FutureWater

Model theory, installation, and data preparation

SPHY v3.1: Spatial Processes in Hydrology

[248]

AUTHORS

S. Khanal
A.F. Lutz
J. Eekhout
W. Terink
C. Aubry-Wake
W.W. Immerzeel

DATE

March 2024

SPHY v3.1: Spatial Processes in Hydrology

Model theory, installation, and data preparation

FutureWater Report [248]

Authors
S. Khanal
A.F. Lutz
J. Eekhout
W. Terink
C. Aubry-Wake
W. W. Immerzeel

Date
February 2024

How to cite
Khanal, S., A.F. Lutz, J. Eekhout, W. Terink, W.W. Immerzeel, 2024. SPHY v3.1: Spatial Processes in Hydrology. Model theory, installation, and data preparation. FutureWater Report 248, 124pp.

The online version of the report is also available at https://futurewater.gitbook.io/sphy-manual/

FutureWater

ADDRESS
FutureWater B.V.
Costerweg 1V
6702 AA Wageningen
The Netherlands

TELEPHONE +31 317 460 050
WEBSITE www.futurewater.eu

Acknowledgements

The development and publication of the SPHY model source code, its binaries, GUIs, and case-studies has been supported through various (research) projects that were partly or completely funded by the following organizations:

- International Centre for Integrated Mountain Development (ICIMOD[1]);
- European Space Agency (ESA[2]);
- Asian Development Bank (ADB[3]);
- World Bank[4];
- Rijksdienst voor Ondernemend Nederland (RVO[5])
- NUFFIC[6]
- Spanish Ministry of Science and Innovation (CGL2013-42009-R, FJCI-2016-28905)

We are very grateful to these organizations and other individual collaborators who made the development of the SPHY model possible. We hope to continue to collaborate with these organizations in the future in order to further develop and improve the SPHY model and its interfaces.

[1] http://www.icimod.org/
[2] http://www.esa.int/ESA
[3] http://www.adb.org/
[4] http://www.worldbank.org/
[5] http://www.rvo.nl/
[6] https://www.nuffic.nl/en

Table of contents

Tables

Figures

1 Introduction

The number and diversity of water-related challenges are large and are expected to increase in the future (Wagener et al., 2010; Lall, 2014). Even today, the ideal condition of having the appropriate amount of good-quality water at the desired place and time is most often not satisfied (Biswas and Tortajada, 2010; Droogers and Bouma, 2014). It is likely that climate variability and change will intensify food insecurity by water shortages (Wheeler and von Braun, 2013), loss of access to drinking water (Rockström et al., 2012), and increased risk of natural hazards from floods and soil erosion. Current and future water-related challenges are location and time specific and can vary from impact of glacier dynamics (Immerzeel et al., 2012b), economic and population growth (Droogers et al., 2012), floods or extended and more prolonged droughts (Dai, 2011), amongst others.

In response to these challenges, hydrologists and water resource specialists are developing modeling tools to analyze, understand and explore solutions to support decision makers and operational water managers (Pechlivanidis et al., 2011). Despite difficulties in connecting the scientific advances in hydrological modeling with the needs of decision makers and water managers, progress has been made and there is no doubt that modeling tools are indispensable in what is called good “water governance” (Droogers and Bouma, 2014; Liu et al., 2008).

The strength of hydrological models is that they can provide output at high temporal and spatial resolutions, and for hydrological processes that are difficult to observe on the large scale that they are generally applied on (Bastiaanssen et al., 2007). The most important aspect of applying models is in their use in exploring different scenarios, expressing for example, possible effects of changes in population and climate on the water cycle (Droogers and Aerts, 2005). Models are also applied at the operational level to explore interventions (management scenarios) to be used by water managers and policy makers. Examples of this are changes in reservoir operation rules, water allocation between sectors, investment in infrastructure such as water treatment or desalination plants, and agricultural and irrigation practices. In other words: models enable hydrologists and water managers to change focus from a re-active towards a pro-active approach.

Over the past decades, the land surface and hydrologic communities have made substantial progress in understanding the spatial presentation of fluxes of water and energy (Abbott et al., 1986; Wigmosta et al., 1994; VanderKwaak and Loague, 2001; Rigon et al., 2006). Their efforts have led to the development of well-known hydrological models, such as, e.g., VIC (Liang et al., 1994, 1996), SWAT (Neitsch et al., 2009), TOPKAPI-ETH (Finger et al., 2011; Ragettli and Pellicciotti, 2012; Ragettli et al., 2014, 2015), LISFLOOD (Van Der Knijff et al., 2010), SWIM (Krysanova et al., 2015, 1998, 2000), HYPE (Lindström et al., 2010), mHM (Samaniego et al., 2010), PCR-GLOBWB (van Beek and Bierkens, 2008; Bierkens and van Beek, 2009; Wada et al., 2010; Sperna Weiland et al., 2010), MIKE-SHE (Refshaard and Storm, 1995; Oogathoo et al., 2008; Deb S.K. and Shukla M.K., 2011) and GEOtop (Rigon et al., 2006; Endrizzi et al., 2011, 2014) amongst others. The number of existing hydrological models is probably in the tens of thousands (Droogers and Bouma, 2014). Some existing model reviews cover a substantial number of models: IRRISOFT (Irrisoft, 2014): 114; USGS (2014): 110; (EPA, 2014): 211; USACE (HEC, 2014): 18.

All these hydrological models are different with respect to (i) the number and detail of hydrological processes that are integrated, (ii) their field and (iii) scale of application, and (iv) the way they are implemented. Whereas, for example, the SWIM (Krysanova et al., 2015, 1998, 2000) and HYPE (Lindström et al., 2010) models both include all major hydrological processes, the SWIM model is typically developed for large-scale (large river basins to continental) applications, and the HYPE model operates on the sub-basin scale. Therefore, these models contain less detail, in contrast to fully distributed models operating at grid level, such as, e.g., GEOtop (Rigon et al., 2006; Endrizzi et al., 2014, 2011) and TOPKAPI-ETH (Finger et al., 2011; Ragettli et al., 2015, 2014; Ragettli and Pellicciotti, 2012).

Models like, e.g., MIKE-SHE (Refshaard and Storm, 1995; Oogathoo et al., 2008; Deb S.K. and Shukla M.K., 2011) and LISFLOOD (Van Der Knijff et al., 2010) have the advantage of being flexible in terms of the spatial and temporal resolutions, but their disadvantages are that they do not include glacier processes and that they are not open source and therefore not available to the larger community.

It is clear that all these models have their pros and cons in terms of (i) processes integrated, (ii) field of application, (iii) scale of application, and (iv) implementation. Table 1 shows the pros and cons of some well-known hydrological models, including the Spatial Processes in HYdrology (SPHY) model. Over the last couple of years, we have developed the SPHY model, and improved its usefulness by applying the model in various research projects. SPHY has been developed with the explicit aim of simulating terrestrial hydrology under various physiographical and hydroclimatic conditions by integrating key components from existing and well-tested models: HydroS (Droogers and Immerzeel, 2010), SWAT (Neitsch et al., 2009), PCR-GLOBWB (van Beek and Bierkens, 2008; Bierkens and van Beek, 2009; Wada et al., 2010; Sperna Weiland et al., 2010), SWAP (van Dam et al., 1997) and HimSim (Immerzeel et al., 2012b). Based on Table 1 it is clear that SPHY (i) integrates most hydrologic processes, including glacier processes, (ii) has the flexibility to study a wide range of applications, including climate and land use change impacts, irrigation planning, and droughts, (iii) can be used for catchment- and river-basin-scale applications as well as farm- and country-level applications, and has a flexible spatial resolution, and (iv) can easily be implemented. Implementation of SPHY is relatively easy because (i) it is open source, (ii) input and output maps can directly be used in GIS, (iii) it is set up modular in order to switch on/off relevant/irrelevant processes and thus decreases model run time and data requirements, (iv) it needs only daily precipitation and temperature data as climate forcing, (v) it can be forced with remote sensing data, and (vi) it uses a configuration file that allows the user to change model parameters and choose the model output that needs to be reported.

Assessing the impacts of environmental change on soil erosion and sediment yield at the large catchment scale remains one of the main challenges in soil erosion modelling (de Vente et al., 2013a; Poesen, 2018). Most soil erosion and sediment yield models adopt simplified model formulations, are applied at low temporal resolutions, and often only partly represent the impacts of changes in land use or climate conditions. This often leads to unreliable results that do not sufficiently increase process understanding or support decision-making (de Vente et al., 2013b). From the available soil erosion models, process-based models aim to incorporate the most relevant processes driving soil detachment, sediment transport and deposition, see (Morgan, 2005) for an overview of process-based models. Process-based models often run at small spatial (hillslope to small catchment) and temporal scales (sub-hourly to daily time steps) and require detailed input data, such as (sub-)hourly precipitation and topographic data, and incorporate a large number of calibration parameters management (Govers, 2011). At larger scales, soil erosion is often assessed using empirical erosion models, see (de Vente et al., 2013) for an overview. These models are derived from field studies where soil erosion has been observed under different land use, management, soil, climate, and topographical conditions. The best-known and applied empirical model is the Universal Soil Loss Equation (Wischmeier and Smith, 1978) and its derivatives RULSE (Renard et al., 1997) and MUSLE (Williams, 1995). While the empirical formulations of the USLE were obtained at plot-scale, the model is often applied at much larger scales, sometimes in combination with a sediment transport capacity equation or a sediment delivery ratio to assess sediment yield (Van Rompaey et al., 2001; de Vente et al., 2008). Due to its simplicity, the USLE can be applied with a relatively limited amount of input data. However, their main restriction is the limited number of processes accounted for (e.g. the USLE and RUSLE based models only consider sheet and rill erosion) and the limited potential to evaluate the impacts of changes in climate and land management (Govers, 2011; de Vente et al., 2013b). Furthermore, these models are typically applied at annual time steps, largely neglecting intra-annual variation of climate and vegetation conditions.

Most current soil erosion models have a limited potential for application at larger temporal and spatial scales (i.e. process-based models) or lack sufficient representation of the underlying soil detachment

and sediment transport processes and sensitivity to changes in land use or climate (i.e. empirical models), making them of limited use for scenario studies and process understanding. We have extended the SPHY model with a soil erosion module based on the process-based Morgan-Morgan-Finney erosion model (Morgan and Duzant, 2008) that allows evaluating the impacts of land use, land management and climate conditions on erosion and sediment yield from local to regional scales (Eekhout et al., 2018b).

The objectives of this manual are:

- Introduce and present the SPHY model (v3.1)
- Present the SPHY model (v3.1) theory and demonstrate some typical applications
- Provide the steps that are required to install the SPHY model as a standalone application
- Learn how-to prepare model data for a SPHY model for your own area of interest

The model source code is in the public domain (open access) and can be obtained from the SPHY model website free of charge (www.sphymodel.com). The three peer-reviewed open-access publications of the SPHY model can be found at https://doi.org/10.5194/gmd-8-2009-2015 (Terink et al., 2015c), https://doi.org/10.1029/2020WR029266 (Khanal et al., 2021) and https://doi.org/10.5194/esurf-6-687-2018 (Eekhout et al., 2018b).

Table 1: Pros (+) and cons (-) of some well-known hydrological models, including the SPHY model. A categorization is made between (i) processes that are integrated, (ii) field of application, (iii) scale of application, and (iv) implementation.

	SPHY	TOPKAPI-ETH	SWAT	VIC	LIS-FLOOD	SWIM	HYPE	mHM	MIKE-SHE	PCRGLOB-WB	GEO-top
Processes integrated											
Rainfall–runoff	+	+	+	+	+	+	+	+	+	+	+
Evapotranspiration	+	+	+	+	+	+	+	+	+	+	+
Dynamic vegetation growth	+	–	+	+	+	+	a	NA	+	+	–
Unsaturated zone	+	+	+	+	+	+	+	+	+	+	+
Groundwater	+	–	+	+	+	+	+	+	+	+	+
Glaciers	+	+	–	–	–	+	+	–	–	–	+
Snow	+	+	+	+	+	+	+	+	+	+	+
Routing	+	+	+	+	+	+	+	+	+	+	+
Lakes incorporated into routing scheme	+	–	+	+	+	+	+	NA	+	+	–
Reservoir management	–	–	+	–	–	+	+	NA	–	+	–
Field of application											
Climate change impacts	+	+	+	+	+	+	+	+	+	+	+
Land use change impacts	+	+	+	+	+	+	+	+	+	+	+
Irrigation planning	+	–	+	+	–	+	+	–	+	–	+
Floods	–	–	–	–	c	–	+	–	+	+	+
Droughts	+	+	+	+	+	+	+	+	+	+	+
Water supply and demand	–	–	+	–	–	–	+	NA	–	–	–
Scale of application											
Catchment scale	+	+	+	+	–	–	+	–	+	–	+
River basin scale	+	+	+	+	+	+	+	+	+	–	–
Mesoscale river basins	+	–	+	+	+	+	+	+	+	+	–
Global scale	–	–	–	+	+	–	–	–	–	+	–
Farm level	+	–	–	–	–	–	+	–	–	–	–
Country level	+	–	–	–	–	–	+	–	–	–	–
Fully distributed	+	+	–	+	+	–	–	+	+	+	+
Sub-grid variability	+	–	–	+	–	–	–	+	–	+	+
Flexible spatial resolution	+	+	–	+	+	–	–	+	+	+	+
Hourly resolution	–	+	+	–	+	–	+	+	+	–	+
Sub-daily resolution	–	–	–	+	+	–	+	NA	+	–	–
Daily resolution	+	+	+	+	+	+	+	NA	+	+	–
Implementation											
Open source	+	–	+	+	–	–	+	–	–	–	+
Forcing with remote sensing	+	+	–	+	+	–	+	NA	–	–	+
GIS compatibility	+	+	+	–	+	+	+	+	+	+	+
Modular set up	+	–	–	+	+	+	+	+	+	–	–
Computational efficient	+	+	+	–	+	+	+	+	–	+	+
Climate forcing requirements	+	+	–	b	–	–	+	+	–	–	–
Flexible output reporting options	+	+	–	+	+	+	+	NA	+	–	+
Graphical user-interface in GIS	a	–	+	–	–	+	–	–	+	–	–

[a] Currently in development. [b] More climate variables are required if the model is run in energy balance mode. [c] Only if run in combination with LISFLOOD-FP. NA: information not available.

2 Theory

2.1 Background

SPHY is a spatially distributed leaky bucket type of model, and is applied on a cell-by-cell basis. The main terrestrial hydrological processes are described in a conceptual way so that changes in storages and fluxes can be assessed adequately over time and space. SPHY is written in the Python programming language using the PCRaster (Karssenberg et al., 2001, 2010; Karssenberg, 2002; Schmitz et al., 2009, 2013) dynamic modeling framework.

SPHY is grid based and cell values represent averages over a cell (Figure 1). For glaciers, sub-grid variability is taken into account: a cell can be glacier free, partially glacierized, or completely covered by glaciers. The cell fraction not covered by glaciers consists of either land covered with snow or land that is free of snow. Land that is free of snow can consist of vegetation, bare soil, or open water. The dynamic vegetation module accounts for a time-varying fractional vegetation coverage, which affects processes such as interception, effective precipitation, and potential evapotranspiration. Figure 2 provides a schematic overview of the SPHY modeling concepts.

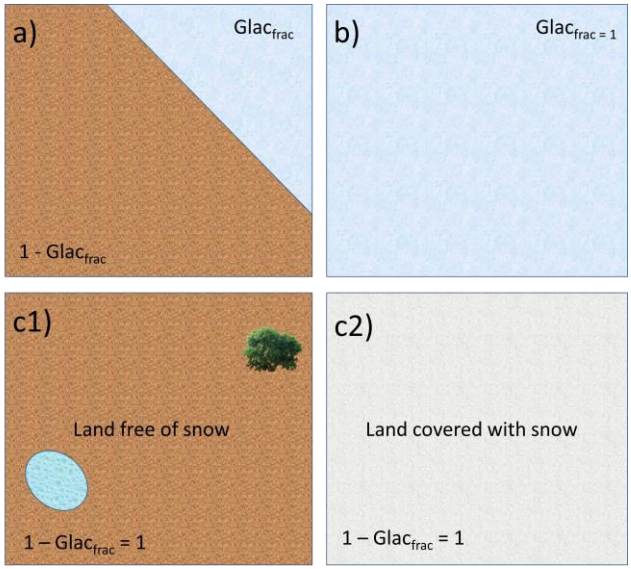

Figure 1: Illustration of SPHY sub-grid variability. A grid cell in SPHY can be (a) partially covered with glaciers, or (b) completely covered with glaciers, or (c1) free of snow, or (c2) completely covered with snow. In the case of (c1), the free land surface can consist of bare soil, vegetation, or open water.

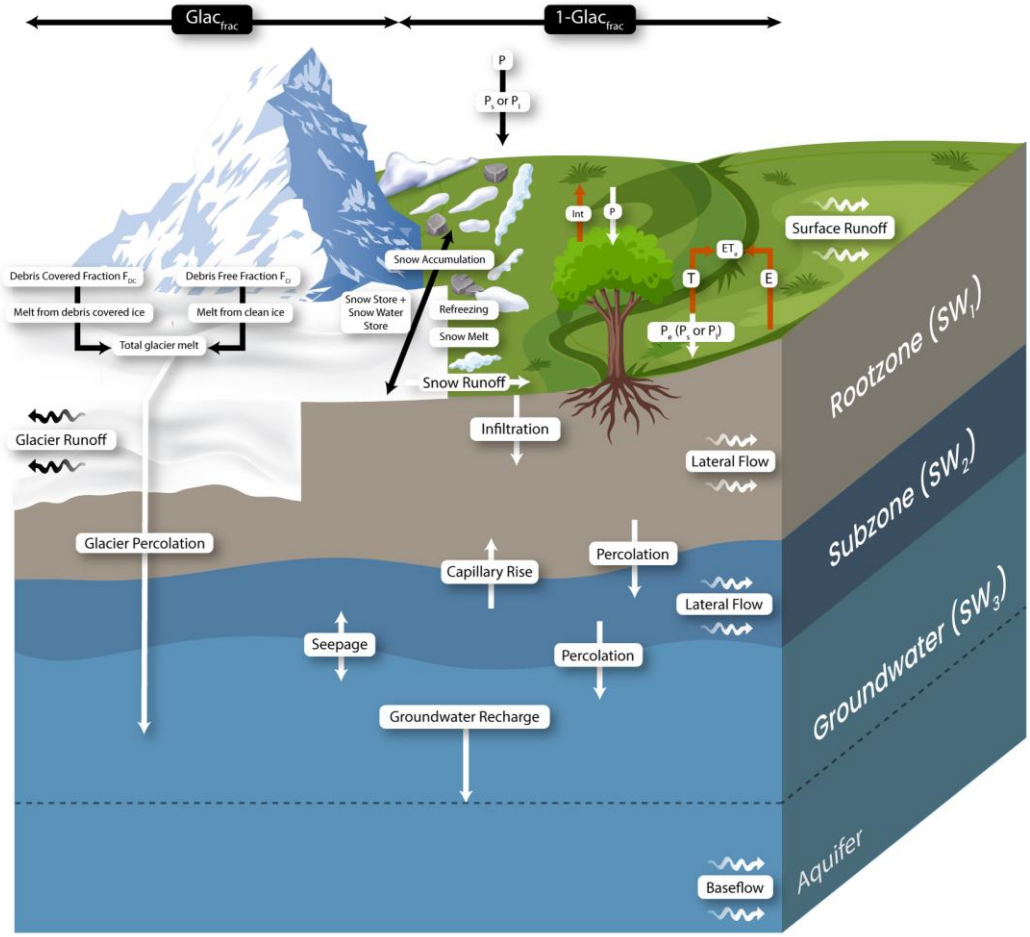

Figure 2: SPHY modeling concepts. Abbreviations are explained in the text.

The soil column structure is similar to VIC (Liang et al., 1994, 1996), with two upper soil storages and a third groundwater storage. Their corresponding drainage components are surface runoff, lateral flow and baseflow. SPHY simulates for each cell precipitation in the form of rain or snow, depending on the temperature. Precipitation that falls on land surfaces can be intercepted by vegetation and evaporated in part or whole. The snow storage is updated with snow accumulation and/or snowmelt. A part of the liquid precipitation is transformed in surface runoff, whereas the remainder infiltrates into the soil. The resulting soil moisture is subject to evapotranspiration, depending on the soil properties and fractional vegetation cover, while the remainder contributes to river discharge by means of lateral flow from the first soil layer, and baseflow from the groundwater layer.

Melting of glacier ice contributes to the river discharge by means of a slow and fast component, being (i) percolation to the groundwater layer that eventually becomes baseflow, and (ii) direct runoff. The cell-specific runoff, which becomes available for routing, is the sum of surface runoff, lateral flow, baseflow, snowmelt and glacier melt.

If no lakes are present, then the user can choose a simple flow accumulation routing scheme: for each cell, the accumulated amount of water that flows out of the cell into its neighboring downstream cell is calculated. This accumulated amount is the amount of water in the cell itself plus the amount of water in upstream cells of the cell, and is calculated using the flow direction network. If lakes are present, then the fractional accumulation flux routing scheme is used; depending on the actual lake storage, a fraction

of that storage becomes available for routing and is extracted from the lake, while the remaining part becomes the updated actual lake storage. The flux available for routing is routed in the same way as in the simple flow accumulation routing scheme.

As input, SPHY requires static data as well as dynamic data. For the static data, the most relevant are digital elevation model (DEM), land use type, glacier cover (including differentiation in debris-free and debris-covered ice surfaces), lakes/reservoirs and soil characteristics. The main dynamic data consist of climate data, such as precipitation, temperature, and reference evapotranspiration. Since SPHY is grid based, optimal use of remote sensing data and global data sources can be made. For example, the Normalized Difference Vegetation Index (NDVI) (Tucker, 1979; Carlson and Ripley, 1997; Myneni and Williams, 1994) can be used to determine the leaf-area index (LAI) in order to estimate the growth stage of land cover. For setting up the model, streamflow data are not necessary. However, to undertake a proper calibration and validation procedure, flow data are required. The model could also be calibrated using actual evapotranspiration, soil moisture contents, and/or snow-covered area (SCA). Section 3.2 contains an example application in which the SPHY model has been calibrated using MODIS snow cover images. An overview of the adjustable SPHY model parameters is shown in Appendix 1 (Table 25).

The soil erosion model is based on the Modified MMF model (Morgan and Duzant, 2008). Total soil erosion is calculated from detachment by raindrop impact and detachment by runoff, considering within cell deposition. Detachment of soil particles from raindrop impact is determined from the total rainfall energy, which is determined for direct throughfall and leaf drainage, respectively. Detachment of soil particles by runoff is determined from the accumulated runoff from the hydrological model. Both soil erosion equations account for the fraction of the soil covered by stones and vegetation or snow and are determined separately for three texture classes (sand, silt, clay). Within cell deposition is calculated as a function of vegetation and surface roughness. The remainder of the detached sediment is taken into transport.

The SPHY model provides a wealth of output variables that can be selected based on the preference of the user. Spatial output can be presented as maps of all the available hydrological processes, i.e., actual evapotranspiration, runoff generation (separated by its components), and groundwater recharge, and storage components, i.e. root zone water content, snow storage, groundwater storage, and canopy storage. These maps can be generated on a daily basis, but can also be aggregated at monthly or annual time periods and as long-term monthly averages or sums. Time series can be generated for each cell in the study area. Time series often used are streamflow, actual evapotranspiration and recharge to the groundwater.

2.2 Modules

SPHY enables the user to turn on/off modules (representing groups of hydrological processes) that are relevant/irrelevant to the area of interest. This concept is very useful if the user is studying hydrological processes in regions where not all hydrological processes are relevant. A user may for example be interested in studying irrigation water requirements in central Africa. For this region, glacier and snow melting processes are irrelevant, and can thus be switched off. The advantages of turning off irrelevant modules are two-fold: (i) decrease model run time, and (ii) decrease the number of required model input data. It should be noted, however, that the hydrologic model structure should be specific to the catchment's characteristics (Pomeroy et al., 2007; Clark et al., 2008; Niu et al., 2011; Essery et al., 2013; Clark et al., 2015a, b). It is therefore essential that the user knows which catchment characteristics and processes should be included in their modeling framework.

Figure 3 represents an overview of the six modules available: glaciers, snow, groundwater, dynamic vegetation, simple routing, lake/reservoir routing, soil erosion and sediment transport. Most modules can run independently of each other, except for the glacier, sediment transport and soil erosion modules. If

glaciers are present, then snow processes are relevant as well (Verbunt et al., 2003; Singh and Kumar, 1997).

Since melting glacier water percolates to the groundwater layer, the glacier module cannot run with the groundwater module turned off. Two modules are available for runoff routing: (i) a simple flow accumulation routing scheme, and (ii) a fractional flow accumulation routing scheme used when lakes/reservoirs are present. The user has the option to turn off routing, or to choose between one of these two routing modules. All hydrological processes incorporated in the SPHY model are described in detail in the following sections.

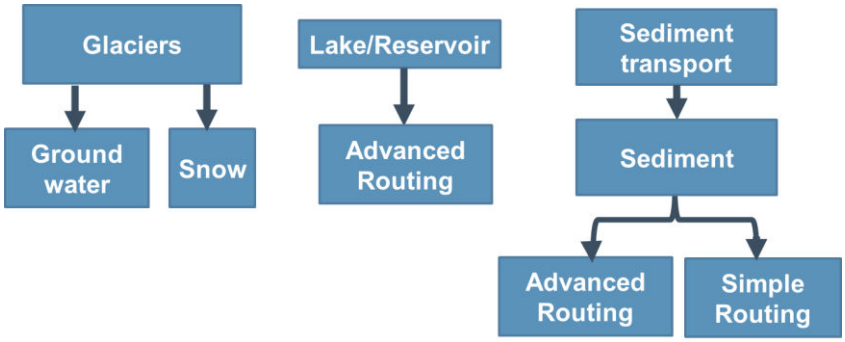

Figure 3: Modules of the SPHY model that can be switched on/off.

2.3 Reference and potential evapotranspiration

Despite the good physical underlying theory of the Penman–Monteith equation (Allen et al. 1998) for calculating the reference evapotranspiration (ET), its major limitation is the high data demand for energy-based methods. This brought Hargreaves and Samani (1985) to derive the modified Hargreaves equation that is based on temperature only. For this reason, this equation has also been implemented in the SPHY model, according to:

$$ET_r = 0.0023 \cdot 0.408 \cdot Ra\left(T_{avg} + 17.8\right) \cdot TD^{0.5}$$

Equation 1

with Ra ($MJm^{-2}d^{-1}$) the extraterrestrial radiation, T_{avg} (C) the average daily air temperature, and TD (C) the daily temperature range, defined as the difference between the daily maximum and minimum air temperature. The constant 0.408 is required to convert the units to mm, and Ra can be obtained from tables (Allen et al., 1998) or equations using the day of the year and the latitude of the area of interest.

According to Allen et al. (1998), ET_r is the evapotranspiration rate from a reference surface with access to sufficient water to allow evapotranspiration at the potential rate. The reference surface is a hypothetical grass reference crop with specific characteristics. The potential evapotranspiration ET_p has no limitations on crop growth or evapotranspiration from soil water and salinity stress, crop density, pests and diseases, weed infestation or low fertility. Allen et al. (1998) determined ET_p by the crop coefficient approach, where the effects of various weather conditions are incorporated into ET_r and the crop characteristics in the crop coefficient (Kc), using:

$$ET_{p,t} = ET_{r,t} \cdot Kc$$

Equation 2

with $ET_{p,t}$ (mm) the potential evapotranspiration on day t, $ET_{r,t}$ (mm) the reference evapotranspiration on day t, and Kc (–) the crop coefficient. The effects of both crop transpiration and soil evaporation are integrated into the Kc.

If the dynamic vegetation module in SPHY is not used, then the user can opt (i) to use a single constant Kc throughout the entire simulation period or (ii) to use a pre-defined time series of crop coefficients as model input. Plausible values for Kc can be obtained from the literature (Allen et al., 1998; FAO, 2013). However, vegetation is generally very dynamic throughout the year. It is therefore more realistic to use a pre-defined time series of crop coefficients or to use the dynamic vegetation module, instead of a single constant Kc. This can be adjusted according to the user's preferences.

Kc can be estimated using remotely sensed data (Rafn et al., 2008; Contreras et al., 2014). In the dynamic vegetation module, Kc is scaled throughout the year using NDVI and the maximum and minimum values for Kc, which are crop specific. These values for Kc can easily be obtained from Allen et al. (1998). Then Kc is calculated using:

$$Kc = Kc_{min} + (Kc_{max} - Kc_{min}) * \frac{(NDVI - NDVI_{min})}{(NDVI_{max} - NDVI_{min})}$$

Equation 3

with $NDVI_{max}$ (-) and $NDVI_{min}$ (-) the maximum and minimum values for NDVI (vegetation type dependent). This approach shows the flexibility of SPHY in using remote sensing data (e.g., NDVI) as input to improve model accuracy.

2.4 Dynamic vegetation processes

2.4.1 Maximum canopy storage

SPHY allows the user to use the dynamic vegetation module in order to incorporate a time-variable vegetation cover and corresponding rainfall interception. In order to calculate the rainfall interception, the canopy storage needs to be calculated, using a time series of NDVI (Carlson and Ripley, 1997). The first step involves the calculation of the fraction photosynthetically active radiation (FPAR). FPAR can be calculated using a relation between NDVI and FPAR, which was found by Peng et al. (2012) and described by Sellers et al. (1996), according to:

$$FPAR = min\left(\frac{(SR - SR_{min})(FPAR_{max} - FPAR_{min})}{(SR_{max} - SR_{min})} + FPAR_{min}, 0.95\right)$$

Equation 4

with

$$SR = \frac{1 + NDVI}{1 - NDVI}$$

Equation 5

and $FPAR_{max}$ (-) and $FPAR_{min}$ (–) having values of 0.95 and 0.001, respectively. An FPAR of 0.95 is equivalent to the maximum LAI for a particular class, and an FPAR of 0.001 is equivalent to a minimum LAI. In order to calculate FPAR, an NDVI time series is required.
The second step is the calculation of the leaf-area index (LAI), which is eventually required to calculate the maximum canopy storage ($Scan_{max}$). According to Monteith (1973), LAI for vegetation that is evenly distributed over a surface can be calculated using a logarithmic relation between LAI and FPAR, according to:

$$LAI = LAI_{max} \cdot \frac{log(1 - FPAR)}{log(1 - FPAR_{max})}$$

Equation 6

with LAI (–) the leaf-area index, and LAI_{max} (–) the maximum leaf-area index (vegetation type dependent). This means that the maximum and minimum LAI values are related to the maximum and minimum of FPAR.
For vegetation that is concentrated in clusters, the linear relation from Goward and Huemmrich (1992) is often used. However, since SPHY is generally applied using grid-cell resolutions between 250m and 1km, we can assume that the effect of having vegetation concentrated in clusters is negligible. Therefore, the calculation of LAI in SPHY is done using the logarithmic relation of Monteith (1973) (Equation 6).

The next step involves the calculation of the maximum canopy storage ($Scan_{max}$ (mm)). Many different relations between $Scan_{max}$ and LAI can be found in the literature, depending on the vegetation type (de Jong and Jetten, 2010). The best results for crop canopies are shown by Kozak et al. (2007) and are archived by Von Hoyningen-Huene (1981), who derived the following relation between $Scan_{max}$ and LAI:

$$Scan_{max} = 0.935 + 0.498LAI - 0.00575LAI^2$$

Equation 7

2.4.2 Interception

Interception is calculated on a daily basis if the dynamic vegetation module is used, and consists of the daily precipitation plus the intercepted water remaining in the canopy storage from the previous day. First, the canopy storage is updated with the amount of precipitation of the current day:

$$Scan_t = Scan_{t-1} + P_t$$

Equation 8

with $Scan_t$ (mm) the canopy storage on day t, $Scan_{t-1}$ (mm) the canopy storage on day $t-1$, and P_t (mm) the amount of precipitation on day t. The portion of precipitation that cannot be stored in the canopy storage is known as precipitation throughfall, or effective precipitation, according to:

$$Pe_t = max\left(0, Scan_t - Scan_{max,t}\right)$$

Equation 9

with Pe_t (mm) the effective precipitation on day t, and $Scan_t$ (mm) the canopy storage on day t. This equation shows that precipitation throughfall only occurs if the water stored in the canopy exceeds the maximum canopy storage. After the effective precipitation has been calculated, the canopy storage is updated as:

$$Scan_t = Scan_t - Pe_t$$

Equation 10

The remaining amount of water stored in the canopy is available for interception, and the amount of water that will be intercepted depends on the atmospheric demand for open water evaporation. A commonly used value for the atmospheric demand for open water evaporation is 1.5 (Allen et al., 1998), which is derived from the ratio between 1 and the mean pan evaporation coefficient Kp (~0.65). The interception can now be calculated using:

$$Int_t = min\left(1.5ET_{r,t}, Scan_t\right)$$

Equation 11

with Int_t (mm) the intercepted water on day t, and $ET_{r,t}$ (mm) the reference evapotranspiration on day t. Finally, the canopy storage is updated by subtracting the interception:

$$Scan_t = Scan_t - Int_t$$

Equation 12

2.5 Snow processes

For each cell, a dynamic snow storage is simulated at a daily time step, adopted from the model presented by Kokkonen et al. (2006). The model keeps track of a snow storage, which is fed by precipitation and generates runoff from snowmelt. Refreezing of snowmelt and rainfall within the snowpack are simulated as well.

2.5.1 Snow and rainfall

Depending on a temperature threshold, precipitation is defined as falling in either solid or liquid form. Daily snow accumulation, which is defined as solid precipitation, is calculated as:

$$P_{s,t} = \begin{Bmatrix} Pe_t & if & T_{avg,t} \leq T_{crit} \\ 0 & if & T_{avg,t} > T_{crit} \end{Bmatrix}$$

Equation 13

with $P_{s,t}$ (mm) the snowfall on day t, Pe_t (mm) the effective precipitation on day t, $T_{avg,t}$ (°C) the mean air temperature on day t, and T_{crit} (°C) a calibrated temperature threshold for precipitation to fall as snow. The precipitation that falls as rain is defined as liquid precipitation, and is calculated as:

$$P_{l,t} = \begin{Bmatrix} Pe_t & if & T_{avg,t} > T_{crit} \\ 0 & if & T_{avg,t} \leq T_{crit} \end{Bmatrix}$$

Equation 14

with $P_{l,t}$ (mm) being the amount of rainfall on day t.

2.5.2 Snowmelt, refreezing, and storage

To simulate snowmelt, the well-established and widely used degree-day melt modeling approach is used (Hock, 2003). The application of degree-day models is widespread in cryospheric models and is based on an empirical relationship between melt and air temperature. Degree-day models are easier to set up compared to energy-balance models, and only require air temperature, which is mostly available and relatively easy to interpolate (Hock, 2005). Using a degree-day modeling approach, the daily potential snowmelt is calculated as follows:

$$A_{pot,t} = \begin{Bmatrix} HT_t \cdot DDF_s, & if\ T_{max,t} > 0 \\ 0, & if\ T_{max,t} \leq 0 \end{Bmatrix}$$

equation 15

$$HT_t = Max\left\{0, \left(\sum_{i=1}^{i=24} T_{avg,t} + \left(T_{avg,t} + \left(T_{avg,t} - T_{max,t}\right)\cos(\pi * i/12)\right)\right)/24\right\}$$

Equation 16

with $A_{pot,t}$ [mm] the potential snow melt on day t, $T_{max,t}$ [°C] the max air temperature on day t and DDF_s [mm °C^{-1}d^{-1}] a calibrated degree day factor for snow. HT_t, calculates the fraction of day where the hourly temperature is above melting point, while the average temperature is below melting point. The actual snow melt is limited by the snow store at the end of the previous day, and is calculated as:

$$A_{act,t} = min(A_{pot,t}, SS_{t-1})$$

Equation 17

with $A_{act,t}$ (mm) the actual snowmelt on day t, and SS_{t-1} (mm) the snow storage on day $t-1$. The snow storage from day $t-1$ is then updated to the current day t, using the actual snowmelt ($A_{act,t}$) and the solid precipitation ($P_{s,t}$). Part of the actual snowmelt freezes within the snowpack and thus does not run off immediately. When temperature is below the melting point, meltwater that has frozen in the snowpack during $t-1$ is added to the snow storage as:

$$SS_t = \begin{cases} SS_{t-1} + P_{s,t} + SSW_{t-1} & if \quad T_{avg,t} < 0 \\ SS_{t-1} + P_{s,t} - A_{act,t} & if \quad T_{avg,t} \geq 0 \end{cases}$$

Equation 18

with SS_t the snow storage on day t, SS_{t-1} the snow storage on day $t-1$, $P_{s,t}$ the solid precipitation on day t, $A_{act,t}$ the actual snowmelt on day t, and SSW_{t-1} the amount of frozen meltwater on day $t-1$. The units for all terms are mm.

The capacity of the snowpack to freeze snowmelt is characterized by introducing a calibrated water storage capacity(SSC ($mm \cdot mm^{-1}$)), which is the total water equivalent of snowmelt (mm) that can freeze per mm water equivalent of snow in the snow storage. The maximum of meltwater that can freeze (SSW_{max}(mm)) is thus limited by the thickness of the snow storage:

$$SSW_{max,t} = SSC \cdot SS_t$$

Equation 19

Then the amount of meltwater stored in the snowpack, and that can freeze in the next time step, is calculated as:

$$SSW_t = \begin{cases} 0, & if\ T_{avg,t} < 0 \\ min(SSW_{max,t}, SSW_{t-1} + P_{l,t} + A_{act,t}), & if\ T_{avg,t} \geq 0 \end{cases}$$

Equation 20

with SSW_t the amount of meltwater in the snowpack on day t, $SSW_{max,t}$ the maximum of meltwater that can freeze on day t, SSW_{t-1} the amount of frozen meltwater on day $t-1$, $P_{l,t}$ the amount of rainfall on day t, and $A_{act,t}$ the actual snowmelt on day t. The units of all terms are in mm.

The total snow storage (SST (mm)) consists of the snow storage and the meltwater that can freeze within it, according to:

$$SST_t = (SS_t + SSW_t) \cdot (1 - GlacF)$$

Equation 21

with $(1 - GlacF)$ (–) the grid-cell fraction not covered with glaciers. In SPHY it is therefore assumed that snow accumulation and snowmelt can only occur on the grid-cell fraction determined as land surface. Snow falling on glaciers is incorporated in the glacier module.

2.5.3 Snow runoff

Runoff from snow (SRo (mm)) is generated when the air temperature is above melting point and no more meltwater can be frozen within the snowpack, according to:

$$SRo_t = \begin{cases} A_{act,t} + P_{l,t} - \Delta SSW & if \quad T_{avg,t} > 0 \\ 0 & if \quad T_{avg,t} \leq 0 \end{cases}$$

Equation 22

with ΔSSW (mm) the change in meltwater stored in the snowpack according to:

$$\Delta SSW = SSW_t - SSW_{t-1}$$

Equation 23

2.6 Glacier processes

Since the SPHY model usually operates at a spatial resolution between 250m and 1km, the dynamics of glaciers such as ice flow cannot be resolved explicitly. However, SPHY has a mass-conserving glacier evolution algorithm to represent changes in glacier cover through time.

2.6.1 Glacier melt

Glacier melt is calculated with a degree-day modeling approach as well (Hock, 2005). Because glaciers that are covered with debris melt at different rates than debris-free glaciers (Reid et al., 2012), a distinction can be made between different degree-day factors for both types. The daily melt from debris-free glaciers (A_{CI} (mm)) is calculated as:

$$A_{CI,t} = \begin{cases} T_{avg,t} \cdot DDF_{CI} \cdot F_{CI} & if \quad T_{avg,t} > 0 \\ 0 & if \quad T_{avg,t} \leq 0 \end{cases}$$

Equation 24

with DDF_{CI} $(mm\,^{\circ}C^{-1}d^{-1})$ a calibrated degree-day factor for debris-free glaciers and F_{CI} (–) the fraction of debris-free glaciers within the fractional glacier cover (GlacF) of a grid cell. The daily melt from debris-covered glaciers (A_{DC} (mm)) is calculated in a similar way, but with a different degree-day factor:

$$A_{DC,t} = \begin{cases} T_{avg,t} \cdot DDF_{DC} \cdot F_{DC} & if \quad T_{avg,t} > 0 \\ 0 & if \quad T_{avg,t} \leq 0 \end{cases}$$

Equation 25

where DDF_{DC} $(mm\,^{\circ}C^{-1}d^{-1})$ is a degree-day factor for debris-covered glaciers and F_{DC} (–) is the fraction of debris-covered glaciers within the fractional glacier cover of a grid cell. The total glacier melt per grid cell (A_{GLAC} (mm)) is then calculated by summing the melt from the debris-covered and debris-free glacier types and multiplying by the fractional glacier cover, according to:

$$A_{GLAC,t} = \left(A_{CI,t} + A_{DC,t}\right) \cdot GlacF$$

Equation 26

2.6.2 Glacier runoff

In SPHY, a fraction of the glacier melt percolates to the groundwater while the remaining fraction runs off. The distribution of both is defined by a calibrated glacier melt runoff factor (GlacROF (–)) that can have any value ranging from 0 to 1. Thus, the generated runoff GRo (mm) from glacier melt is defined as:

$$GRo_t = A_{GLAC,t} \cdot GlacROF$$

Equation 27

2.6.3 Glacier percolation

The percolation from glacier melt to the groundwater (G_{perc} (mm)) is defined as:

$$G_{perc,t} = A_{GLAC,t} \cdot (1 - GlacROF)$$

Equation 28

The percolated glacier water is added to the water that percolates from the soil layers of the non-glacierized part of the grid cell (Section 2.7.1 and 2.7.7), which eventually recharges the groundwater.

2.6.4 Glacier ice redistribution

The model takes sub-grid variability into account by calculating the snow and glacier melt runoff from glaciers. By intersecting the glacier outlines with the coarse model grid, the glaciers or parts thereof (fraction) that lie within each model grid cell can be identified. Future changes in (parts of) glaciers in response to the precipitation and temperature are taken into account by using a mass-conserving ice redistribution approach (Khanal et al., 2021). The ice redistribution is done once per year at the end of the hydrological year, which is also the end of the melting season (October 1st). At that moment the accumulated snow in the accumulation zone is transformed into ice and distributed downwards to the ablation area. The net imbalance (I), that is, the difference in the volume of total snow accumulated (SnowS) and total volume of melt generated from the glaciers (GM), forms the basis of ice redistribution:

$$I_{n,j} = SnowS_{n,j} - GM_{n,j}$$

equation 29

where the subscript n is the glacier id, and j is a unique-id. Only when the net imbalance is negative, the volume of ice is redistributed (V_{red}) over the ablation zone according to:

$$Vred_{n,j} = \begin{cases} 0 & , \quad j \epsilon B_{n,j} \\ \sum_{j \epsilon B_{n,j}} I_{n,j} \times \frac{Vini_{n,j}}{\sum_{j \epsilon A_{n,j}} Vini_{n,j}} & , \quad j \epsilon A_{n,j} \end{cases}$$

equation 30

where Aj is the part of the glacier with a negative imbalance, Bj is the part of the glacier with a positive imbalancein any glacier-id n. The redistribution is proportional to the initial total volume of ice (Vini), that is, glacier parts with a larger initial ice volume will receive a large volume of accumulated ice from the accumulation zone to the ablation zone.

2.7 Soil water processes

2.7.1 Soil water balances

The soil water processes in SPHY are modeled for three soil layers (Figure 2), being (i) the first soil layer (root zone), (ii) second soil layer (subzone), and (iii) third soil layer (groundwater layer). The water balance of the first soil layer is:

$$SW_{1,t} = SW_{1,t-1} + Pe_t - ET_{a,t} - RO_t - LF_{1,t} - Perc_{1,t} + Cap_t$$

Equation 31

with $SW_{1,t}$ and $SW_{1,t-1}$ the water content in the first soil layer on days t and $t-1$, respectively, Pe_t the effective precipitation on day t, $ET_{a,t}$ the actual evapotranspiration on day t, RO_t the surface runoff on day t, $LF_{1,t}$ the lateral flow from the first soil layer on day t, $Perc_{1,t}$ the percolation from the first to the second soil layer on day t, and Cap_t the capillary rise from the second to the first soil layer on day t. The second soil layer water balance is:

$$SW_{2,t} = SW_{2,t-1} + Perc_{1,t} - Perc_{2,t} - Cap_t$$

Equation 32

with $SW_{2,t}$ and $SW_{2,t-1}$ the water content in the second soil layer on day t and $t-1$, respectively, and $Perc_{2,t}$ percolation from the second to the third soil layer on day t. The third soil layer water balance is given as:

$$SW_{3,t} = SW_{3,t-1} + Gchrg_t - BF_t$$

Equation 33

with $SW_{3,t}$ and $SW_{3,t-1}$ the water content in the third soil layer on day t and $t-1$, respectively, $Gchrg_t$ groundwater recharge from the second to the third soil layer on day t, and BF_t baseflow on day t. If the glacier module is used, then groundwater recharge consists of percolation from the second soil layer and percolated glacier melt; otherwise, only percolation from the second soil layer is taken into account.

The user can opt to run SPHY without the third soil layer (groundwater). This may be desirable if the user for example is mainly interested in simulating soil moisture conditions in the root zone, instead of evaluating for instance the contribution of baseflow to the total routed river flow. In that case, only the two upper soil layers are used where the bottom boundary of soil layer two is controlled by a seepage flux (positive outward), and instead of baseflow from the third soil layer, water leaves the second soil layer through lateral flow. With the groundwater module turned off, the water balance for the second soil layer is:

$$SW_{2,t} = SW_{2,t-1} + Perc_{1,t} - LF_{2,t} - Cap_t - Seep$$

Equation 34

with $LF_{2,t}$ lateral flow from the second soil layer, and Seep seepage in or out of the second soil layer (positive is outgoing). The units for all water balance terms are in mm.

2.7.2 Actual evapotranspiration

Evapotranspiration refers to both the transpiration from vegetation and the evaporation from soil or open water. As was mentioned in Section 2.3, the Kc accounts for both the crop transpiration and soil evaporation. The additional use of the dynamic vegetation module accounts for a time-variable vegetation cover, meaning that the role of evaporation becomes more dominant as soon as vegetation cover decreases.

Many limiting factors (e.g., salinity stress, water shortage, water excess, diseases) can cause a reduction in potential evapotranspiration (ET_p), resulting in the actual evapotranspiration rate (ET_a). Since SPHY is a water-balance model, SPHY only accounts for stresses related to water shortage or water excess. If there is too much water in the soil profile, then the plant is unable to extract water because of oxygen

stress (Bartholomeus et al., 2008). The calculation of evapotranspiration reduction due to water excess (oxygen stress) is quite complex and requires a substantial number of plant and soil properties (e.g., soil temperature, root dry weight, plant respiration, and minimum gas filled soil porosity; (Bartholomeus et al., 2008) that are generally not available for the spatial scale that SPHY is applied on. Therefore, SPHY uses an evapotranspiration reduction parameter ($ETred_{wet}$) that has a value of 0 if the soil is saturated, and otherwise it will have a value of 1. This parameter is used in the following equation to calculate the actual evapotranspiration:

$$ET_{a,t} = ET_{p,t} \cdot ETred_{wet} \cdot ETred_{dry}$$

Equation 35

with $ET_{a,t}$ (mm) the actual evapotranspiration on day t, $ET_{p,t}$ (mm) the potential evapotranspiration on day t, and $ETred_{wet}$ and $ETred_{dry}$ the reduction parameters for water excess and water shortage conditions, respectively. $ETred_{dry}$ is either calculated using the Feddes equation (Feddes et al., 1978) or the plant water stress method (Allen et al., 1998). The Feddes equation assumes a linear decline in rootwater uptake if the water pressure head drops below a critical value. This critical value can be determined using the soil water retention curve (pF curve), which relates the moisture content of the soil to its binding capacity. This relation is unique for each soil type. The binding capacity is a suction force (H) and is therefore often expressed in cm negative water column. The pF value is simply a conversion of the suction force (H), and is calculated as:

$$pF = log_{10}(-H)$$

Equation 36

Soils that are at field capacity generally have a pF of 2, meaning −100cm of water column, and soils that are at permanent wilting point have a pF of 4.2, or −16000cm of water column. The permanent wilting point is often referred to as the point where the crop dies. In SPHY it is assumed that the linear decline in rootwater uptake starts at a pF of 3 (−1000cm water column). Therefore, $ETred_{dry}$ (–) is calculated as:

$$ETred_{dry,t} = \frac{SW_{1,t} - SW_{1,pF4.2}}{SW_{1,pF3} - SW_{1,pF4.2}}$$

Equation 37

with $ETred_{dry,t}$ (–) the reduction in rootwater uptake due to water shortage on day t, $SW_{1,t}$ (mm) the actual soil water content in the first soil layer on day t, and $SW_{1,pF3}$ (mm) and $SW_{1,pF4.2}$ (mm) the soil water content in the first soil layer at pF3 and pF4.2, respectively. $ETred_{dry}$ can therefore have values ranging between 0 and 1, where a value of 1 represents optimal plant growing conditions, and 0 means no rootwater uptake at all.

The plant water stress method (Allen et al., 1998) accounts for plant-specific characteristics, in addition to soil hydraulic properties. With this method $ETred_{dry}$ (–) is determined with the following equation:

$$ETred_{dry,t} = \frac{TAW - D_r}{(1-p)TAW}$$

Equation 38

Where $ETred_{dry,t}$ is the reduction parameter for water shortage (-),TAW is the total available water in the rootzone (mm), D_r the root zone depletion (mm) and p the depletion fraction (-). The total available water TAW is defined as:

$$TAW = SW_{l,fc} - SW_{1,pF4.2}$$

Equation 39

Where $SW_{l,fc}$ is the soil water content at field capacity (mm) and $SW_{1,pF4.2}$ the soil water content at wilting point (mm). The root zone depletion D_r is defined as:

$$D_r = SW_{l,fc} - SW_{1,t}$$

Equation 40

Where $SW_{1,t}$ is the current soil water content of the first soil layer (mm). The depletion fraction p is defined as the fraction of TAW that a crop can extract from the root zone without suffering water stress, which is determined by the following equation:

$$p = p_{\text{tab}} + 0.04(5 - ET_{p,t})$$

Equation 41

Where p_{tab} is a landuse-specific tabular value of the depletion fraction (-) and $ET_{p,t}$ is the potential evapotranspiration (mm). Values for the landuse-specific tabular value of the depletion fraction can be obtained from (Allen et al., 1998).

$ETred_{dry}$ is eventually used in Equation 35 to calculate the ET_a.

2.7.3 Open-water evaporation

Open-water evaporation is determined in the open-water cells. In these cells all soil hydraulic processes are turned off and runoff equals precipitation minus open-water evaporation. Reservoir cells cannot dry up, i.e. we assume that there is always water present in the reservoir cells. Open-water evaporation is determined as follows:

$$ET_{\text{open-water}} = Kc_{\text{open-water}} ET_r$$

Equation 42

Where $Kc_{\text{open-water}}$ is the crop coefficient value for open-water evaporation (-) and ET_r is the reference evapotranspiration (mm). We suggest to set $Kc_{\text{open-water}}$ to a value of 1.2, after (Allen et al., 1998). In each time step the open-water evaporation is subtracted from the reservoir and lake storage.

2.7.4 Surface runoff

SPHY accounts for both infiltration excess (Horton, 1933) and saturation excess surface runoff (Hewlett, 1961). Infiltration excess surface runoff occurs when the precipitation intensity exceeds the infiltration capacity of the first soil layer; hence, it is a sub-daily process. Since SPHY runs with a daily time step, we have developed a new infiltration excess surface runoff equation, which is inspired by the Green-Ampt formula (Heber Green and Ampt, 1911). We assumed a constant infiltration rate f (mm hr^{-1}), which is determined for each cell and each day by:

$$f = \frac{K_{\text{eff}}}{24}\left[1 + \frac{SW_{1,sat} - SW_1}{SW_{1,sat}}\right]^{\lambda}$$

Equation 43

where K_{eff} is the effective hydraulic conductivity (mm day^{-1}), SW_1 (mm) the water content in the first soil layer, $SW_{1,sat}$ (mm) the saturated water content of the first soil layer and λ is a calibration parameter (-). (Bouwer, 1969) suggested an approximation of $K_{\text{eff}} \approx 0.5K_{\text{sat}}$.

Infiltration excess surface runoff occurs when the precipitation intensity exceeds the infiltration rate f (Beven, 2012). We assume that highest precipitation intensity is recorded in the first hour of the rain storm and decreases linearly until the end of the storm. Furthermore, we assume a triangular-shaped precipitation intensity $p(t)$ (mm hr^{-1}) according to:

$$p(t) = \frac{1}{2}\alpha^2 Pt + \alpha P$$

Equation 44

where α is the fraction of daily rainfall that occurs in the hour with the highest intensity (-), P is the daily rainfall (mm), and t is an hourly time step (hr). Daily infiltration excess surface runoff Q_{surf} is determined as follows:

$$Q_{\text{surf}} = \begin{cases} \dfrac{(\alpha P - f)^2}{\alpha^2 P} & \text{if } \alpha P > f \\ 0 & \text{if } \alpha P \leq f \end{cases}$$

Equation 45

When the hourly precipitation intensity αP is higher than the infiltration rate f, surface runoff equals the triangular shaped area of the precipitation above the infiltration rate. The amount of precipitation below the infiltration rate will infiltrate into the rootzone.

Saturation excess surface runoff occurs when the first soil layer gets saturated and is calculated as:

$$RO = \begin{Bmatrix} SW_1 - SW_{1,sat} & if & SW_1 > SW_{1,sat} \\ 0 & if & SW_1 \leq SW_{1,sat} \end{Bmatrix}$$

Equation 46

with RO (mm) surface runoff, SW_1 (mm) the water content in the first soil layer, and $SW_{1,sat}$ (mm) the saturated water content of the first soil layer.

2.7.5 Lateral flow

Lateral flow is substantial in catchments with steep gradients and soils with high hydraulic conductivities (Beven, 1981; Beven and Germann, 1982; Sloan and Moore, 1984). In SPHY, it is assumed that only the amount of water exceeding field capacity can be used for lateral flow. Therefore, the drainable volume of water (excess water) needs to be calculated first:

$$W_{l,exc} = \begin{Bmatrix} SW_l - SW_{l,fc} & if & SW_l > SW_{l,fc} \\ 0 & if & SW_l \leq SW_{l,fc} \end{Bmatrix}$$

Equation 47

with $W_{l,exc}$ (mm) the drainable volume of water from soil layer l, SW_l (mm) the water content in soil layer l, and $SW_{l,fc}$ (mm) the field capacity of soil layer l. According to Sloan and Moore (1984), the lateral flow at the hillslope outlet can be calculated as:

$$LF_l^* = W_{l,excfrac} \cdot v_{lat,l}$$

Equation 48

with LF_l^* (mm) lateral flow from soil layer l, $W_{l,excfrac}$ (–) the drainable volume of water as a fraction of the saturated volume, and $v_{lat,l}$ $(mm \cdot d^{-1})$ the flow velocity at the outlet. In SPHY, the drainable volume as a fraction of the saturated volume is calculated as:

$$W_{l,excfrac} = \frac{W_{l,exc}}{SW_{l,sat} - SW_{l,fc}}$$

Equation 49

The velocity of flow at the outlet, $v_{lat,l}$ $(mm \cdot d^{-1})$, depends on both the saturated hydraulic conductivity $K_{sat,l}$ $(mm \cdot d^{-1})$ and the slope of the hill slp (–), and is defined as:

$$v_{lat,l} = K_{sat,l} \cdot slp$$

Equation 50

The slope (slp) in SPHY is calculated for each grid cell as the increase in elevation per unit distance.

According to (Neitsch et al., 2009), only a fraction of lateral flow will reach the main channel on the day it is generated if the catchment of interest has a time of concentration greater than 1 day. This concept is also implemented in the SPHY model, and uses a lateral flow travel time $TT_{lag,l}$ (d) to lag a portion of lateral flow release to the channel:

$$LF_l = \left(LF_l^* + LF_{l,t-1}^*\right) \cdot \left(1 - exp\left[\frac{-1}{TT_{lag,l}}\right]\right)$$

Equation 51

with LF_l (mm) the amount of lateral flow entering the channel on a given day, LF_l^* (mm) the lateral flow (Equation 48) generated within the cell on a given day, and $LF_{l,t-1}^*$(mm) the lateral flow lagged from the previous day. SPHY assumes the lateral flow travel time to be dependent on the field capacity $SW_{l,fc}$ (mm), saturated content $SW_{l,sat}$ (mm), and the saturated conductivity $K_{sat,l}$ $(mm \cdot d^{-1})$, according to:

$$TT_{lag,l} = \frac{SW_{l,sat} - SW_{l,fc}}{K_{sat,l}}$$

Equation 52

A longer lateral flow travel time will result in a smoother streamflow hydrograph.

2.7.6 Percolation

If the groundwater module is used, then water can percolate from the first to the second soil layer, and from the second to the third soil layer. If the user decides to run SPHY without the groundwater module, percolation only occurs from the first to the second soil layer. In SPHY, water can only percolate if the water content exceeds the field capacity of that layer, and the water content of the underlying layer is not saturated. A similar approach has been used in the SWAT model (Neitsch et al., 2009). The water volume available for percolation to the underlying layer is calculated as:

$$W_{l,exc} = \begin{cases} 0, & if\ SW_l \leq SW_{l,fc}\ or\ SW_{l+1} \geq SW_{l+1,sat} \\ SW_{l+1,sat} - SW_{l+1}, & if\ SW_l - SW_{l,fc} > SW_{l+1,sat} - SW_{l+1} \\ SW_l - SW_{l,fc}, & else \end{cases}$$

Equation 53

with $W_{l,exc}$ (mm) the drainable volume of water from layer l, SW_l (mm) the water content in layer l, $SW_{l,fc}$ (mm) the field capacity of layer l, SW_{l+1} (mm) the water content in layer $l+1$, and $SW_{l+1,sat}$ (mm) the

saturated water content of layer $l+1$. Only a certain amount of $W_{l,exc}$ will percolate to the underlying soil layer, depending on the percolation travel time $TT_{perc,l}$ (d). This approach follows the storage routing methodology, which is also implemented in the SWAT model (Neitsch et al., 2009):

$$w_{l,perc} = W_{l,exc} \cdot \left(1 - exp\left[\frac{-1}{TT_{perc,l}}\right]\right)$$

Equation 54

with $w_{l,perc}$ (mm) the amount of water percolating to the underlying soil layer. Since the speed at which water can move through the soil is mainly dependent on the saturated hydraulic conductivity (K_{sat}), the travel time for percolation is calculated the same way as the travel time for lateral flow (Equation 52).

2.7.7 Groundwater recharge

Water that percolates from the second to the third soil layer will eventually reach the shallow aquifer. This process is referred to as groundwater recharge hereafter. If the glacier module is used as well, then glacier melt that percolates also contributes to the groundwater recharge. Groundwater recharge often does not occur instantaneously, but with a time lag that depends on the depth of the groundwater table and soil characteristics. SPHY uses the same exponential decay weighting function as proposed by Venetis(1969) and used by Sangrey et al. (1984) in a precipitation groundwater response model. This approach has also been adopted in the SWAT model (Neitsch et al., 2009), using:

$$Gchrg_t = \left(1 - exp^{\frac{-1}{\delta_{gw}}}\right) \cdot w_{2,perc} + exp^{\frac{-1}{\delta_{gw}}} \cdot \ Gchrg_{t-1}$$

Equation 55

with $Gchrg_t$ (mm) and $Gchrg_{t-1}$ (mm) the groundwater recharge on days t and $t-1$, respectively. δ_{gw} (d) is the delay time and $w_{2,perc}$ (mm) is the amount of water that percolates from the second to the third layer on day t.

2.7.8 Baseflow

After groundwater recharge has been calculated, SPHY calculates baseflow, which is defined as the flow going from the shallow aquifer to the main channel. Baseflow only occurs when the amount of water stored in the third soil layer exceeds a certain threshold (BF_{thresh}) that can be specified by the user. Baseflow calculation in SPHY is based on the steady-state response of groundwater flow to recharge (Hooghoudt, 1940) and the water table fluctuations that are a result of the non-steady response of groundwater flow to periodic groundwater recharge (Smedema and Rycroft, 1983). The SWAT model (Neitsch et al., 2009) assumes a linear relation between the variation in groundwater flow (baseflow) and the rate of change in water table height, according to:

$$\frac{dBF}{dt} = 10 \cdot \frac{K_{sat}}{\mu L_{gw}^2} \cdot (Gchrg - BF) = \alpha_{gw} \cdot (Gchrg - BF)$$

Equation 56

with BF (mm) the groundwater flow (baseflow) into the main channel on day t, K_{sat} ($mm\ d^{-1}$) the hydraulic conductivity of the shallow aquifer, μ (–) the specific yield of the shallow aquifer, L_{gw} (m) the distance from the subbasin divide for the groundwater system to the main channel, $Gchrg$ (mm) the amount of groundwater (Equation 55) recharge entering the shallow aquifer on day t, and α_{gw} (–) the

baseflow recession coefficient. Equation 56 can be integrated and rearranged to calculate baseflow, according to:

$$BF_t = \begin{cases} 0, & if\ SW_3 \leq BF_{thresh} \\ BF_{t-1} \cdot exp^{-\alpha_{gw}} + Gchrg_t \cdot (1 - exp^{-\alpha_{gw}}), & if\ SW_3 > BF_{thresh} \end{cases}$$

Equation 57

with BF_t (mm) the baseflow into the channel on day t, and BF_{t-1} (mm) the baseflow into the channel on day $t-1$. Since this equation has proven its success in the SWAT model (Neitsch et al., 2009) throughout many applications worldwide, this equation has been adopted in the SPHY model as well.

The baseflow recession coefficient (α_{gw}) is an index that relates the baseflow response to changes in groundwater recharge. Lower values for α_{gw} therefore correspond to areas that respond slowly to groundwater recharge, whereas higher values indicate areas that have a rapid response to groundwater recharge. The baseflow recession coefficient is generally used as a calibration parameter in the SPHY model, but a good first approximation of this coefficient can be calculated using the number of baseflow days (Neitsch et al., 2009):

$$\alpha_{gw} = \frac{2.3}{BFD}$$

Equation 58

with BFD (d) the number of baseflow days, which is defined as the number of days required for baseflow recession to decline.

2.8 Soil erosion processes

The SPHY model allows modeling soil erosion with 6 different soil erosion models, i.e. MUSLE (1), MMF (2), INCA (3), SHETRAN (4), DHSVM (5) and HSPF (6). The MUSLE model is an empirical model, which is forced by accumulated runoff, as generated by the hydrological part of the SPHY model. The implementation of MUSLE in SPHY was part of a study in which three different soil erosion model concepts were compared (Eekhout and De Vente, 2020). All other models are process-based models that determine the detachment of soil particles separately for raindrop impact and accumulated runoff. Subsequently, these two different detachment processes are summed and sediment taken into transport is determined accounting for immediate deposition. The first of these 5 process-based models that was implemented was the MMF model (Eekhout et al., 2018). The other 4 process-based soil erosion models were part of the soil erosion model ensemble, with the aim to assess the uncertainty of process-based soil erosion models in climate change impact studies (Eekhout et al., 2021).

All soil erosion models make use of model parameters related to the infiltration excess surface runoff equation. It is therefore advisable to use this equation, i.e. Infil_excess = 1. Furthermore, most of the process-based soil erosion models use the LAI (leaf area index) from the vegetation module to determine the canopy cover, hence, it is also advisable to use the vegetation module when applying one of the process-based soil erosion models.

2.8.1 MUSLE

The Modified Universal Soil Loss Equation (MUSLE) is a modification of the USLE, where the rainfall erosivity factor is replaced by a runoff factor, and applied at a daily time step. MUSLE is incorporated in various widely used hydrological models, such as SWAT, in which a separate hydrological module is used to calculate runoff. MUSLE is determined as follows (Williams, 1995):

$$sed = 11.8 \left(Q_{surf}\ q_{peak}\ A\right)^{0.56} K\ LS\ C\ P\ CFRG$$

Equation 59

Where sed is the sediment yield (kg m^{-2} day^{-1}), Q_{surf} is the surface runoff depth (mm), q_{peak} is the peak runoff rate (m^3 s^{-1}), A is the cell area (m^2), K is the soil erodibility factor (kg h MJ^{-1} mm^{-1}), LS is the topographic factor (-), C is the crop and management factor (-), P is the erosion control practice factor (-) and $CFRG$ is the coarse fragment factor (-).

The surface runoff Q_{surf} is determined within SPHY as described in other parts of the manual. The peak runoff rate is determined as follows:

$$q_{peak} = \frac{\alpha_{tc}\ Q_{surf}\ A}{3.6\ t_{conc}}$$

Equation 60

Where α_{tc} is the fraction of daily rainfall that occurs during the time of concentration (-) and t_{conc} is the time of concentration (hr). The time of concentration is the amount of time from the beginning of a rainfall event until the entire cell area contributes to flow at the cell outlet.

The fraction of daily rainfall that occurs during the time of concentration is determined as follows:

$$\alpha_{tc} = 1 - e^{2\ t_{conc} \ln(1-\alpha_{0.5})}$$

Equation 61

Where $\alpha_{0.5}$ is the fraction of the daily rain falling in the half-hour highest intensity (-), which is obtained from a model parameter of the infiltration excess surface runoff equation and can be determined within the calibration of the hydrological model.

The time of concentration is determined accounting for both channel flow and overland flow:

$$t_{conc} = \frac{t_{conc,ch} + t_{conc,ov}}{60}$$

Equation 62

Where $t_{conc,ch}$ is the channel flow time of concentration (minutes) and $t_{conc,ov}$ the overland flow time of concentration (minutes). The channel flow time of concentration ($t_{conc,ch}$) is determined using the Kirpich (1940) method:

$$t_{conc,ch} = 0.0195\ L^{0.77}\ S^{-0.385}$$

Equation 63

Where L is the slope length (m) and S the slope (m m^{-1}).

The overland flow time of concentration $t_{conc,ov}$ is determined using the Kerby (1959) method:

$$t_{conc,ov} = 1.44(L\ N)^{0.467} S^{-0.235}$$

Equation 64

Where N is the retardance coefficient (-).

The soil erodibility factor was determined using the equation developed by Wischmeier et al. (1971):

$$K = \frac{0.00021M^{1.14}(12 - OM) + 3.25(c_{soilstr} - 2) + 2.5(c_{perm} - 3)}{100}$$

Equation 65

Where K is the particle-size parameter (-), OM is the organic matter content (%), $c_{soilstr}$ is the soil structure class (-) and c_{perm} is the profile permeability class (-).

The particle-size parameter is calculated as follows:

$$M = (m_{silt} + m_{vfs})(100 - m_c)$$

Equation 66

Where m_{silt} is the silt content (%), m_{vfs} is the very fine sand content (%) and m_c is the clay content (%). The profile permeability classes are defined according to the saturated hydraulic conductivity.

The coarse fragment factor is determined as follows:

$$CFRG = e^{-0.053\, p_{rock}}$$

Equation 67

Where p_{rock} is the rock content in the root zone layer (%).

The topographic factor LS is the expected ratio of soil loss per unit area from a field slope of 22.1 m length with uniform slope of 9%. We applied the following equation (Wischmeier et al., 1971):

$$LS = \left(\frac{L}{22.1}\right)^m (65.41\ sin^2(\alpha_{hill}) + 4.56\ sin(\alpha_{hill}) + 0.065)$$

Equation 68

Where m is an exponential term (-) and α_{hill} is the slope angle (°). The exponential term m is calculated as follows:

$$m = 0.6(1 - e^{-35.835S})$$

Equation 69

2.8.2 MMF

The Morgan-Morgan-Finney model (Morgan and Duzant, 2008) was originally implemented as an annual model, however, Eekhout et al. (2018) included MMF as a daily model in SPHY. In MMF, the detachment by raindrop impact is a function of the highest daily precipitation intensity and the canopy cover, which are obtained from the infiltration excess surface runoff equation and the vegetation module, respectively. Detachment by runoff is a function of the accumulated runoff. Both detachment by raindrop impact and runoff are determined for each of the three textural classes (sand, silt and clay) separately and later aggregated to determine the total detachment. Immediate deposition is a function of the particle fall number, in which the flow velocity is determined with the Manning equation. A detailed explanation is given below.

2.8.2.1 Detachment by raindrop impact

Detachment by raindrop impact (F, kg m^{-2}) is determined for each of the soil texture classes separately and subsequently summed and is calculated as follows:

$$F_i = K_i \frac{\%i}{100}(1 - \mathrm{GC})\mathrm{KE}\cdot 10^{-3}$$

Equation 70

Where F is the detachment by raindrop impact for textural class i (kg m^{-2}), i the textural class, K the detachability of the soil by raindrop impact (g J^{-1}), GC the ground cover (-) and KE the kinetic energy of the effective precipitation (J m^{-2}). The ground cover (GC), expressed as a proportion between zero and unity, protects the soil from detachment and is determined by the proportion of vegetation and rocks covering the surface. The ground cover is set to 1 in case the surface is covered with snow, which is determined by the snow module.

The total kinetic energy of the effective precipitation (KE) is calculated as follows:

$$KE = KE_{\mathrm{LD}} + KE_{\mathrm{DT}}$$

Equation 71

Where KE_{LD} is the kinetic energy of the leaf drainage (J m^{-2}) and KE_{DT} is the kinetic energy of the direct throughfall (J m^{-2}).

The kinetic energy of the leaf drainage KE_{LD} is based on (Brandt, 1990):

$$\mathrm{KE}_{\mathrm{LD}} = \begin{cases} 0 & \text{for } PH < 0.15 \\ \mathrm{LD}\left(15.8\sqrt{PH} - 5.87\right) & \text{for } PH \geq 0.15 \end{cases}$$

Equation 72

Where LD is the leaf drainage (mm) and PH is the plant height (m), specified for each landuse class.

Leaf drainage is determined as:

$$LD = P_{eff}\mathrm{CC}$$

Equation 73

Where P_{eff} is the precipitation throughfall (mm) and CC is the canopy cover (fraction, -). The canopy cover is either introduced by a landuse-class specific tabular value or determined by the vegetation module. When the vegetation module is used, the canopy cover is obtained from the LAI (Equation 6), maximized by 1. The effective precipitation from the hydrological model is first corrected for the slope angle, following (Choi et al., 2017):

$$P_{eff} = P_{eff}\cos S$$

Equation 74

Where P_{eff} is the effective precipitation (mm) and S is the slope (°).

The kinetic energy of the direct throughfall is based on a relationship described by Brown and Foster, 1987):

$$\mathrm{KE}_{\mathrm{DT}} = DT\left(0.29\left(1 - 0.72\, e^{-0.05\, I}\right)\right)\cdot 100$$

Equation 75

Where DT is the direct throughfall (mm) and I is the intensity of the erosive precipitation (mm h^{-1}). The intensity of the erosive precipitation is a model parameter and varies according to geographical location.

Direct throughfall (DT) is calculated as follows:

$$DT = P_{eff} - \mathrm{LD}$$

Equation 76

2.8.2.2 Detachment by runoff

Detachment by runoff (H) is calculated as follows:

$$H_i = DR_i \frac{\%i}{100} Q^{1.5}(1 - \mathrm{GC})\, sin^{0.3}\, S \cdot 10^{-3}$$

Equation 77

Where H is the detachment by runoff (kg m^{-2}), DR the detachability of the soil by runoff (g mm^{-1}), Q is the volume of accumulated runoff (mm) and S is the slope (m m^{-1}).

2.8.2.3 Sediment transported

A proportion of the detached soil is deposited in the cell of its origin as a function of the abundance of vegetation and the surface roughness. The percentage of the detached sediment that is deposited (DEP) is estimated from the relationship obtained by (Tollner et al., 1976) and calculated separately for each texture class:

$$DEP = 44.1 N_{f_i}^{0.29}$$

Equation 78

Where N_f is the particle fall number (-), defined as:

$$N_{f_i} = \frac{l v_{s_i}}{v d}$$

Equation 79

Where l is the length of a grid cell (m), v_s the particle fall velocity (m s^{-1}), v the flow velocity (m s^{-1}) and d the depth of flow (m).

The particle fall velocities v_s are estimated from:

$$v_s = \frac{\frac{1}{18}\delta^2(\rho_s + \rho)g}{\eta}$$

Equation 80

Where δ is the diameter of the particle (m), ρ_s the sediment density (kg m^{-3}), ρ the flow density (kg m^{-3}) (Abrahams et al., 2001) g gravitational acceleration (m s^{-2}) and η the fluid viscosity (kg m^{-1} s^{-1}).

The flow velocity v from Equation 79 is obtained by the Manning formula:

$$v = \frac{1}{n} d^{\frac{2}{3}} S^{\frac{1}{2}}$$

equation 81

Where n' is the modified Manning's roughness coefficient (s $m^{-1/3}$), which is a combination of the Manning's roughness coefficient for the soil surface and vegetation, defined as (Petryk and Bosmajian, 1975):

$$n' = \sqrt{n_{\text{soil}}^2 + n_{\text{vegetation}}^2}$$

Equation 82

Where n_{soil} is the Manning's roughness coefficient for soil (s $m^{-1/3}$) and $n_{vegetation}$ the Manning's roughness coefficient for vegetation (s $m^{-1/3}$). The Manning's roughness coefficient for soil can either be defined by bare soil (Figure 4a) or tilled soil (Figure 4b). The Manning's roughness coefficient for vegetation can either be obtained for regular spaced vegetation (Figure 4c) or irregular spaced vegetation (Figure 4d).

For tilled conditions (Figure 4b) the following equation is applied to obtain the Manning's roughness coefficient for the soil:

$$n_{\text{soil}} = exp(-2.1132 + 0.0349\ \text{RFR})$$

Equation 83

Where RFR is the surface roughness parameter (cm m^{-1}).

The Manning's roughness coefficient for regular spaced vegetation (Figure 4c) is obtained from the following equation (Jin et al., 2000):

$$n_{\text{vegetation}} = \frac{d^{\frac{2}{3}}}{\sqrt{\frac{2g}{D\ NV}}}$$

Equation 84

Where D is the stem diameter (m) and NV the stem density (stems m^{-2}).

Equation 79, equation 81 and Equation 84 require a flow depth d, a model parameter that can be used in the model calibration. The value for d should be taken such that it corresponds to a water depth from runoff generated within the cell margins, i.e. without accumulation of flow from upstream located cells.

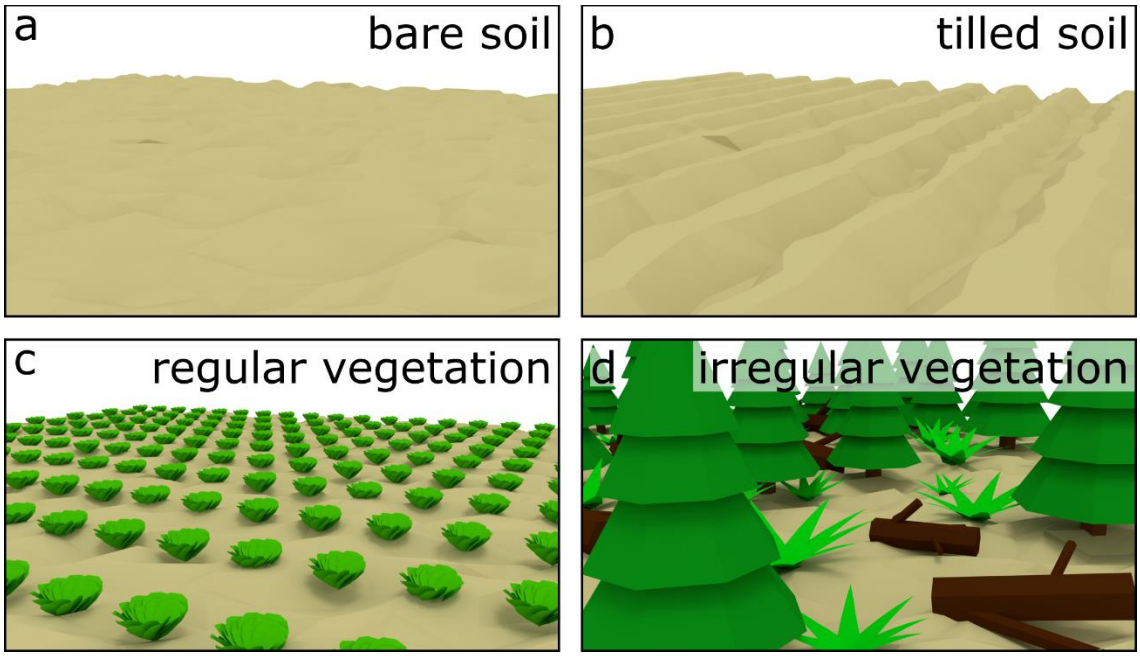

Figure 4. Surface and vegetation roughness options: (a) bare soil, (b) tilled soil (Equation 83), (c) regular vegetation (Equation 84), and (d) irregular vegetation.

The amount of sediment that is taken into transport is determined from the sum of the detached sediment from raindrop impact (F_i; Equation 70) and runoff (H_i; Equation 77), subtracting the proportion of the sediment that is deposited within the cell of its origin (DEP_i; Equation 78):

$$G_i = (F_i + H_i)\left(1 - \frac{DEP_i}{100}\right)$$

Equation 85

Where G is the amount of sediment taken into transport for textural class i (kg m^{-2}). The amount of sediment that is routed to downstream cells is the summation of the individual amounts for clay, silt and sand.

2.8.3 INCA

The Integrated Catchments model for Sediments (Lazar et al., 2010) is originally applied in a semi-distributed manner, however, here the model is implemented in a spatially distributed manner. Detachment by raindrop impact is a function of the daily precipitation intensity and the canopy cover, for which the latter is obtained from the vegetation module. For model calibration purposes, we included the ground cover as a model parameter in the detachment by raindrop impact formulation. Detachment by runoff is a function of the sediment transport, the surface runoff and the detachment by raindrop impact. Sediment that is taken into transport is determined from the before mentioned formulations, accounting for sediment storage.

2.8.3.1 Detachment by raindrop impact

Detachment by raindrop impact (S_{SP}) is calculated as follows:

$$\boldsymbol{S_{SP} = \left(1 - C_g\right) C_{X1}\, p_{Sed}\, E_{sp}^{\left(\frac{10}{10-V}\right)} 8.64 \cdot 10^{10}}$$

Equation 86

Where S_{SP} the detachment by raindrop impac (kg km^{-2}), C_g is the ground cover (-), C_{X1} a scaling parameter (s m^{-1}), p_{Sed} the precipitation throughfall (mm), E_{sp} a soil specific erosion potential parameter (kg m^{-2} s^{-1}) and V the vegetation cover (-), here estimated with the canopy cover from the vegetation module, multiplied by 10.

2.8.3.2 Detachment by runoff

Detachment by runoff (S_{FL}) is calculated as follows:

$$S_{FL} = \frac{K(S_{TC} - S_{SP})}{S_{TC} + K}$$

Equation 87

Where S_{FL} is the detachment by runoff (kg km^{-2}), K a function of runoff (kg km^{-2}) and S_{TC} the transport capacity (kg km^{-2}).

The function K is calculated as follows:

$$K = a_1 E_{FL} \left(\frac{A\, q_{DR}}{L} - a_2 \right)^{a_3} \cdot 86400$$

Equation 88

Where E_{FL} is the soil erosion potential (kg km^{-2} s^{-1}), A the grid cell area (km^2), q_{DR} the routed runoff (m^3 s^{-1} km^{-2}), L the slope length (km), a_1 is the flow erosion scaling factor (s m^{-2}), a_2 the flow erosion direct runoff threshold (m^2 s^{-1}) and a_3 the flow erosion non-linear coefficient (-).

Sediment transport capacity (S_{TC}) is calculated as follows:

$$S_{TC} = a_4 \left(\frac{A\, q_{DR}}{L} - a_5 \right)^{a_6} \cdot 86400$$

Equation 89

Where a_4 is the transport capacity scaling factor (kg m^{-2} km^{-2}), a_5 the transport capacity direct runoff threshold (m^2 s^{-1}) and a_6 the transport capacity non-linear coefficient (-).

2.8.3.3 Sediment transported

The amount of sediment that is taken into transport depends on the amount of sediment in the sediment storage. The daily change in sediment storage is calculated as follows:

$$\frac{dS_{store}}{dt} = \begin{cases} S_{SP} - S_{TC} & \text{for } S_{store} + S_{SP} > S_{TC} \\ \dfrac{-K(S_{SP} - S_{TC})}{S_{TC} + K} & \text{for } S_{store} + S_{SP} < S_{TC} \end{cases}$$

Equation 90

Where S_{store} is the sediment storage (kg km^{-2}), which is subsequently updated following:

$$S_{store} = S_{store} + \frac{dS_{store}}{dt}$$

equation 91

The amount of sediment taken into transport is calculated as follows:

$$M_{out} = \begin{cases} S_{TC} & \text{for } S_{store} + S_{SP} > S_{TC} \\ S_{SP} + S_{FL} & \text{for } S_{store} + S_{SP} < S_{TC} \end{cases}$$

Equation 92

Where M_{out} is the mass of sediment taken into transport (kg km^{-2}).

2.8.4 SHETRAN

The SHETRAN model (Lukey et al., 1995) is a sediment transport model implemented in the Système Hydrologique Européen (SHE) hydrological model. The detachment by raindrop impact formulations are similar to the ones used in DHSVM, with some small differences in the leaf drip formulations. The canopy cover is obtained from the vegetation module. Detachment by runoff is a function of the shear stress and critical shear stress, which are both a function of the water depth. We obtained the water depth using the Manning equation, assuming a triangular-shaped flow profile, with the width-depth ratio as the model parameter. For model calibration purposes, we included the ground cover as a model parameter in the detachment by runoff formulation. Immediate deposition of sediment is determined with a sediment transport equation.

2.8.4.1 Detachment by raindrop impact

Detachment by raindrop impact is determined with the following empirical equation, which is derived from Wicks (1988):

$$D_r = k_r F_w (1 - C_g - C_r)(M_r + M_d)$$

Equation 93

where D_r is the rate of detachment of soil (kg m^{-2} s^{-1}), k_r the raindrop impact soil erodibility coefficient (J^{-1}), F_w the protective effect of ponding (-), C_g the proportion of ground shielded by near ground cover (fraction, -), C_r the proportion of ground shielded by ground level (rock) cover (fraction, -), M_r the momentum squared of raindrops reaching the ground (kg^2 s^{-3}) and M_d the momentum squared of leaf drip reaching the ground (kg^2 s^{-3}).

The original SHETRAN model accounts for the protective effect of ponding on detachment by raindrop impact by model parameter F_w (Park et al., 1982). The hydrological model SPHY does not account for ponding, hence, we assume $F_w = 1$.

The momentum squared of raindrops reaching the ground (M_r) is based on the formulations by Marshall and Palmer (1948):

$$M_r = (1 - C_c) a_1 I^{b_1}$$

Equation 94

Where I is the rainfall intensity (mm h^{-1}) and a_1 and b_1 are coefficients dependent on I and are given in Table 2. The rainfall intensity is obtained from the infiltration excess surface runoff equation and a_1 and b_1 are determined inside the model code.

Table 2: Values for the empirical coefficients a_1 and b_1 used to determine the momentum squared of raindrops.

Range for I (mm h^{-1})	a_1	b_1
0 - 10	2.6893 · 10^{-8}	1.6896
10 - 50	3.7514 · 10^{-8}	1.5545
50 - 100	6.1192 · 10^{-8}	1.4242
≥ 100	11.737 · 10^{-8}	1.2821

The momentum squared of leaf drip reaching the ground (M_d) is calculated as follows:

$$M_d = \frac{\pi}{6} V_d^2 \rho^2 d_l^3 L_d DRAINA$$

Equation 95

Where V_d is the leaf drip fall speed (m s^{-1}), ρ the density of water (kg m^{-3}), d_l the leaf drip diameter (m), L_d the proportion of drainage that falls as leaf drip (fraction, -) and $DRAINA$ the water drainage rate from canopy (m s^{-1}). The proportion of drainage that falls as leaf drip (L_d) is assumed to be equal to the canopy cover (C_c). The water drainage rate from canopy ($DRAINA$) is assumed to be equal to the daily precipitation intensity in m s^{-1}.

The leaf drip fall speed (V_d) is calculated as follows:

$$V_d = \sqrt{\frac{M}{\beta} g \left(1 - e^{-\frac{2X\beta}{M}}\right)}$$

Equation 96

Where M the average mass of leaf drips (kg), β the friction constant (kg m^{-1}), g the acceleration due to gravity (m s^{-2}) and X is the average leaf drip fall distance (m).

The fraction $\frac{M}{\beta}$ is a function of the leaf drip diameter d_l and two coefficients, a_2 and b_2.

$$\frac{M}{\beta} = a_2 + b_2 d_l$$

Equation 97

where a_2 and b_2 are given in Table 3 and are determined inside the model code.

Table 3: Values for the empirical coefficients a_2 and b_2 used to determine the fraction $\frac{M}{\beta}$.

Range for d_l (m)	Range for X (m)	a_2	b_2
< 0.0033	all X	0	2200
≥ 0.0033	< 7.5	1.93	1640
≥ 0.0033	≥ 7.5	5.14	6600

2.8.4.2 Detachment by runoff

Detachment by runoff is determined using the approach of Ariathurai and Arulanandan (1978):

$$D_q = \begin{cases} k_f (1 - C_g - C_r)\left[\frac{\tau}{\tau_{cr}} - 1\right] & \text{for } \tau > \tau_{cr} \\ 0 & \text{for } \tau < \tau_{cr} \end{cases}$$

Equation 98

Where D_q is the rate of detachment of soil per unit area (kg m^{-2} s^{-1}), k_f the overland flow soil erodibility coefficient (kg m^{-2} s^{-1}), τ the shear stress due to overland flow (N m^{-2}), τ_{cr} the critical shear stress for initiation of sediment motion (N m^{-2}).

The shear stress due to overland flow (τ) is given by:

$$\tau = \rho g h S$$

Equation 99

with ρ the water density (kg m^{-3}), g the acceleration due to gravity (m s^{-2}), h the water depth (m) and S the water surface slope in the direction of the flow (m m^{-1}).

The water depth (h) is determined with the Manning equation. We assumed a triangular shaped profile on which the Manning equation is applied, where the width-to-depth ratio is a model parameter. First the flow area is determined with an algebraic re-arrangement of the Manning equation:

$$A = \left[\frac{Q\, n \left(2\sqrt{\frac{WD^2 + 1}{WD}} \right)^{2/3}}{\sqrt{S}} \right]^{3/4}$$

Equation 100

where Q is the discharge (m^3 s^{-1}), n the Manning's coefficient (s m$^{-1/3}$) and WD the width-to-depth ratio (-). The discharge (Q) is obtained from the hydrological model and the Manning's coefficient (n) is defined per land use class.

The water depth (h) is calculated as follows:

$$h = \sqrt{\frac{A}{WD}}$$

Equation 101

The critical shear stress τ_{cr} is calculated as follows:

$$\tau_{cr} = (\rho_s - \rho)\, g\, D_{50}\, a_3\, R_*^{b_3}$$

Equation 102

Where ρ_s is the density of sediment particles (kg m^{-3}), D_{50} the median sediment particle diameter (m), R_* the particle Reynolds number (-), and a_3 and b_3 are given in Table 4 and are determined inside the model code.

Table 4. Values for the empirical coefficients a_3 and b_3 used to determine the particle Reynolds number (R_*).

Range for R_*	a_3	b_3
0.03 - 1	0.1	-0.3
1 – 6	0.1	-0.62
6 – 30	0.033	0
30 – 135	0.013	0.28
135 – 400	0.03	0.1
> 400	0.056	0

The particle Reynolds number R_* is calculated as follows:

$$R_* = \max\left[0.03, \frac{D_{50}\sqrt{\tau/\rho}}{\nu}\right]$$

Equation 103

where ν is the water viscosity (m^2 s^{-1}).

2.8.4.3 Sediment transported

The total sediment taken into transport (G) is calculated as follows:

$$G = \begin{cases} D_r + D_q & \text{for } D_r + D_q < TC \\ TC & \text{for } D_r + D_q > TC \end{cases}$$

Equation 104

Where TC the transport capacity (kg m^{-2} s^{-1}), which is calculated as follows:

$$TC = G_{tot} \frac{\rho_s}{A_{cell}}$$

Equation 105

Where G_{tot} is the capacity particulate transport rate for overland flow (m^3 s^{-1}) and A_{cell} the cells area (m^2).

The capacity particulate transport rate for overland flow (G_{tot}) is determined with the formulations from Hansen and Engelund (1967):

$$G_{tot} = \begin{cases} \dfrac{0.05\, Q^2\, S^{3/2}}{\sqrt{g\, h}\left(\frac{\rho_s}{\rho} - 1\right)^2 D_{50}\, l} & \text{for } h > 0 \\ 0 & \text{for } h < 0 \end{cases}$$

Equation 106

Where l is the width of the flow (m), Q the water flow rate (m^3 s^{-1}). The width of the flow l is determined as:

$$l = WD \cdot h$$

Equation 107

2.8.5 DHSVM

The distributed hydrology-soil-vegetation model (DHSVM; (Doten et al., 2006) simulates hillslope erosion based on detachment energy of raindrops, leaf drip and surface runoff. The detachment by raindrop impact formulations originate from the SHESED model Wicks and Bathurst (1996). These formulations require hourly precipitation intensity as input. While the SPHY hydrological model runs at a daily time step, the model includes a sub-daily infiltration formulation. This formulation determines hourly precipitation intensity, which was subsequently used as input for the DHSVM model. Furthermore, the detachment by raindrop impact formulations require the canopy cover as input, which was obtained from the vegetation module.

Detachment by runoff is determined from a detachment coefficient, the settling velocity, and the transport capacity. The detachment coefficient is a function of the soil cohesion, which is determined from the sum of the soil cohesion and root cohesion. The transport capacity is based on the unit stream power approach from the KINEROS model (Woolhiser et al., 1990), which requires the water depth of the flow as input. We obtained the water depth by applying the Manning equation, assuming a triangular-shaped flow profile, with the width-depth ratio as model parameter.

2.8.5.1 Detachment by raindrop impact

Detachment by raindrop impact is based on the sum of the momentum squared for rain (M_R) and the momentum squared for leaf drip (M_D) (Wicks and Bathurst, 1996):

$$D_R = k_r\, F_w (1 - C_G)[(1 - C_C)\, M_R + M_D]$$

Equation 108

where D_R is the soil detached by raindrop impact (kg m^{-2} s^{-1}), k_r the raindrop soil erodibility coefficient (J^{-1}), F_w the protective effect of ponding (-), C_G the ground cover (fraction, -), C_C the canopy cover (fraction, -), M_R the momentum squared for rain (kg^2 s^{-3}) and M_D the momentum squared for leaf drip (kg^2 s^{-3}).

The original DHSVM model accounts for the protective effect of ponding on detachment by raindrop impact by model parameter F_w (Park et al., 1982). The hydrological model SPHY does not account for ponding, hence, we assume $F_w = 1$.

The momentum squared for the rain (M_R) is determined as follows:

$$M_R = \alpha\, I^{\beta}$$

Equation 109

Where I is the rainfall intensity (mm h^{-1}) and α and β are empirical coefficients (Wicks, 1988). The rainfall intensity I is determined from the infiltration excess surface runoff formulations of the hydrological model. In these formulations, the hourly rainfall is assumed to decrease linearly over time, where the fraction of the daily rainfall that falls in the first hour is a model parameter. Hence, from these assumptions the hourly rainfall intensity was determined as input for the DHSVM model. Values for α and β for each rainfall intensity interval are given in Table 5 and are determined inside the model code.

Table 5. Values for the empirical coefficients α and β used to determine the momentum squared for the rain.

Range for I (mm h^{-1})	α	β
0 – 10	$2.69 \cdot 10^{-8}$	1.6896
10 - 50	$3.75 \cdot 10^{-8}$	1.5545
50 - 100	$6.12 \cdot 10^{-8}$	1.4242
≥ 100	$11.75 \cdot 10^{-8}$	1.2821

Momentum squared for leaf drip (M_D) is calculated as follows:

$$M_D = \frac{\left(\frac{V\, \rho\, \pi\, D^3}{6}\right) DRIP\%\; DRAIN}{\left(\frac{\pi\, D^3}{6}\right)}$$

Equation 110

where V is the leaf drip fall velocity (m s^{-1}), ρ the density of water (kg m^{-3}), D the leaf drip diameter (m), $DRIP\%$ the proportion of drainage that falls as leaf drip and $DRAIN$ the canopy drainage rate (m s^{-1}). The proportion of the drainage that falls as leaf drip ($DRIP\%$) is assumed to be equal to the canopy cover (C_C). The canopy drainage rate ($DRAIN$) is assumed to be equal to the daily precipitation intensity in m s^{-1}.

The leaf drip fall speed V is calculated as follows (Epema and Riezebos, 1983):

$$V = \sqrt{\frac{M}{\beta_V}\, g\, \left(1 - e^{-\frac{2X\,\beta}{M}}\right)}$$

Equation 111

where X is the average leaf drip fall distance (m), M the average mass of leaf drips (kg), β_V a friction constant (kg m^{-1}) and g the acceleration due to gravity (m s^{-2}).

The fraction $\frac{M}{\beta_V}$ is a function of the leaf drip diameter D and two coefficients, a and b.

$$\frac{M}{\beta_V} = a + b\ D$$

Equation 112

where a and b are a function of the drip diameter and fall distance and are given in Table 6 and are determined inside the model code.

Table 6. Values for the empirical coefficients a and b used to determine the fraction $\frac{M}{\beta_V}$.

Drip diameter $\boldsymbol{D}$ (m)	Fall distance $\boldsymbol{X}$ (m)	$\boldsymbol{a}$	$\boldsymbol{b}$
< 0.0033	all X	0	2200
≥ 0.0033	< 7.5	1.93	1640
≥ 0.0033	≥ 7.5	5.14	6600

2.8.5.2 Detachment by runoff

Detachment by runoff is calculated as follows:

$$D_{of} = \beta_{de}\ dy\ v_s\ TC$$

Equation 113

where D_{of} is the soil detachment by overland flow (kg m^{-2} s^{-1}), β_{de} the detachment efficiency (-), dy the length of a grid cell (m), v_s the settling velocity (m s^{-1}) and TC the transport capacity (m^3 sediment m^{-3} water).

The detachment efficiency β_{de} is calculated as follows:

$$\beta_{de} = 0.79\ e^{-0.6\ COH}$$

Equation 114

Where COH is the soil cohesion (kPa), which is determined from the combination of soil cohesion (COH_s) and root cohesion (COH_r).

The settling velocity (v_s) is calculated following the method used in the KINEROS model (Woolhiser et al., 1990):

$$v_s = \sqrt{\frac{\left(\frac{4}{3} g \frac{\rho_s}{\rho} - 1\right) d_{50}}{C_d}}$$

Equation 115

where ρ_s the sediment density (kg m^{-3}), d_{50} the median grain size (m) and C_d the drag coefficient, which is a function of the particle Reynolds number:

$$C_d = \frac{24}{R_n} + \frac{3}{\sqrt{R_n}} + 0.34$$

Equation 116

where R_n is the particle Reynolds number, defined as:

$$R_n = \frac{v_{s_0}\, d_{50}}{\nu}$$

Equation 117

where v_{s_0} is an initial estimate of the settling velocity (m s^{-1}) and ν is the kinematic viscosity of water (m^2 s^{-1}), assumed to be equal to $1 \cdot 10^{-6}$ m^2 s^{-1}. The initial estimate of the settling velocity v_{s_0} is calculated as follows:

$$v_{s_0} = \sqrt{\left(\frac{4}{3} g \frac{\rho_s}{\rho} - 1\right) d_{50}}$$

Equation 118

The transport capacity (TC) is determined according to the unit stream power method from the KINEROS model (Woolhiser et al., 1990):

$$TC = \frac{0.05}{d_{50}\left(\frac{\rho_s}{\rho} - 1\right)^2} \sqrt{\frac{S\, h}{g}} (SP - SP_{cr})$$

Equation 119

where S is the slope (m m^{-1}), h the water depth (m), SP the stream power (kg m s^{-3}) and SP_{cr} the critical stream power (kg m s^{-3}).

The water depth (h) is determined with the Manning equation. We assumed a triangular shaped profile on which the Manning equation is applied, where the width-to-depth ratio is a model parameter. First the flow area is determined with an algebraic re-arrangement of the Manning equation:

$$A = \left[\frac{Q\, n \left(2\sqrt{\frac{WD^2 + 1}{WD}}\right)^{2/3}}{\sqrt{S}}\right]^{3/4}$$

Equation 120

where Q is the discharge (m^3 s^{-1}), n the Manning's coefficient (s $m^{-1/3}$) and WD the width-to-depth ratio (-). The discharge (Q) is obtained from the hydrological model and the Manning's coefficient (n) is defined per land use class.

The water depth (h) is calculated as follows:

$$h = \sqrt{\frac{A}{WD}}$$

Equation 121

The stream power (SP) is calculated as follows:

$$SP = \rho\, g\, Q\, S$$

Equation 122

2.8.5.3 Sediment transported

The sediment taken into transport is simply the sum of detachment by raindrop impact and runoff:

$$sed = D_R + D_{of}$$

Equation 123

Where sed is the sediment taken into transport (kg m^{-2} s^{-1}).

2.8.6 HSPF

The Hydrological Simulation Program-Fortran (HSPF) model (Bicknell et al., 1993) simulates detachment by raindrop impact with daily precipitation intensity as input. The soil erodibility is based on the USLE K-factor, here estimated using the method proposed by Wischmeier et al. (1971). Detached sediment by raindrop impact is stored in the sediment storage, which decreases as a result of soil crusting, simulated by a reduction parameter. The amount of detached sediment by raindrop impact taken into transport is a function of the sediment storage and the transport capacity. Detachment by runoff is a function of surface runoff and a coefficient for scour of the soil matrix.

2.8.6.1 Detachment by raindrop impact

The original HSPF model accounts for the surface water storage ($SURS$), for instance as a result of ponding. Since the hydrological model SPHY does not account for ponding, we assume the surface water storage to be equal to 0. The detachment by raindrop impact, which is called washoff of detached sediment by raindrop impact in Bicknell et al. (1993), is calculated as follows:

$$WSSD = \begin{cases} DETS & \text{for } STCAP > DETS \\ STCAP & \text{for } STCAP < DETS \end{cases}$$

Equation 124

Where $WSSD$ is the detachment by raindrop impact (ton $acre^{-1}$), $DETS$ is the sediment storage (ton $acre^{-1}$) and $STCAP$ is the capacity for removing detached sediment (ton $acre^{-1}$).

The sediment storage is calculated as follows:

$$DETS = DETS\,(1 - AFFIX) + DET$$

Equation 125

Where DET is the sediment detached from the soil matrix by rainfall (ton $acre^{-1}$) and $AFFIX$ is the fraction by which $DETS$ decreases each day as a result of soil compaction (-).

The sediment detached from the soil matrix by rainfall DET is calculated as follows:

$$DET = DELT60\,(1 - CR)\,SMPF\,KRER\left(\frac{RAIN}{DELT60}\right)^{JRER}$$

Equation 126

Where $DELT60$ is the number of hours per interval (-), CR the fraction of the land covered by vegetation (-), $SMPF$ the supporting management practice factor (-), $KRER$ the detachment coefficient dependent on soil properties (-), $RAIN$ the rainfall (inch $interval^{-1}$) and $JRER$ the detachment exponent dependent on soil properties (-).

The supporting management practice factor $SMPF$ is assumed to be 1 for all land use classes. The detachment coefficient dependent on soil properties $KRER$ is estimated with the USLE K-factor developed by (Wischmeier et al., 1971):

$$KRER = \frac{0.00021M^{1.14}(12 - OM) + 3.25(c_{soilstr} - 2) + 2.5\left(c_{perm} - 3\right)}{100}$$

Equation 127

Where $KRER$ is the particle-size parameter (-), OM is the organic matter content (%), $c_{soilstr}$ is the soil structure class (-) and c_{perm} is the profile permeability class (-).

The particle-size parameter is calculated as follows:

$$M = (m_{silt} + m_{vfs})(100 - m_c)$$

Equation 128

Where m_{silt} is the silt content (%), m_{vfs} is the very fine sand content (%) and m_c is the clay content (%).

The capacity for removing detached sediment $STCAP$ is calculated as follows:

$$STCAP = DELT60\ KSER \left(\frac{SURO}{DELT60}\right)^{JSER}$$

Equation 129

Where $KSER$ the coefficient for transport of detached sediment (-), $SURO$ the surface outflow of water (inch interval^{-1}) and $JSER$ the exponent for transport of detached sediment (-). The surface water storage $SURO$ is estimated by the (routed) runoff from the hydrological model.

2.8.6.2 Detachment by runoff

Detachment by runoff, which is called scour of matrix soil in Bicknell et al. (1993), is calculated as follows:

$$SCRSD = DELT60\ KGER \left(\frac{SURO}{DELT60}\right)^{JGER}$$

Equation 130

Where $SCRSD$ is the scour of matrix soil (ton acre^{-1}), $KGER$ is the coefficient for scour of the matrix soil (-) and $JGER$ the exponent for scour of the matrix soil (-).

2.8.6.3 Sediment transported

The sediment taken into transport is simply the sum of detachment by raindrop impact and runoff:

$$SOSED = WSSD + SCRSD$$

Equation 131

Where $SOSED$ is the total removal of soil and sediment from the surface by water (ton acre^{-1}).

2.9 Routing

After calculating the different runoff components, the cell-specific total runoff ($QTot$) is calculated by adding these different runoff components. Depending on the modules being switched on, the different runoff components are i) rainfall runoff (RRo), (ii) snow runoff (SRo), (iii) glacier runoff (GRo), and iv) baseflow (BF). Rainfall runoff is the sum of surface runoff (RO, Section 2.7.4) and lateral flow from the first soil layer (LF_1, Section 2.7.5). If the groundwater module is not used, then baseflow is calculated as being the lateral flow from the second soil layer. QTot is eventually calculated according to:

$$QTot = RRo + SRo + GRo + BF$$

Equation 132

with $QTot$ (mm) the cell-specific total runoff, RRo (mm) rainfall runoff, SRo (mm) snow runoff, GRo (mm) glacier runoff, and BF (mm) baseflow from the third soil layer or lateral flow from the second soil layer. In order to obtain river discharge, $QTot$ needs to be routed through a flow direction network. SPHY allows the user to opt between the use of a simple routing scheme (Section 2.9.1) or a more complex routing scheme (Section 2.9.2) that involves the calculation of lake outflow through $Q(h)$ relations. Both methods require a flow direction network map, which can be obtained by delineating a river network using PCRaster or GIS software in combination with a digital elevation model (DEM).

2.9.1 Runoff routing

In hydrology, streamflow routing is referred to as the transport of water through an open-channel network. Since open-channel flow is unsteady, streamflow routing often involves solving complex partial differential equations. The St. Venant equations (Brutsaert, 1971; Morris and Woolhiser, 1980) are often used for this, but these have high data requirements related to the river geometry and morphology, which are unavailable for the spatial scale SPHY is generally applied on. Additionally, solving these equations requires the use of very small time steps, which result in large model calculation times. The use of very small time steps in the St. Venant equations is required to provide numerical stability. Other models, such as, e.g., SWAT (Neitsch et al., 2009), use the Manning equation (Manning, 1891) to define the rate and velocity of river flow in combination with the variable storage (Williams, 1975) or Muskingum (Gill, 1978) routing methods to obtain river streamflow. But, the Manning equation also requires river bed dimensions, which are generally unknown on the spatial scale that SPHY generally is applied on.

Therefore, SPHY calculates for each cell the accumulated amount of water that flows out of the cell into its neighboring downstream cell. This can easily be obtained by using the accuflux PCRaster built-in function, which calculates for each cell the accumulated specific runoff from its upstream cells, including the specific runoff generated within the cell itself. If only the accuflux function is used, then it is assumed that all the specific runoff generated within the catchment on one day will end up at the most downstream location within one day, which is not plausible. Therefore, SPHY implements a flow recession coefficient (kx (–)) that accounts for flow delay, which can be a result of channel friction. Using this coefficient, river flow in SPHY is calculated using the three equations shown below:

$$QTot_t^* = \frac{QTot_t \cdot 0.001 \cdot A}{24 \cdot 3600}$$

Equation 133

$$Q_{accu,t} = accuflux(F_{dir}, QTot_t^4)$$

Equation 134

$$Q_{rout,t} = (1 - kx) \cdot Q_{accu,t} + kx \cdot Q_{rout,t-1}$$

Equation 135

with $QTot_t^*$ $(m^3 s^{-1})$ the specific runoff on day t, $QTot_t$ the specific runoff in mm on day t, A (m^2) the grid-cell area, $Q_{accu,t}$ $(m^3 s^{-1})$ the accumulated streamflow on day t without flow delay taken into account, $Q_{rout,t}$ $(m^3 s^{-1})$ the routed streamflow on day t, $Q_{rout,t-1}$ $(m^3 s^{-1})$ the routed streamflow on day $t-1$, F_{dir} the flow direction network, and kx (–) the flow recession coefficient.The kx coefficient has values ranging between 0 and 1, where values close to 0 correspond to a fast responding catchment, and values approaching 1 correspond to a slow responding catchment. This coefficient is typically used for model calibration.

The user can opt to route each of the four streamflow contributors separately, which may be useful if one wants to evaluate, for example, the contribution of glacier melt or snowmelt to the total routed runoff. However, this increases model run time substantially, because the accuflux function, which is a time-consuming function, needs to be called multiple times, depending on the number of flow contributors to be routed.

2.9.2 Lake/reservoir routing

Lakes or reservoirs act as a natural buffer, resulting in a delayed release of water from these water bodies. SPHY allows the user to choose a more complex routing scheme if lakes/reservoirs are located in their basin of interest. The use of this more advanced routing scheme requires a known relation between lake outflow and lake level height ($Q(h)$ relation) or lake storage.

To use this routing scheme, SPHY requires a nominal map with the lake cells having a unique ID, and the non-lake cells having a value of 0. The user can supply a Boolean map with "True" for cells that have measured lake levels, and "False" for lake cells that do not have measured lake levels. This specific application of SPHY is discussed in detail in Section 3.3.

Four different relations can be chosen to calculate the lake outflow from the lake level height or lake storage, being (i) an exponential relation, (ii) a first-order polynomial function, (iii) a second-order polynomial function, and (iv) a third-order polynomial function. The user needs to supply maps containing the coefficients used in the different functions.

The lake/reservoir routing scheme simply keeps track of the actual lake storage, meaning that an initial lake storage should be supplied. Instead of the simple accuflux function described in the previous section, the lake/reservoir routing scheme uses the PCRaster functions accufractionstate and accufractionflux. The accufractionflux calculates for each cell the amount of water that is transported out of the cell, while the accufractionstate calculates the amount of water that remains stored in the cell. For non-lake cells, the fraction that is transported to the next cell is always equal to 1, while the fraction that is transported out of a lake/reservoir cell depends on the actual lake storage. Each model time step, the lake storage is updated by inflow from upstream. Using this updated storage, the lake level and corresponding lake outflow can be calculated using one of the four relations mentioned before. The lake outflow can then be calculated as a fraction (Q_{frac} (–)) of the actual lake storage. Instead of using Equation 134, Q_{frac} is then used in Equation 136 and Equation 137 to calculate the accumulated streamflow and updated storage, respectively:

$$Q_{accu,t} = accufractionflux\left(F_{dir}, S_{act,t}, Q_{frac,t}\right)$$

Equation 136

$$S_{act,t+1} = accufractionstate\left(F_{dir}, S_{act,t}, Q_{frac,t}\right)$$

Equation 137

with $S_{act,t}$ (m^3) and $S_{act,t+1}$ (m^3) the actual storage and updated storage to be used in the next time step, respectively, and $Q_{accu,t}$ $(m^3 d^{-1})$ the accumulated streamflow on day t, without flow delay taken into account. Since Q_{frac} is always equal to 1 for the non-lake cells, the accufractionflux function becomes equal to the accuflux function used in the previous section. This actually means that for the river network, the same routing function from Section 2.9.1 is used, and that Equation 136 and Equation 137 only apply to lake/reservoir cells.

In order to account for non-linearity and slower responding catchments, the same kx coefficient is used again. This involves applying Equation 135 a last step after Equation 136 and converting the units from

$m^3 d^{-1}$ to $m^3 s^{-1}$. Since the accufractionflux and accufraction state functions are more complex to compute, the use of these functions increases model run time.

2.9.3 Sediment transport

Sediment is transported using a routing scheme that takes into account both the transport capacity TC (ton ha^{-1}) of the accumulated runoff and the trapping efficiency of the reservoirs TE (-). The latter only applies when the reservoir module is used. The transport capacity TC (Figure 5a) of the accumulated runoff is based on

$$TC = \mathrm{k}\ q_{\mathrm{surf}}^{\beta} S^{\gamma}$$

Equation 138

Where k is a spatially distributed roughness factor (-),q_{surf} accumulated runoff per unit width (m^2 day^{-1}), S the local energy gradient (°), approximated by the slope, and β and γ are model parameters (-). As suggested by (Prosser and Rustomji, 2000) $\gamma = 1.4$ and β is used for model calibration.

The roughness factor k is determined as follows:

$$\mathrm{k} = \frac{v_{\mathrm{actual}}}{v_{\mathrm{bare}}}$$

Equation 139

Where v_{actual} is the actual flow velocity (m s^{-1}) and v_{actual} is the flow velocity for bare soil conditions (m s^{-1}). The actual flow velocity v_{actual} is obtained from equation 81 - Equation 84, applying a water depth d_{actual} of 0.25 m, which coincides with deeper rills from (Morgan and Duzant, 2008). The flow velocity for bare soil conditions v_{actual} is obtained from equation 81, applying values for $n' = 0.015$ s m$^{-1/3}$ and $d_{\mathrm{bare}} = 0.005$ m

Reservoir sediment trapping efficiency TE (Figure 5b), the percentage of sediment trapped by the reservoir, is calculated according to (Brown, 1943):

$$TE = 100\left[1 - \frac{1}{1 + 0.0021D\frac{C}{A_{\mathrm{basin}}}}\right]$$

Equation 140

Where D is a constant (-) within the range 0.046-1, depending on the reservoir operation characteristics that we set at 0.1, C the reservoir capacity (m^3), and A_{basin} the drainage area of the subcatchment (km^2).

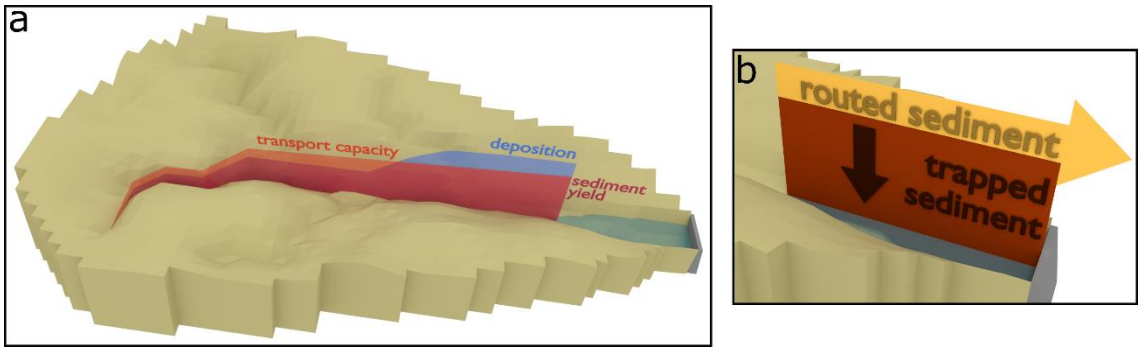

Figure 5: Sediment routing: (a) transport of sediment through the catchment (Equation 138), and (b) trapping efficiency at the reservoirs (Equation 140).

3 Applications

The SPHY model has been applied and tested in various studies, including real-time soil moisture predictions in lowlands, operational reservoir inflow forecasting in mountainous catchments, irrigation scenarios in the Nile basin, and climate change impact studies in the snow–glacier–rain dominated Himalayan region. Some example applications will be summarized in the following sections.

3.1 Irrigation management in lowland areas

As SPHY produces spatial outputs for the soil moisture content in the root zone and the potential and actual evapotranspiration (ET), it is a useful tool for application in agricultural water management decision support. By facilitating easy integration of remote sensing data, crop growth stages can be spatially assessed at different moments in time. The SPHY dynamic vegetation module ensures that all relevant soil water fluxes correspond to crop development stages throughout the growing season. Spatially distributed maps of root water content and ET deficit can be produced, enabling both the identification of locations where irrigation is required and a quantitative assessment of crop water stress.

SPHY has been applied with the purpose of providing field-specific irrigation advice for a large-scale farm in western Romania, comprising 380 individual fields and approximately ten different crops. Contrary to the other case studies highlighted in this paper, a high spatial resolution is very relevant for supporting decisions on variable-rate irrigation. The model has therefore been set up using a 30m resolution, covering the 2013 and 2014 cropping seasons on a daily time step. Optical satellite data from Landsat 8 (USGS, 2013) were used as input to the dynamic vegetation module. Soil properties were derived from the Harmonized World Soil Database (Batjes et al., 2012), which for Romania contains data from the Soil Geographical Database for Europe (Lambert et al., 2003). Using the Van Genuchten equation (van Genuchten, 1980), soil saturated water content, field capacity, and wilting point were determined for the HWSD classes occurring at the study site. Elevation data was obtained from the EU-DEM data set (EEA, 2014), and air temperature was measured by two on-farm weather stations.

In irrigation management applications like these, a model should be capable of simulating the moisture stress experienced by the crop due to insufficient soil moisture contents, which manifests itself by an evapotranspiration deficit (potential ET−actual ET>0). Figure 6 shows the spatial distribution of ET deficit, as simulated by the SPHY model for the entire farm on 03 April 2014. When SPHY is run in an operational setting, this spatial information can be included in a decision support system that aids the farmer in irrigation planning for the coming days.

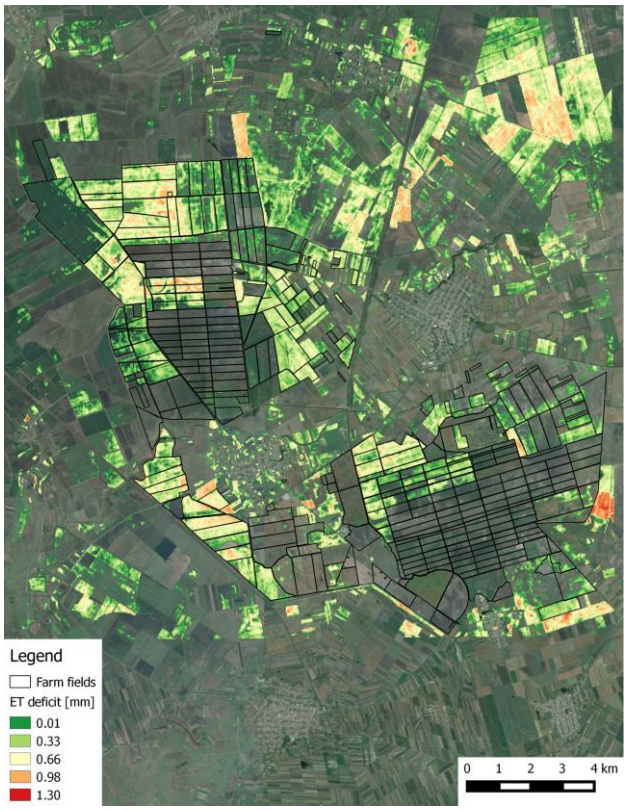

Figure 6: Spatial distribution of evapotranspiration (ET) deficit, as simulated by the SPHY model for a Romanian farm on 03 April 2014. Transparency means no ET deficit.

For calibration purposes, field measurements of soil moisture and/or actual ET are desired. In this case study, one capacitance soil moisture sensor was installed in a soybean field to monitor root-zone water content shortly after 01 May 2014, which is the start of the soybean growing season. The sensor measures volumetric moisture content for every 10cm of the soil profile up to a depth of 60cm. It is also equipped with a rain gauge measuring the sum of rainfall and applied irrigation water, which was used as an input to SPHY. Soil moisture measured over the extent covered by the crop root depth was averaged and compared to simulated values (Figure 7).

Since this study was a demonstration project, only an initial model calibration was performed. The model was in this case most sensitive for the crop coefficient (Kc), affecting the evaporative demand for water. As can be seen in Figure 7, the temporal patterns as measured by the soil moisture sensor are well simulated by the SPHY model. Based on daily soil moisture values, a Nash–Sutcliffe (Nash and Sutcliffe, 1970) model efficiency coefficient of 0.6 was found, indicating that the quality of prediction of the SPHY model is “good” (Foglia et al., 2009). Soil moisture simulations could be further improved by conducting a full model calibration, adjusting the soil physical parameters $K_{sat,1}$, $SW_{1,fc}$, $SW_{1,pF3}$, and $SW_{1,pF4.2}$. Remotely sensed sensed evapotranspiration can be used in the calibration process (Immerzeel and Droogers, 2008), although such data are often not available on these small scales as ET is a very complex variable to assess (Samain et al., 2012). It should also be noted that soil moisture content is typically highly variable in space; a very high correlation between point measurements and grid-cell simulations of soil moisture may therefore not always be feasible (Bramer et al., 2013).

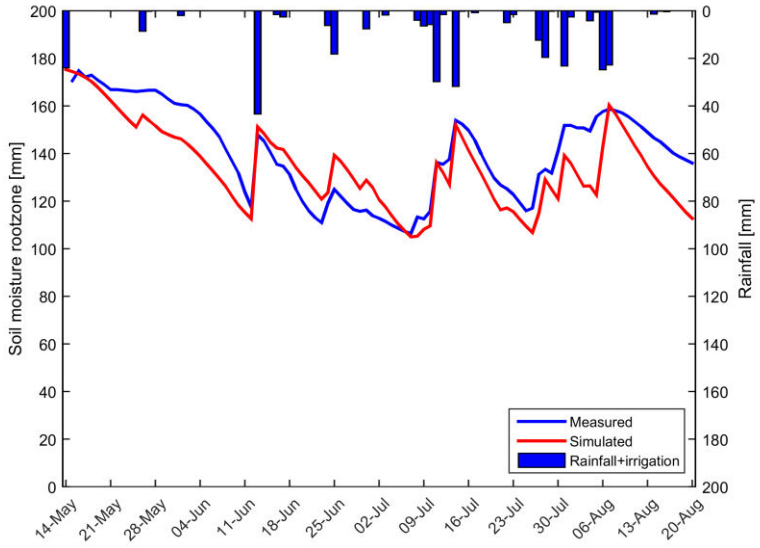

Figure 7: Measured and simulated daily root-zone soil moisture content during the 2014 growing season. Rainfall+irrigation has been measured by the rain gauge that was attached to the moisture sensor.

3.2 Snow- and glacier-fed river basins

SPHY is being used in large Asian river basins with significant contribution of glacier melt and snowmelt to the total flow (Khanal et al., 2021a; Immerzeel et al., 2012b; Lutz et al., 2012, 2014, 2016). The major goals of these applications are two-fold:

- Assess the current hydrological regimes at high resolution; e.g., assess spatial differences in the contributions of glacier melt, snowmelt and rainfall–runoff to the total flow.
- Quantify the effects of climate change on the hydrological regimes in the future and how these affect the water availability.

Rivers originating in the high mountains of Asia are considered to be the most meltwater-dependent river systems on Earth (Schaner et al., 2012). In the regions surrounding the Himalayas and the Tibetan Plateau, large human populations depend on the water supplied by these rivers (Immerzeel et al., 2010). However, the dependency on meltwater differs strongly between river basins as a result of differences in climate and differences in basin hypsometry (Immerzeel and Bierkens, 2012). Only by using a distributed hydrological modeling approach that includes the simulation of key hydrological and cryospheric processes, and inclusion of transient changes in climate, snow cover, glaciers and runoff, can appropriate adaptation and mitigation options be developed for this region (Sorg et al., 2012). The SPHY model is very suitable for such goals, and has therefore been widely applied in the region (Khanal et al., 2021).

For application in this region, SPHY was set up at a 1km spatial resolution using a daily time step, and forced with historical air temperature (T_{avg}, T_{max}, T_{min}) and precipitation data, obtained from global and regional data sets (e.g., APHRODITE, (Yatagai et al., 2012); Princeton, (Sheffield et al., 2006); TRMM, (Gopalan et al., 2010) or interpolated WMO station data from a historical reference period. For this historical reference period, SPHY was calibrated and validated using observed streamflow. For the future period, SPHY was forced with downscaled climate change projections obtained from general circulation models (GCMs), as available through the Climate Model Intercomparison Projects (e.g., CMIP3, (Meehl et al., 2007); CMIP5, (Taylor et al., 2012), which were used as a basis for the Assessment Reports prepared by the Intergovernmental Panel on Climate Change (IPCC).

In central Asia, SPHY was applied in a study (ADB, 2012; Immerzeel et al., 2012a; Lutz et al., 2012) that focused on the impacts of climate change on water resources in the Amu Darya and Syr Darya river basins. SPHY was used to quantify the hydrological regimes in both basins, and subsequently to project the outflow from the upstream basins to the downstream areas by forcing the model with an ensemble of five CMIP3 GCMs. The SPHY model output fed into a water allocation model that was set up for the downstream parts of the Amu Darya and Syr Darya river basins.

In the Himalayan Climate Change Adaptation Programme (HICAP), led by the International Centre for Integrated Mountain Development (ICIMOD), SPHY has been successfully applied in the upstream basins of the Indus, Ganges, Brahmaputra, Salween and Mekong rivers (Lutz et al., 2013, 2014). In this study the hydrological regimes of these five basins have been quantified and the calibrated and validated model (Figure 8) was forced with an ensemble of eight GCMs to create water availability scenarios until 2050. Table 7 lists the calibration and validation results. Based on the validation results, we concluded that the model performs satisfactorily given the large scale, complexity and heterogeneity of the modeled region and data scarcity (Lutz et al., 2014). We use one parameter set for the entire domain, which inherently means some stations perform better than others. In the particular case of the upper Indus, another possible explanation could be uncertainty in air temperature forcing in the highest parts of the upper Indus basin (locations Dainyor bridge, Besham Qila and Tarbela inflow in Table 7), since especially in this area, the used forcing data sets are based on very sparse observations. SPHY allowed the assessment of the current contribution of glacier melt and snowmelt to total flow (Figure 9), and how total flow volumes and the intra-annual distribution of river flow will change in the future (Lutz et al., 2014).

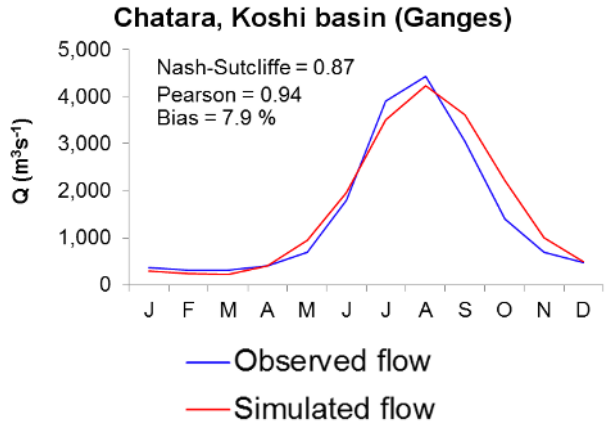

Figure 8: Average monthly observed and SPHY-simulated flow (1998–2007) for the Chatara major discharge measurement location in the Ganges basin (Lutz et al., 2014)**. Metrics are calculated based on monthly time steps.**

Table 7: Station locations used for calibration and validation of the SPHY model in HICAP (Lutz et al., 2014)**. Three stations were used for calibration for 1998–2007. Five stations were used for an independent validation for the same period. The Nash–Sutcliffe efficiency (NS) and bias metrics were calculated at a monthly time step.**

Location	NS (–)	Bias (%)	Validation/calibration
Dainyor bridge	0.39	58.2	Validation
Besham Qila	0.66	24.7	Validation
Tarbela inflow	0.63	34.6	Calibration
Marala inflow	0.65	12.0	Validation
Pachuwarghat	0.90	−1.6	Validation
Rabuwa Bazar	0.65	−22.5	Validation
Turkeghat	0.87	−5.4	Calibration
Chatara	0.87	7.9	Calibration

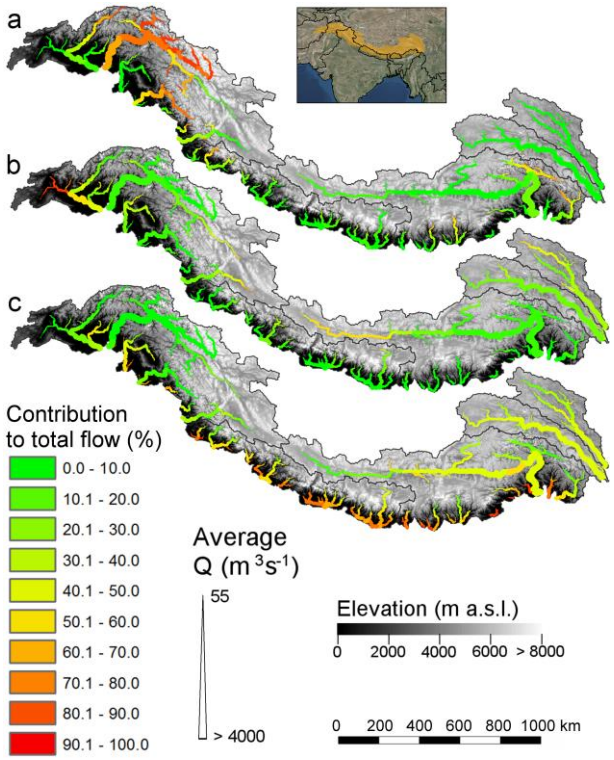

Figure 9: The contribution of glacier melt (a), snowmelt (b), and rainfall (c) to the total flow for major streams in the upstream basins of the Indus, Ganges, Brahmaputra, Salween and Mekong during 1998–2007 (Lutz et al., 2014)**.**

For basins with snowmelt being an important contributor to the flow, besides calibration to observed flow, the snow-related parameters in the SPHY model can also be calibrated to observed snow cover. For the Upper Indus basin, the snow-related parameters degree-day factor for snow (DDF_s) and snow water storage capacity (SSC) were calibrated independently using MODIS snow cover imagery (Lutz et al., 2016). The same MODIS data set was used as in (Immerzeel et al., 2009). From the beginning of 2000 until halfway through 2008, the snow cover imagery was averaged for 46 different periods of 8 days (5 days for the last period) to generate 46 different average snow cover maps. For example, period 1 is the average snow cover for 01–08 January for 2000 until 2008, whereas period 2 is the average snow

cover for 09–16 January for 2000 until 2008, etc. The SPHY model was run for 2000–2007 at a daily time step and, for each 1×1km grid cell, the average snow cover was calculated for the same 46 periods as in the MODIS observed snow cover data set. Subsequently, these simulated snow cover maps were resampled to 0.05 spatial resolution, which is the native resolution of the MODIS product. Figure 10 shows the basin-average observed and simulated fractional snow cover for the 46 periods during 2000–2007 and Figure 11 shows the same at the 0.05 grid-cell level. As a final step, the baseflow recession coefficient (α_{gw}) and routing coefficient (kx) were calibrated to match the simulated streamflow with the observed streamflow.

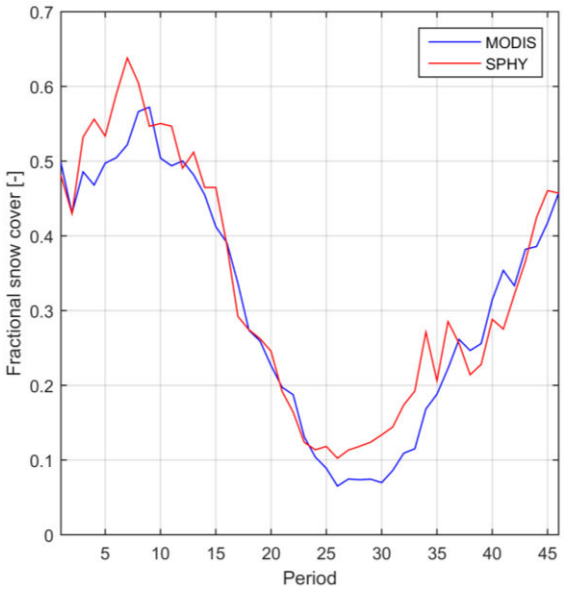

Figure 10: Observed and simulated average fractional snow cover in the upper Indus basin. The values represent the 9-year average for 46 (8-day) periods during 2000–2007.

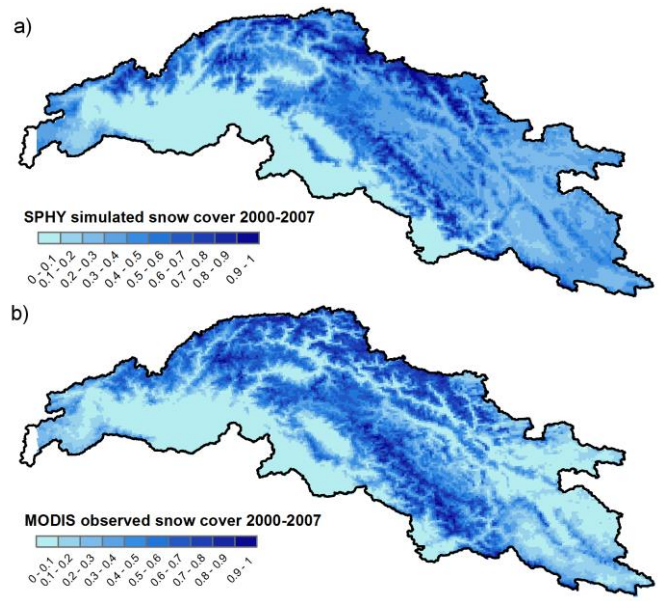

Figure 11: (a) SPHY simulated snow cover 2000–2007 and (b) MODIS observed snow cover 2000–2007.

In the Pan-Third Pole Environment study for a Green Silk Road (Pan-TPE), SPHY has been successfully applied in the 15 major river basins of the High Mountains of Asia (HMA) (Khanal et al., 2021)This study explores changes in climate, water supply and demand, and suitable adaptation measures for green development of the Silk Road Economic Belt (SREB) in the river basins crossed by the SREB transect. To robustly assess the 21st-century climate change impact on hydrology in the entire HMA at a wide range of scales (annual, decadal and multi-decadal), this study uses a 5km spatial and daily time step temporal resolution SPHYv3.0 model. The SPHYv3.0 model results are then used to understand the regional hydrological patterns (Figure 12) and then quantify the compound effects of future changes in precipitation and temperature based on the range of climate change projections in the CMIP6 climate model ensemble. The SPHYv3.0 model in this study uses ERA5 (Hersbach et al., 2020) as input meteorological forcings. The SPHYv3.0 uses dynamic glacier module as described in section 2.6.4. For more details regarding the study readers are referred to (Khanal et al., 2021).

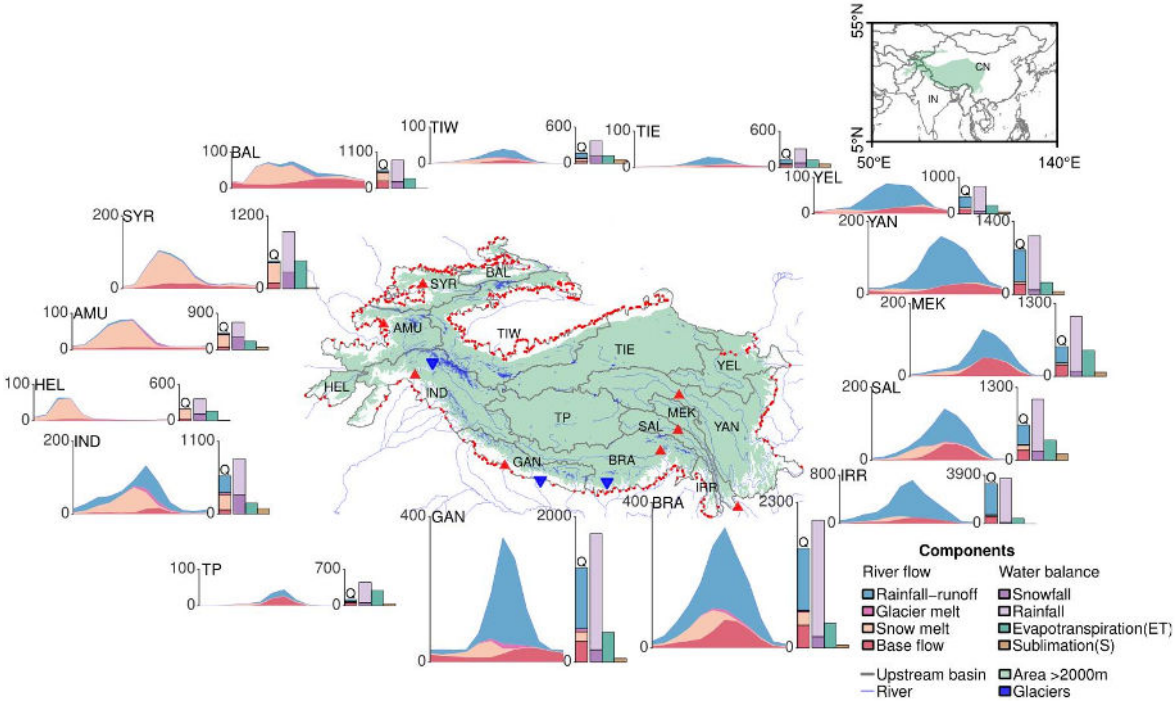

Figure 12: The upstream mountainous basins of HMA analyzed in Pan-TPE project (grey boundaries). The green color represents the area above 2000 m. Shown are 1985–2014 mean seasonal cycles of discharge (Q, in mm yr-1) contributed by baseflow (red), snowmelt (orange), glacier melt (magenta), and rainfall-runoff (blue). Stacked bar plots aside show the average annual contributions of the discharge components (Q, 1st bar), the precipitation (P, 2nd bar) falling as rain (light purple) and snow (purple), the actual evapotranspiration (light green, 3rd bar), and sublimation (brown, 4th bar). The red triangles in the geographical map represent the station locations used for the calibration and validation of the hydrological model with observed discharge. The blue downward triangles represent the station locations where independent model validation with observed discharge is performed. Note the difference in vertical scale for each of the basins.

3.3 Flow forecasting

In data-scarce environments and inaccessible mountainous terrain, like in the Chilean Andes, it is often difficult to install instrumentation and retrieve real-time physical data from these instruments. These real-time data can be useful to capture the hydroclimatic variability in this region, and improve the forecasting capability of hydrological models. Although statistical models can provide skillful seasonal forecasts,

using large-scale climate variables and in situ data (Piechota et al., 1998; Grantz et al., 2005; Regonda et al., 2006; Bracken et al., 2010), a particular hydropower company in Chile was mainly interested in the potential use of an integrated system, using measurements derived from both Earth observation (EO) satellites and in situ sensors, to force a hydrological model to forecast seasonal streamflow during the snow melting season. The objective of the INTOGENER (INTegration of EO data and GNSS-R signals for ENERgy applications) project was therefore to demonstrate the operational forecasting capability of the SPHY model in data-scarce environments with large hydroclimatic variability.

During INTOGENER, data retrieved from EO satellites consisted of a DEM and a time series of snow cover maps. Snow cover images were retrieved on a weekly basis, using RADARSAT and MODIS (Parajka and Blöschl, 2008; Hall et al., 2002) imagery. These images were used to update the snow storage (SS (mm)) in the model in order to initialize it for the forecasting period. Figure 13 shows the snow storage as simulated by the SPHY model during the snow melting season in the Laja basin. These maps clearly show the capability of SPHY to simulate the spatial variation of snow storage, with more snow on the higher elevations, and a decrease in snow storage throughout the melting season. Discharge, precipitation and temperature data were collected using in situ meteorological stations. In order to calculate the lake outflow accurately, the SPHY model was initialized with water level measurements retrieved from reflected Global Navigation Satellite System (GNSS) signals in Laja Lake. Static data that were used in the SPHY model consisted of soil characteristics derived from the Harmonized World Soil Database (HWSD) (Batjes et al., 2009) and land use data obtained from the GLOBCOVER (Bontemps et al., 2011) product. The SPHY model was set up to run at a spatial resolution of 200m.

Figure 14 shows the observed vs. simulated daily streamflow for two locations within the Laja River basin for the historical period 2007–2008. It can be seen that model performance is quite satisfactory for both locations, with volume errors of −4 and −9.4% for the Abanico Canal (downstream of Lake Laja) and Rio Laja en Tucapel, respectively. The NS coefficient, which is especially useful for assessing the simulation of high discharge peaks, is less satisfactory for these locations. Hydropower companies, however, have more interest in expected flow volumes for the coming weeks/months than in accurate day-to-day flow simulations, and therefore the NS coefficient is less important in this case. If the NS coefficient is calculated for the same period on a monthly basis, then the NS coefficients are 0.53 for the Abanico Canal and 0.81 for Rio Laja en Tucapel. It is likely that SPHY model performance would even have been better if a full model calibration would have been performed.

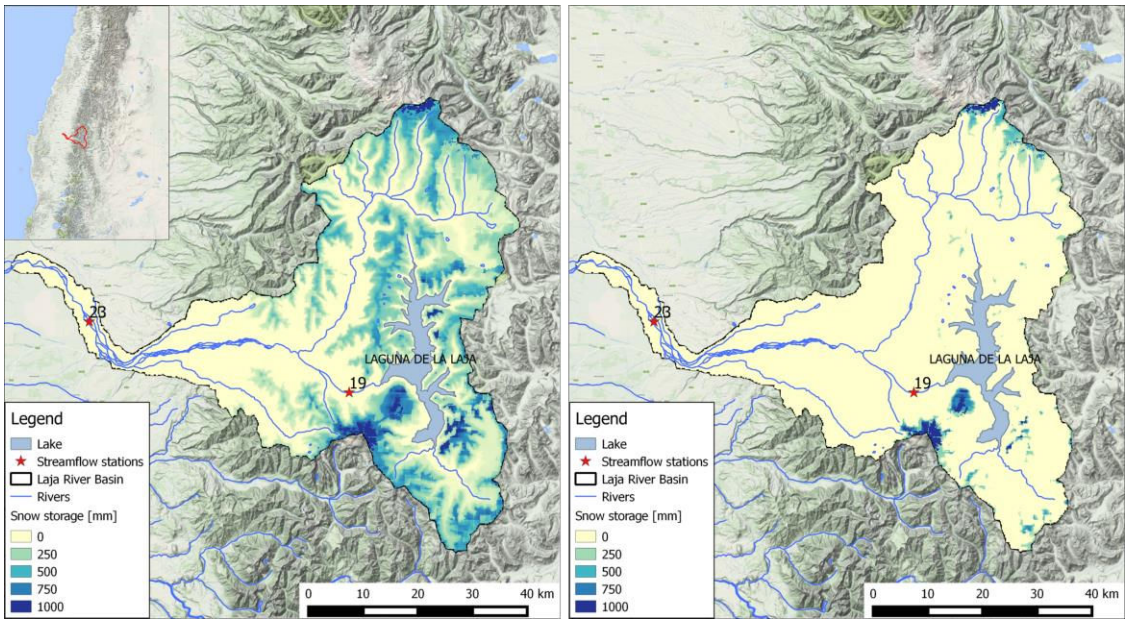

Figure 13: Snow storage (mm) as simulated by the SPHY model on 12 August (left) and 01 October (right) during the snow melting season of 2013 in the Laja River basin.

The hydropower company's main interest is the model's capacity to predict the total expected flow for the coming weeks during the melting season (October 2013 through March 2014). To forecast streamflow during the snow melting season, the SPHY model was forced with gridded temperature and precipitation data from the European Centre for Medium-range Weather Forecasts (ECMWF) Seasonal Forecasting System (SEAS) (Andersson, 2013)(Andersson, 2013)(Andersson, 2013)(Andersson, 2013). The SEAS model provided daily forecasts at a spatial resolution of 0.75, 7 months ahead, and was used to forecast streamflow up till the end of the melting season. Figure 15 shows the bias between the total cumulative forecasted flow and observed flow for the 23 model runs that were executed during operational mode. Although there are some bias fluctuations in the Rio Laja en Tucapel model runs, it can be concluded that the bias decreases for each next model run for both locations, which is a logical result of a decreasing climate forcing uncertainty as the model progresses in time. It can be seen that the SPHY model streamflow forecasts for Canal Abanico, which is downstream of Laja Lake, are substantially better than for Rio Laja en Tucapel (the most downstream location). The reason for this has not been investigated during the demonstration study, but since model performance for these two locations was satisfactory during calibration, a plausible explanation could be the larger climate forecast uncertainty in the higher altitude areas (Hijmans et al., 2005; Rollenbeck and Bendix, 2011; Vicuña et al., 2011; McPhee et al., 2010; Mendoza et al., 2012; Ragettli and Pellicciotti, 2012; Ragettli et al., 2014) in the northeastern part of the basin that contributes to the streamflow of Rio Laja en Tucapel. Additionally, only two in situ meteorological stations were available during operational mode, whereas during calibration, 20+ meteorological stations were available. Moreover, these operational meteorological stations were not installed at higher altitudes, where precipitation patterns tend to be spatially very variable (Wagner et al., 2012; Rollenbeck and Bendix, 2011).

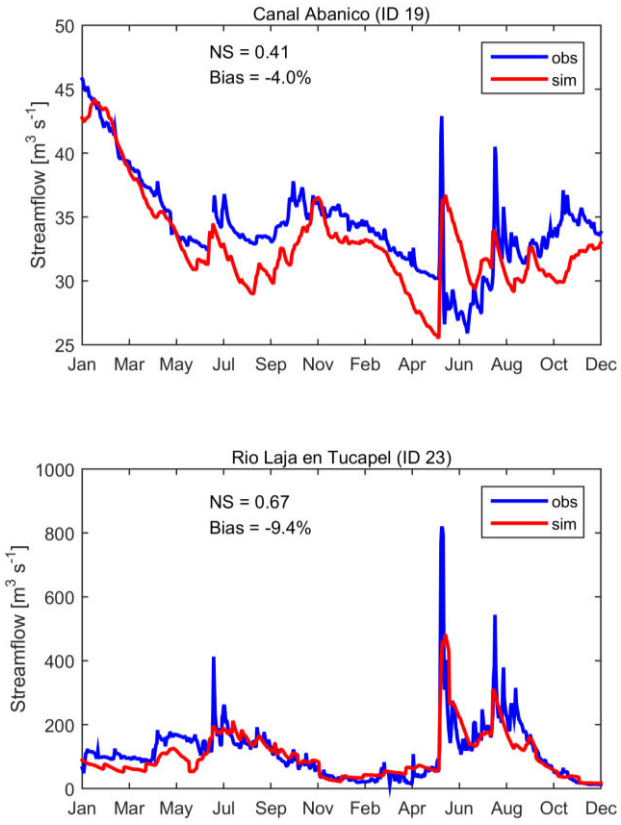

Figure 14: Daily observed vs. SPHY simulated streamflow (period 2007–2008) for the streamflow stations Canal Abanico (ID 19) and Rio Laja en Tucapel (ID 23). The Nash–Sutcliffe (NS) and bias model performance indicators are shown as well.

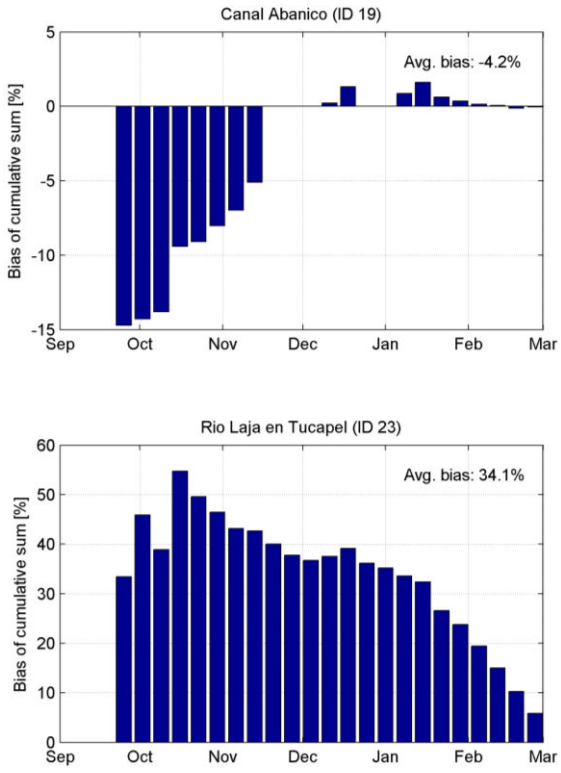

Figure 15: Bias between total cumulative forecasted flow and observed flow for the 23 model runs that were executed between the end of September 2013 and March 2014. Results are shown for the locations Canal Abanico (ID 19) and Rio Laja en Tucapel (ID 23).

3.4 Soil erosion and sediment transport

The soil erosion and sediment transport modules were applied in the Upper Segura River catchment (2,589 km^2) under present and future projected climate conditions. The Upper Segura catchment is located in the headwaters of the Segura River in southeastern Spain. The climate in the catchment is classified as temperate (80% of the catchment) and semi-arid (20%). The catchment-average annual precipitation is 570 mm (1981-2000) and the mean annual temperature is 13.2 ºC (1981-2000). The main landuse types are forest (45%), shrubland (40%), cereal fields (7%) and almond orchards (4%). The main soil classes are Leptosols (38%), Luvisols (27%), Cambisols (16%) and Calcisols (11%). There are 5 reservoirs located in the catchment with a total capacity of 663 Hm^3, which are mainly used to store water for irrigation purposes.

All input data were prepared at a 200 m grid size. Daily precipitation data were obtained from the SPREAD dataset (Serrano-Notivoli et al., 2017 and temperature data were obtained from the SPAIN02 dataset (Herrera et al., 2016). Soil textural fractions (sand, clay and silt) and soil organic matter content were obtained from the global SoilGrids dataset (Hengl et al., 2017). A Digital Elevation Model was obtained from the SRTM dataset (Farr et al., 2007)(). The spatially distributed rock fraction map was obtained by applying the empirical formulations from (Poesen et al., 1998), which determine rock fraction based on slope gradient.

The soil erosion model requires landuse-specific input for plant height (PH), stem density (NV), stem diameter (D), ground cover fraction (GC) and, optionally, the Manning's roughness coefficient for vegetation ($n_{vegetation}$). The user needs to specify whether the landuse class is non-erodible (e.g. pavement and water), tilled or non-vegetated (e.g. bare soil or tilled orchards). We obtained values for each of these parameters through observations from aerial photographs, expert judgement and as part

of the calibration procedure (Table 8). The tillage parameter RFR was set to 6, which corresponds to Cultivator tillage (Morgan and Duzant, 2008). The input parameters change when a crop is harvested, therefore, we varied the input parameters according to the sowing-harvest cycle representing the cropping cycle for horticulture and cereals.

Table 8: Input parameters for the soil erosion model ([1] T = tillage, NE = no erosion, NV = no vegetation, [2] Day of the Year, [3] Obtained from (Chow, (1959)

Landuse class	PH	NV	D	GC	mannin g	sowing	harvest	other[1]
	(m)	(stems m-2)	(m)	(fraction)	(s $m^{-1/3}$)	$(doy)^2$	$(doy)^2$	
Cereal	0.75	500	0.025	0.31	n.a.	288	166	T
(harvested)	0	0	0	0	n.a.			T
Huerta	0.5	500	0.01	0.5	n.a.	n.a.	n.a.	T
Horticulture	0.3	6.25	0.25	0.39	n.a.	288	166	T
(harvested)	0	0	0	0	n.a.			T
Tree crops	2	n.a.	n.a.	< 0.01	n.a.	n.a.	n.a.	T,NV
Vineyard	1	n.a.	n.a.	0.02	n.a.	n.a.	n.a.	T,NV
Forest	10	n.a.	n.a.	0.53	0.2[3]	n.a.	n.a.	
Shrubland	0.5	n.a.	n.a.	0.45	0.1[3]	n.a.	n.a.	
Water/urban	0	0	0	0	n.a.	n.a.	n.a.	NE

Here we present a selection of model results to illustrate the main capabilities of soil erosion and sediment transport modules. Soil erosion shows an important intra-annual variability due to seasonal changes in climate forcing and vegetation cover (Figure 16). Soil erosion follows the precipitation sum for crops with little to no ground cover (i.e. tree crops and vineyard), with high values in the winter, spring and autumn months and low values in the summer months. Some crops show a distinct peak in the vegetation development in the spring (April-May), e.g. huerta and horticulture. While this period has a relatively high precipitation sum, soil erosion decreases as a consequence of the increased vegetation cover indicated by the NDVI in this period. The temporal variation of the vegetation development of cereals and horticulture shows a slightly distinct pattern from the other land use classes. Both crops show an increase in the spring months (March-May), which indicates the rapid growth of these crops in these months. However, during the summer months (June-August) the NDVI decreases, which coincides with the period when the crops are harvested, followed by the post-harvest period. In the latter period, we assume bare soil conditions for these crops. For both crops this ultimately results in the highest annual erosion rates in the post-harvest period (October).

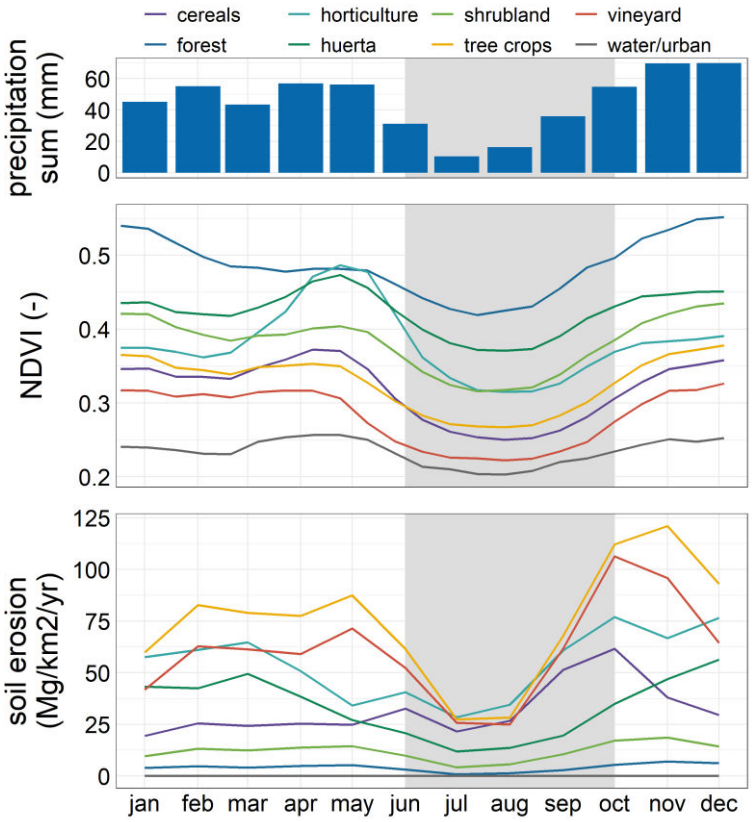

Figure 16: Monthly precipitation sum (mm), NDVI (-) and soil erosion (Mg km^{-2} yr^{-1}) per landuse class for the period 1981-2000. The gray area indicates the period when cereals and horticulture are harvested and model parameters are changed to bare soil conditions

We simulated also the impacts of a projected climate change scenario, by comparing predicted soil erosion rates and sediment yield under the reference scenario (1981-2000) with a future scenario (2081-2100). We used a future emission scenario from the Representative Concentration Pathways (van Vuuren et al., 2011). For this exercise we used projected climate data for RCP8.5 obtained from one Regional Climate Model (CLMcom MPI-ESM-LR) from the EURO-CORDEX initiative (Jacob et al., 2014). The climate forcing (precipitation and temperature) was bias-corrected using quantile mapping (Themeßl et al., 2012). The climate change scenario projects a decrease of the annual precipitation sum decreases, however, extreme precipitation is projected to increase, which is most relevant for soil erosion.

In the reference scenario the highest hillslope erosion (SSY) is projected in the river network (Figure 17), where accumulated runoff causes an increase of soil erosion rates. In the future climate scenario, the catchment-median hillslope erosion increases from 43.3 to 55.2 Mg km^{-2} yr^{-1}, an increase of 27.7%. This shows that the increase in extreme precipitation has a more pronounced impact on soil erosion than the decrease of annual precipitation sum. Reservoir sediment yield (SY) decreases in all five reservoirs between 42.4-59.0% in the future climate scenario. While it is likely that a decrease of hillslope erosion in the western part of the catchment causes a decrease of reservoir SY, it is less obvious why in the eastern part of the catchment an increase in hillslope erosion is not reflected in an increase in reservoir SY. The explanation for this lies in the fact that a decrease in precipitation sum causes a decrease of accumulated runoff and, subsequently, a decrease of sediment transport capacity, increased sediment deposition and decreased reservoir SY.

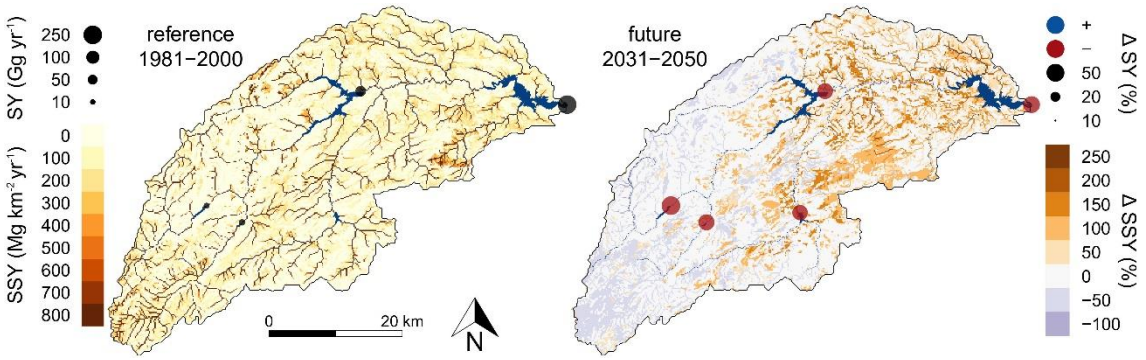

Figure 17: Specific sediment yield (Mg km^{-2} yr^{-1}) and reservoir sediment yield (Gg yr^{-1}) for the reference (1981-2000) scenario and the change (%) for the future (2081-2100) scenario.

4 Installation of SPHY

4.1 General

SPHY v3.1 can only be installed at the moment as a stand-alone application, where the user can run the model from the command prompt. The earlier versions of SPHY 2.0 and 2.1 have Graphical User-Interfaces (GUI) as plugins and have the advantage that changing the model input and output, as well as changing model parameters, is more clear and user-friendly. The GUIs developed using QGIS[1] Geographical Information System (GIS) are not available for the SPHYv3.1. Section 4.2 describes the installation of SPHY v3.1 as a stand-alone application. The main differences between SPHY 2.0/2.1 and SPHY v3.1 are that SPHY v3.1 includes a mass conserving glacier change routine, whereas 2.0/2.1 treats glaciers as static entities, and that SPHYv3.1 includes modules for soil erosion and sediment transport, which are not included in SPHY 2.0/2.1.

4.2 Installing SPHY as a stand-alone application

In order to install SPHY as a stand-alone application it is required to have a PC with a Windows operating system. The software packages that are required to run the SPHY model as a stand-alone application are:

1. Miniconda
2. SPHY v3.1 source code

These packages need to be installed in the same order as shown above, and the installation of each package is described in the following sections.

4.2.1 Miniconda

First download and install Miniconda from https://docs.conda.io/en/latest/miniconda.html. It is important to ensure that you download the Miniconda3 Windows 64-bit version. You may need to check which version of Python is supported by the PCRaster. Here we use py310 64-bit version. It is not mandatory to change the destination folder for Miniconda but we prefer to install it in *'C:\Miniconda'*. Note you need to create the Miniconda folder (see below).

[1] http://www.qgis.org/en/site/

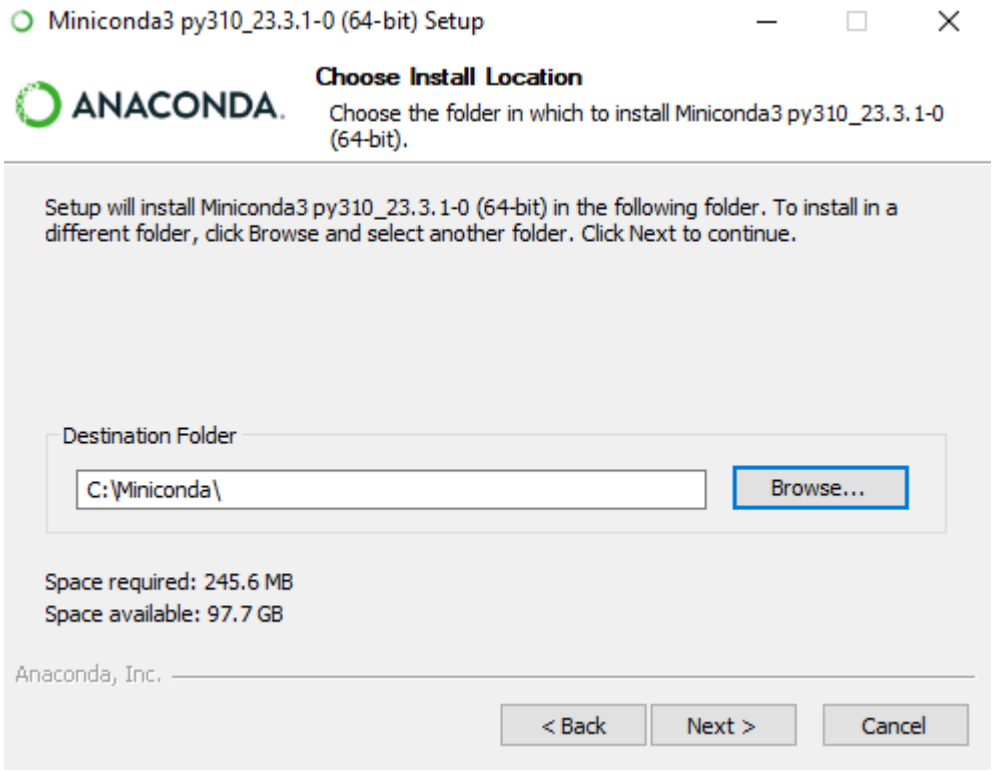

Figure 18: Installation of Miniconda.

After Miniconda installation check if the following paths have been added to the system environment. If paths were not added then add the followings to the 'Path' in system environment variables:

C:\Miniconda\Scripts
C:\Miniconda
C:\Miniconda \Library\bin

To add this path, open control panel and search for 'edit the system environment variables' (see below).

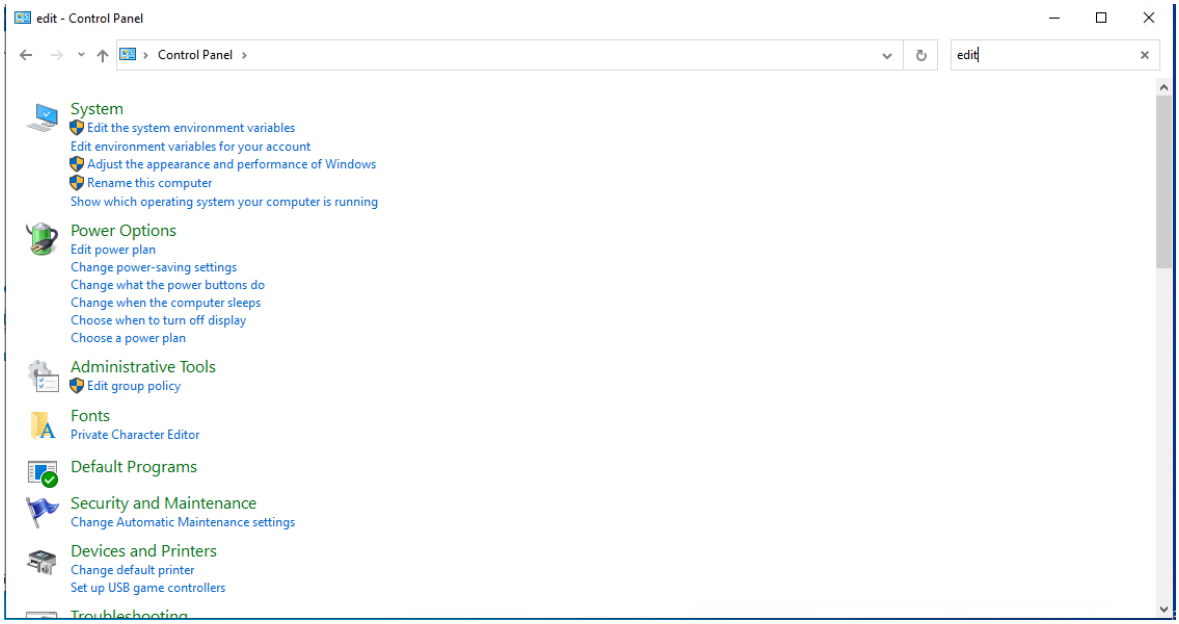

Figure 19: Finding the environment variable.

A new window will popup. Click on Environment variables.

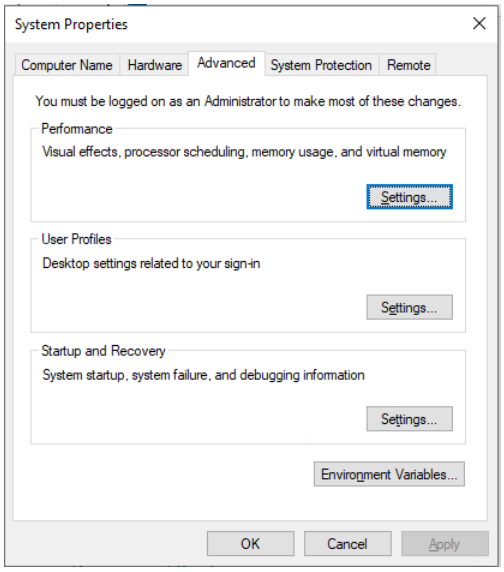

Figure 20: Setting the Path variable.

In the System variables tab click on Path and edit it.

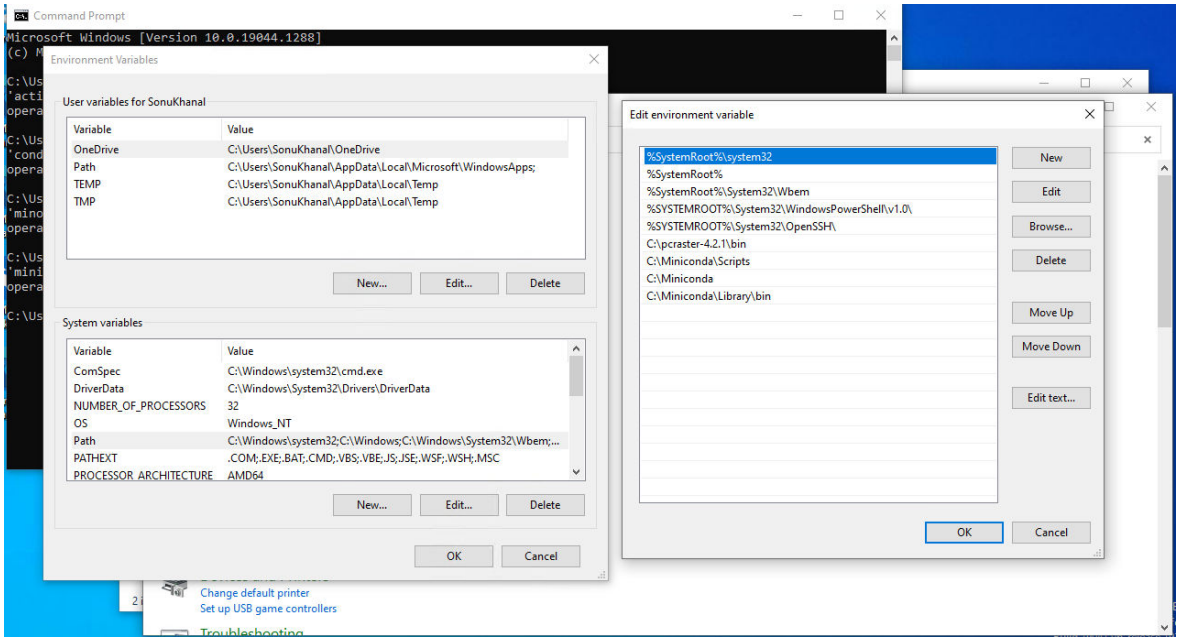

Figure 21: Copying the path.

Open command prompt by typing '*cmd*' in search bar of windows. A command prompt will open. Type *'conda'* and it will populate the command prompt screen with the following commands.

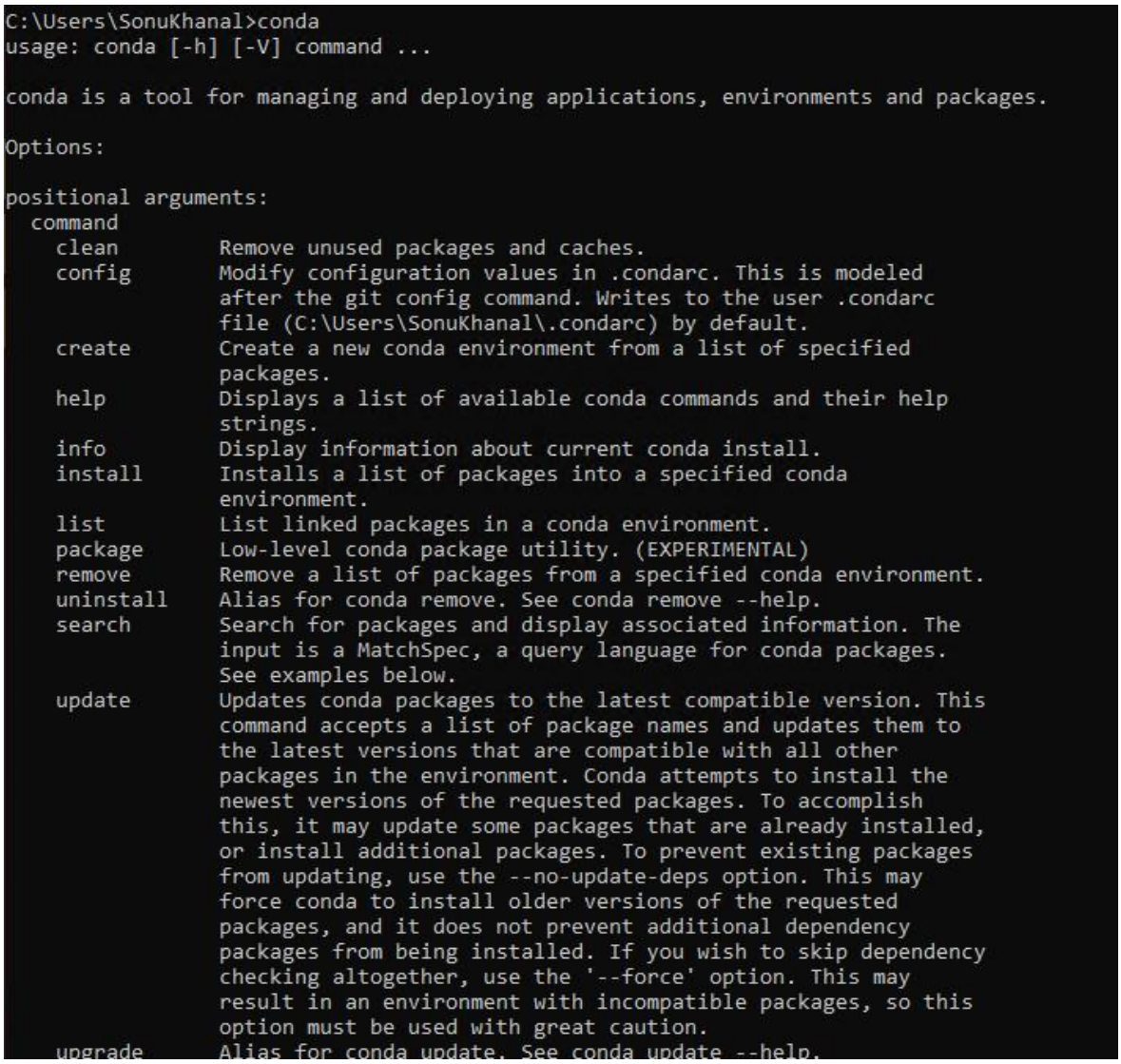

Figure 22: Checking if conda works.

From the command prompt type '*activate C:\Miniconda*'

To run SPHYv3.1 several packages need to be installed so we need to install the specific version of Python and the other dependent packages. This process takes a bit of time. Type:

conda create --name pcraster -c conda-forge python pcraster spyder matplotlib pandas netCDF4 scipy pyproj

In case error messages related to missing packages appear when trying to run the SPHY model, the missing packages can be installed separately.

Add additional packages (if needed):
conda install --name pcraster -c conda-forge pandas

4.2.2 SPHY v3.1 source code

The SPHY v3.1 source code can be obtained from the SPHY model website (https://github.com/FutureWater/SPHY/tags). The source code is available as a zip-file (SPHY3.1.zip)

and needs to be extracted to a folder on your hard drive. This folder can be zipped anywhere on the PC depending on where you want to keep all the model files (D:\SPHY3_1). It is important to note that do not use space in the folder names for SPHY. After unzipping the contents of the SPHY3.1 zip to a folder of your preference, installation has been completed successfully. Alternatively the code can be cloned using git from the github page.

Open the command prompt and browse to the SPHY3.1 folder where all the SPHY source codes (.py) files are copied. This can be done by copying and pasting the SPHY source code folder:

- *cd D:\SPHY3_1* to the command prompt.

Also, activate the environment by typing:

- *conda activate pcraster*.

After creating the required input files (see section 5), the SPHY model can be run from the command line by typing *python sphy.py sphy_config.cfg*.

5 Build your own SPHY-model

A SPHY model preprocessor has been developed that enables the user to automatically generate SPHY model input data for a selected area of interest. This preprocessor has been developed as a plugin for QGIS, and generates the input data using a database that can be selected by the user. Currently, only one database can be used by the preprocessor: the “Hindu Kush-Himalaya” database (xmin: 65, xmax: 100, ymin: 20, ymax: 40). The name of the SPHY model preprocessor is “SphyPreProcess” (v1.0), and is described together with the SPHY model plugin in the SPHY GUIs manual (Terink et al., 2015b).

If your area of interest is not covered by the extent of the database, then you can choose to create your model input data manually (as is done in the Pungwe case-study (Terink et al., 2015a). You will need the PCRaster command line functions and GIS software, like the open source QGIS. The steps that are required to do this are described in the sections below.

5.1 Select projection extent and resolution

First you need to start a new project within QGIS. Give it a useful name and save your project regularly during the steps in the following sections. Because all calculations in SPHY are metric, you will need to project your data in a metric coordinate system. In the example of the Pungwe basin, we chose the WGS84 UTM Zone 36 South projection (EPSG:32736). Define the minimum and maximum x and y values in the projection that you have chosen that cover the entire area you want to model. Then, define the spatial resolution of your model. The choice of resolution will be a tradeoff of the resolution of your input data, computation resources availability, number of runs you intend to do and required detail for your modelling purpose. For your reference, the model for the Pungwe case study has an extent of 275 x 255 km. For this model the spatial resolution is 1000 x 1000 m, and thus the model contains ~70.000 grid cells. Running this model at a daily time step for 5 years takes about 5 minutes.

In order to create your own model, you need to setup the directory structure. This means you need to create a new **SPHY** model directory (containing the SPHY model source *.py files) and in that directory you need to create a new **input** and **output** directory.

5.2 Clone map

You will need to define a ‘clone’ map, which is a map in PCRaster format, with the model extent and resolution. This map is used as the ‘template’ for your model. You can create a clone map using PCRaster’s mapattr command in the Windows Command line window. Make sure you are in the model’s **input** directory. This can be done using commands as for example:

- *c: enter* → go to your c-drive
- *cd c:\SPHY\input enter* → go to the SPHY\input directory on your c-drive
- *d: enter → go to your d-drive*
- *cd d:\SPHY\input enter* → go to the SPHY\input directory on your d-drive
- etc.

If you are in the model’s input directory, then type following in the Command line:

mapattr clone.map

You will enter a menu, where you can set the clone map’s properties:

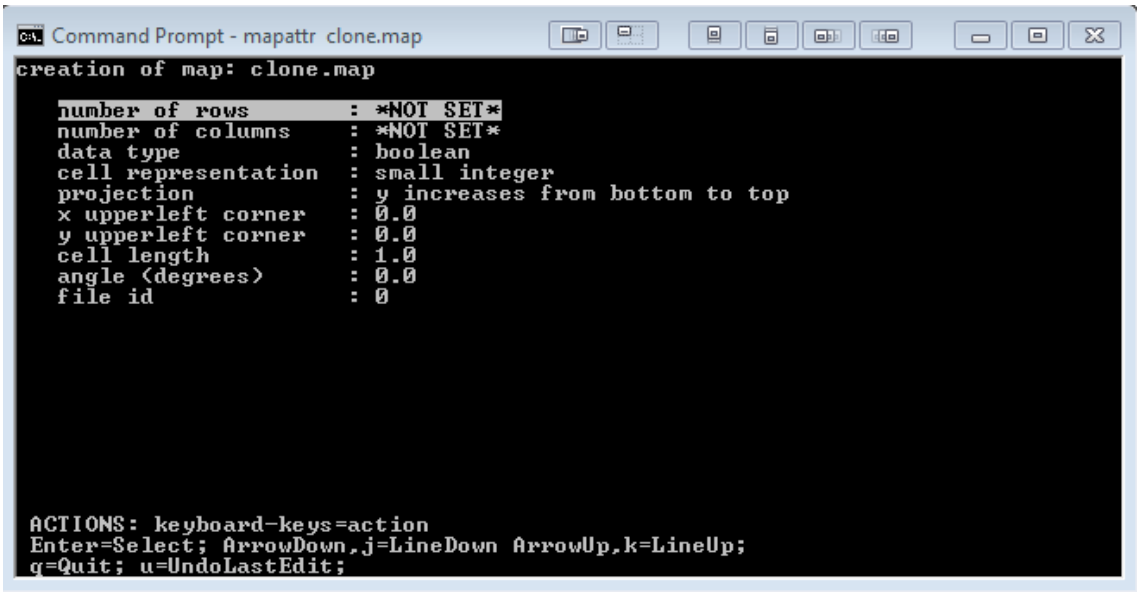

Figure 23: Command line menu for clone creation

Change the settings of the number of rows, number of columns, check if the y values in your model projection increase from bottom to top or from top to bottom, define the x and y values of the upperleft corner of your model's extent, and define the cell length (spatial resolution).

When all is set, press "*q*" to quit and then press "*y*" to confirm the map creation. Then drag the newly created map into QGIS to check if the map has the correct extent. Remember to set the CRS of the "clone.map" after dragging the map into QGIS.

5.3 DEM and Slope

Before you continue with the next steps, make sure that you have opened the "Processing Toolbox" in QGIS (see Figure 24). Next make sure that you select the "Advanced interface" from the "Processing Toolbox" (see Figure 25).

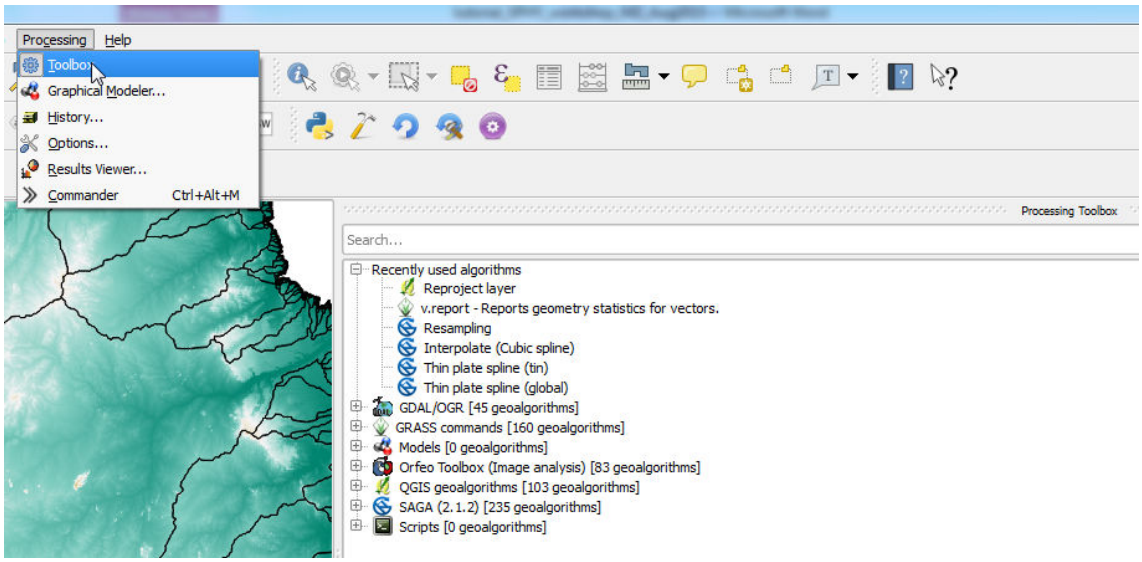

Figure 24: Opening the "Processing Toolbox".

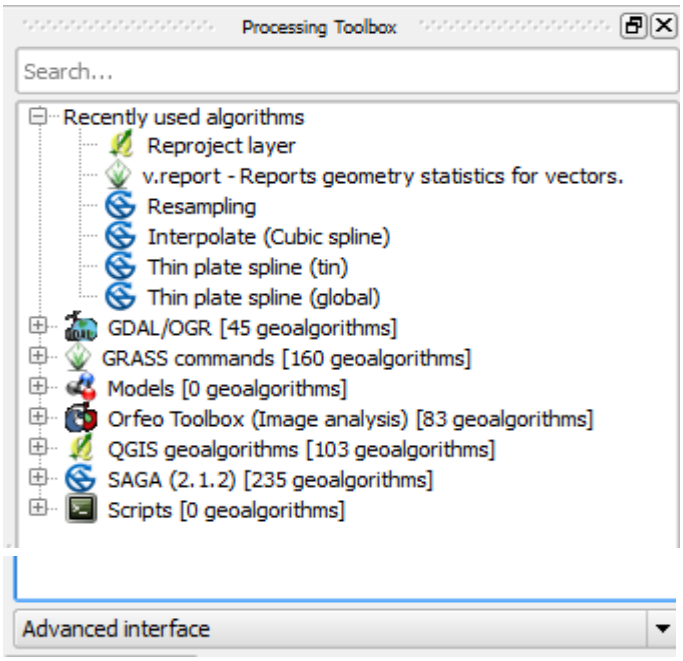

Figure 25: Selecting the "Advanced interface" in the "Processing Toolbox".

Use your own DEM or otherwise the DEM provided in the database. You will need to project your DEM in the model's projection and resample the DEM to model resolution and extent. You can do that using the following steps:

1. Drag the DEM inside the QGIS canvas;
2. Use the Warp tool in QGIS to reproject the DEM to the Coordinate Reference System (CRS) of your basin (EPSG:XXXXXX). This can be found under Raster → Projections → Warp (Reproject) (see Figure 26).
3. Within the Warp tool you need to select the "Input file", the "Output file", and the "Target SRS". The "Input file" is the layer that you need to reproject, which is in this case the **dem**. The "Output file" is the file to which you want to save the reprojected **dem** in GeoTiff format (*.tif). Give it a useful name and save it in a directory that is useful. In the example of Figure 27, the reprojected dem is saved under the **SPHY/input/** directory with the name: **dem_pr.tif**. Finally, it is important that you select the correct "Target SRS" (EPSG:XXXXX), which you defined in Section 5.1. In the example of Figure 27 it is EPSG:32737. Then click OK to do the reprojection. After the reprojection is finished click OK, and again OK, and finally Close.

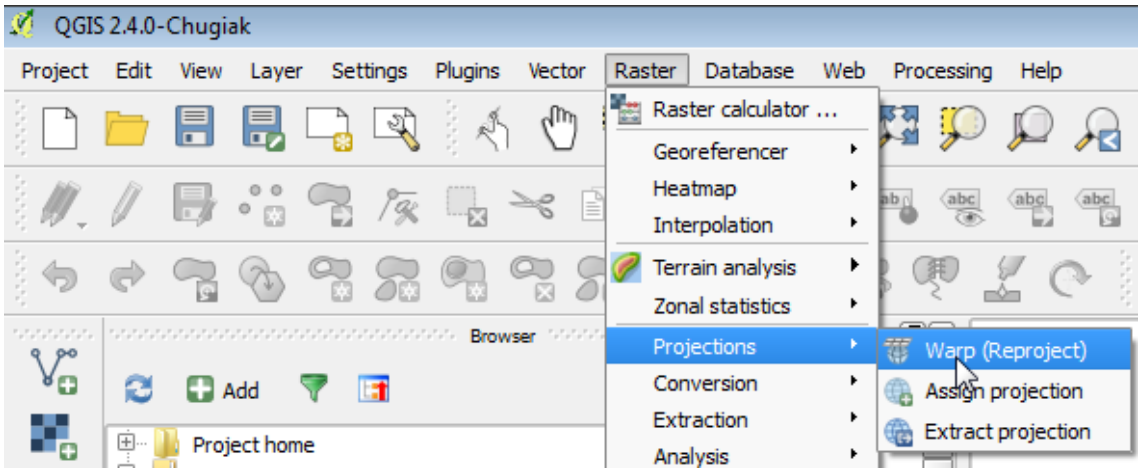

Figure 26: Warp tool

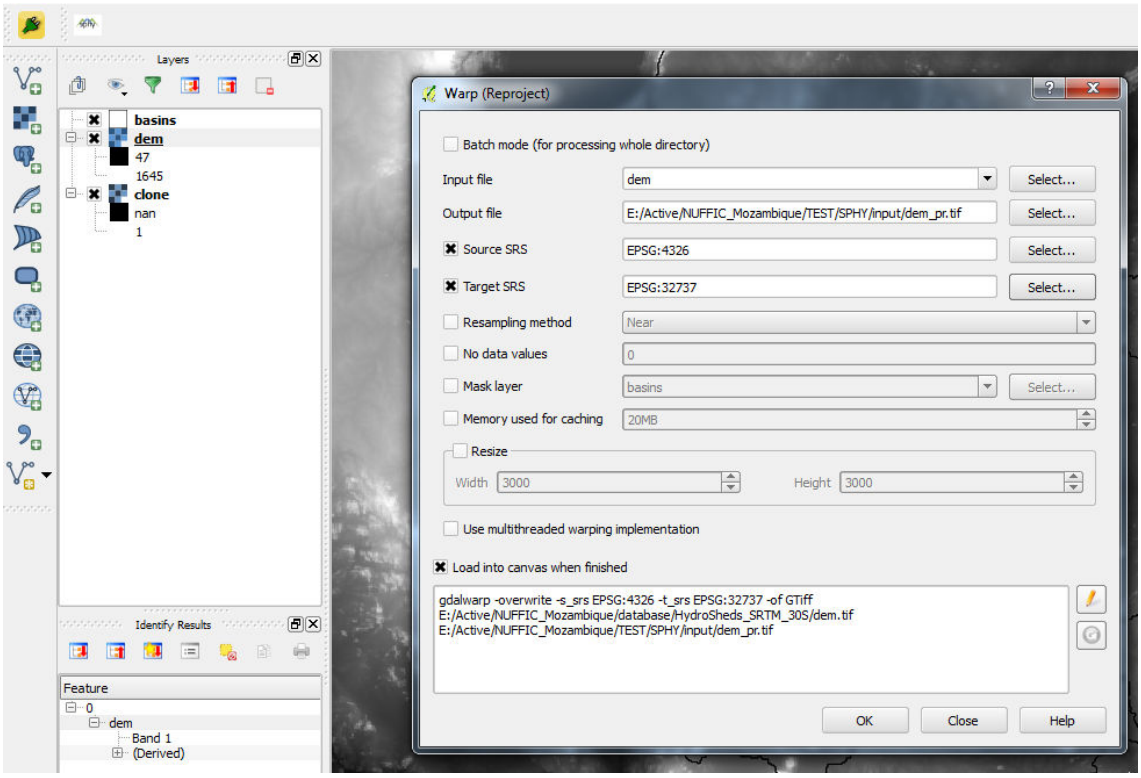

Figure 27: Setting the files and Source and Target SRS in the Warp Tool.

4. The next step involves resampling the projected dem from step 3) to the extent and spatial resolution of the **clone.map**. For this you need to type “resampling” in the “Processing Toolbox” search window (see Figure 28).

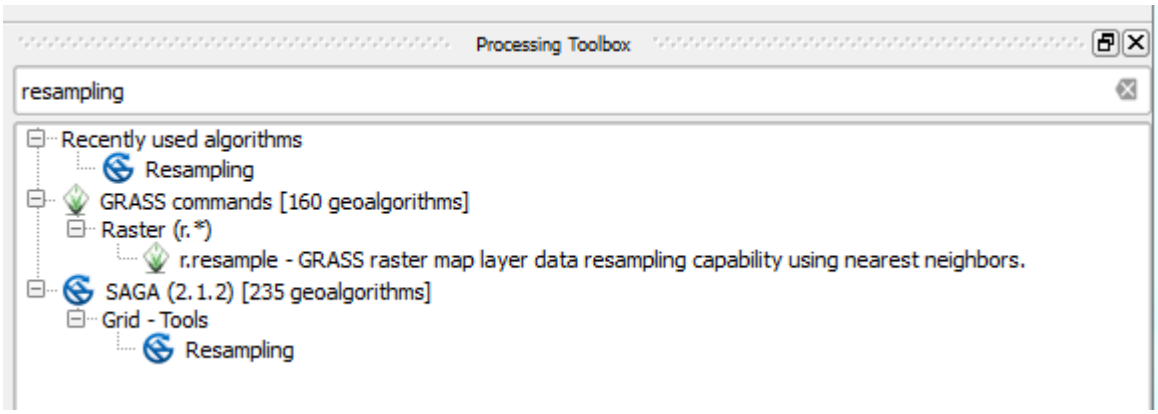

Figure 28: Selecting the Resampling tool in the Processing Toolbox.

5. Then double click “Resampling” under SAGA → Grid – Tools to open the Resampling tool as shown in Figure 29.
6. Within this tool you need to select the “Grid” file that you want to resample, the “Interpolation Methods” for scaling up and for scaling down, the “Output extent”, the “Cellsize”, and the “Grid” to which you want to save the resampled file. You also need to check or uncheck the “Preserve Data Type” option. You can use Table 9 to determine which options to set for the “Preserve Data Type”, and the “Interpolation Methods” for scaling up and for scaling down.

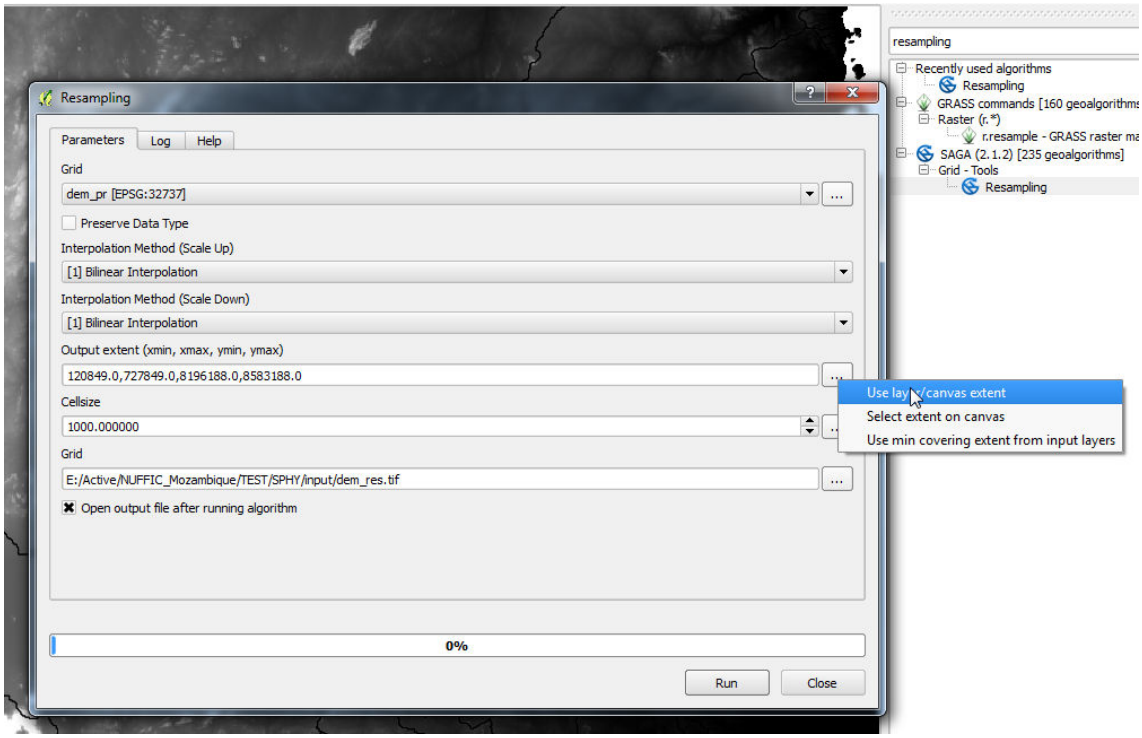

Figure 29: Setting the Resampling tool options.

Table 9: Resampling settings based on the layer data type.

Layer data type	Preserve Data Type	Interpolation Method (scale Up)	Interpolation Method (scale Down)	Example layer
Continuous	No	Bilinear	Bilinear	DEM
Classified	No	Majority	Nearest neighbor	Landuse

7. Since the projected dem that we want to resample is continuous data, we select “Bilinear Interpolation” for both the interpolation methods, and we uncheck the “Preserve Data Type” option. For the “Grid” we select the projected dem from step 3). For the “Output extent” we use the layer extent (see Figure 29) of the **clone.map**. For the “Cellsize” (=cell length) you can fill in the value that you determined in Section 5.1. Then, save the resampled Grid as GeoTiff in the “Grid” in a useful directory. In the example of Figure 29 the file is saved as **dem_res.tif** under the directory **SPHY/input/**. Finally, click Run to finish the resampling. If these steps are performed correctly, then your resampled **dem** should have the same extent and spatial resolution as your **clone.map**.
8. The final step involves converting the GeoTiff format to the PCRaster *.map format. This can be done using the Translate function under Raster → Conversion →Translate (Convert Format) (see Figure 30).

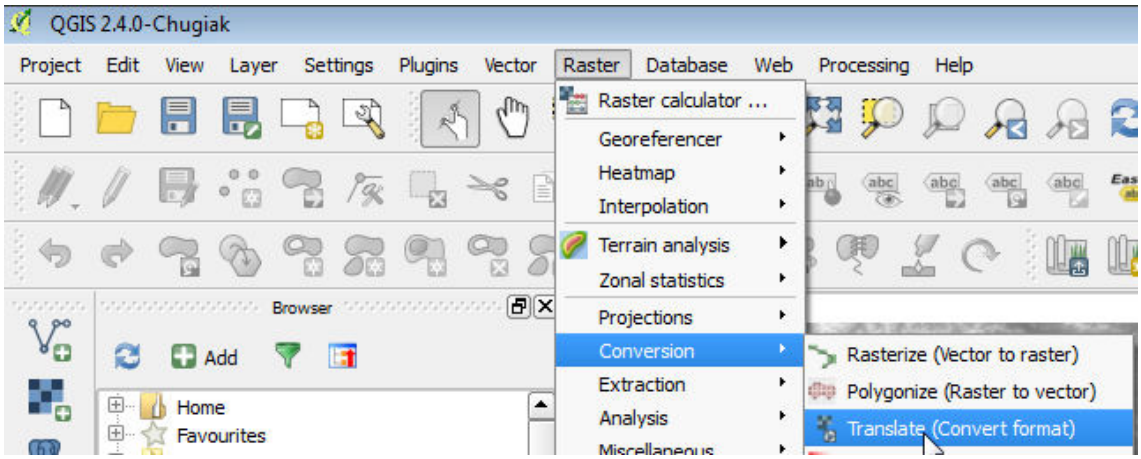

Figure 30: Translate tool (convert raster format)

9. In the "Translate" box (see Figure 31) make sure that you select the "Input Layer" (result from step 7) and set the "Output Layer". The "Output Layer" should be save as PCRaster Raster File format (*.map). In the example of Figure 32 we save it in the **SPHY\input** directory with the name **dem.map**. Finally click OK, and OK, and OK, and Close to finish this step.

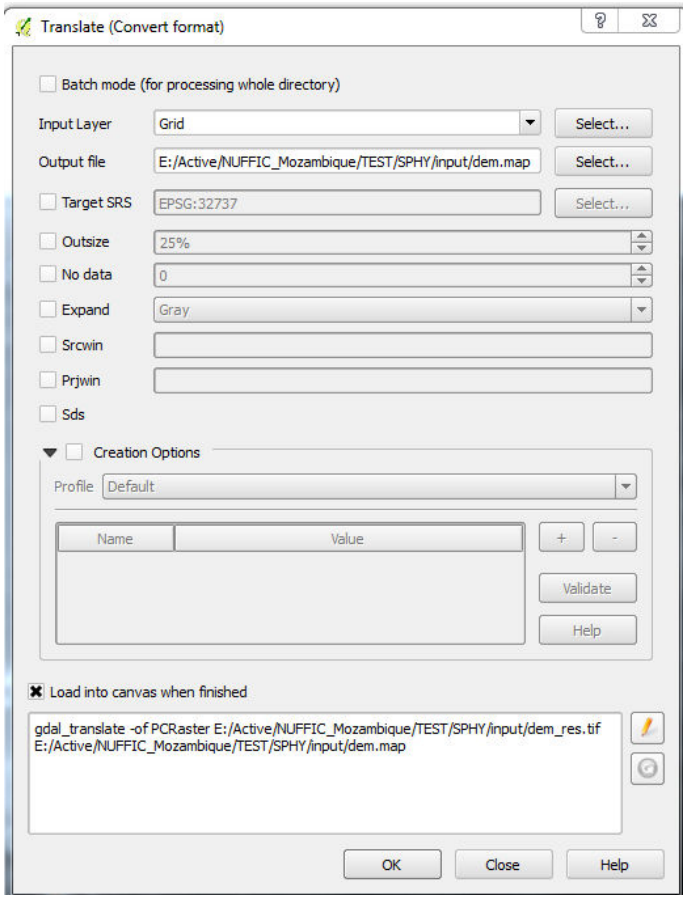

Figure 31: Setting the Translate options.

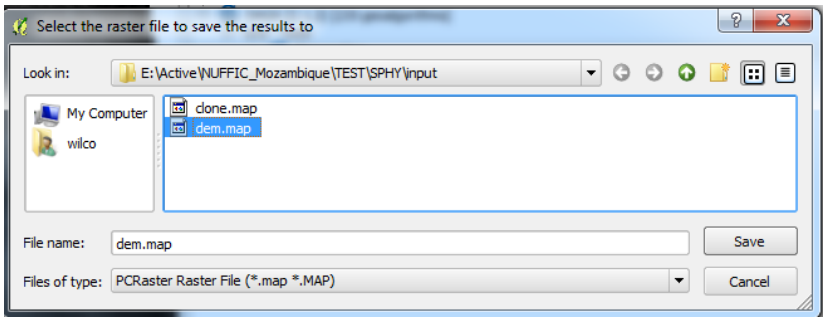

Figure 32: Saving the translated raster as a PCRaster Raster File (*.map).

Now you should have the DEM in the model resolution and extent and in PCRaster format.

The slope map can be derived from the DEM using the slope command. This can be done in the Windows Command line window by typing:

pcrcalc slope.map = slope(dem.map)

5.4 Delineate catchment and create local drain direction map

You can now use the DEM you created in the previous section to generate a local drain direction (LDD) map for your own model area.

To create a flow direction map (or local drain direction (LDD)), you can use the pcraster command lddcreate. Type the following command in the Windows Command line window:

pcrcalc ldd.map = lddcreate(dem.map, 1e31,1e31,1e31,1e31)

This command should also fill the sinks in the DEM to avoid that pits are generated in the depression in the DEM, which could hamper the water to flow to the basin's outlet. A good way to test if the LDD map is correct is to calculate for each cell how many cells are upstream. You can do this using the pcraster command accuflux. Type:

pcrcalc accuflux.map = accuflux(ldd.map,1)

Drag the newly generated accuflux.map to the QGIS canvas. Check if the stream network is complete, and all branches are connected to the outlet point.

If the generated LDD is not entirely correct and not all streams are connected toward the downstream outlet point, this happens because during the creation of the LDD map, pits have been generated where depressions in the landscape are present. More details on the LDD generation can be found in the PCRASTER online manual. There are multiple ways to overcome the problem of pit generation. The first and most easy option is to try this command in the Windows Command line window:

pcrcalc ldd.map = lddrepair(ldd.map)

If this does not solve the correct creation of the ldd.map, then you can try the following options:

- Test different values for the parameters in the lddcreate command
- Remove pits manually by changing the values for those cells.
- Use a map with the streams present in your study area and "burn" them into the DEM to force the other cells to drain in into them.

5.5 Preparing stations map and sub-basins.map

To prepare a stations map it is easiest to use a vector file with the point locations (for example a shapefile), to a PCRaster grid (.map file). You can create a new shapefile with points in QGIS under Layer → New → New Shapefile layer:

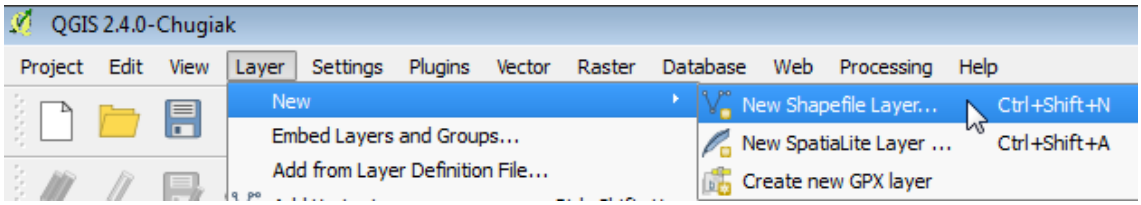

Figure 33: Create new shapefile layer

Make sure that you select "Point" and that the CRS corresponds (see Figure 34) with the EPSG that you have defined in Section 5.1. Finally click OK to create the New Shapefile Layer and save it under a useful name, for example **locations.shp**.

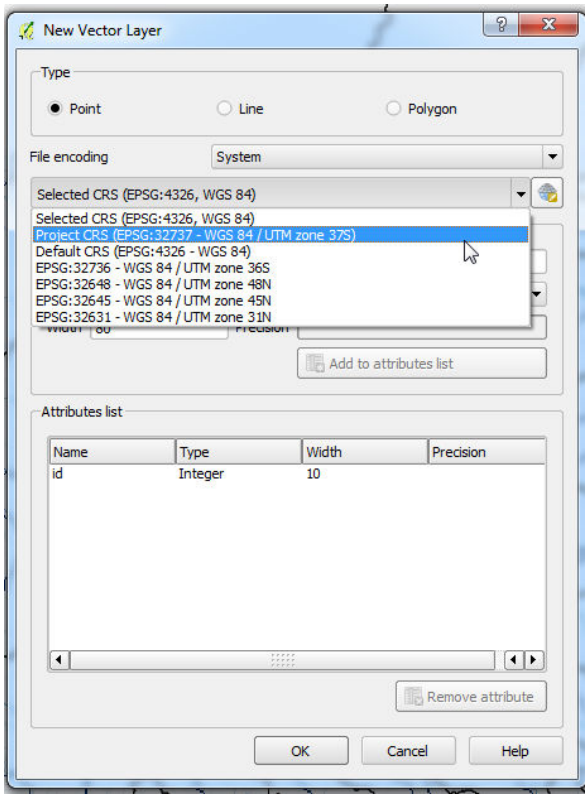

Figure 34: Setting the properties of the New Shapefile Layer.

The next step involves adding points to the Shapefile where you want the SPHY model to report time-series. Often these points correspond with the locations of discharge measurement stations. If you have an existing Shapefile of discharge measurement stations in your basin, then you can easily drag this file into QGIS to identify these locations. Now you can start adding points to the newly created Shapefile by following these steps:

1. Make sure the "locations" layer is selected. Then click "Toggle Editing" to change the layer to editing mode (see Figure 35).

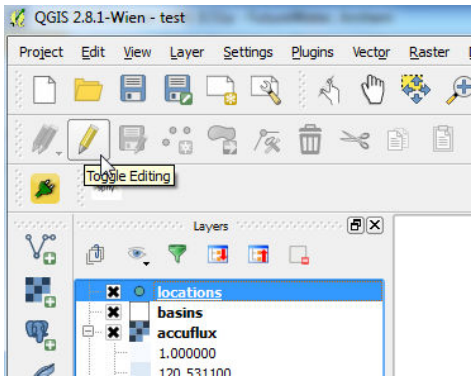

Figure 35: Toggle Editing for Shapefiles.

2. Then click the “Add Feature” option (see Figure 36). Now you can start adding points to the map where you want the SPHY model to create time-series output. The **accuflux.map** can help you determining if you are adding a point to the river network. Add as many as points as you like. For each point you need to provide an ID number. Start with ID 1, then ID 2, etc. In the example of Figure 37 we added 3 points to the “locations” layer.

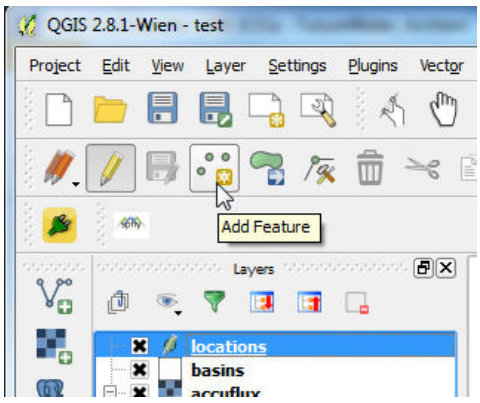

Figure 36: Add Feature for Shapefiles.

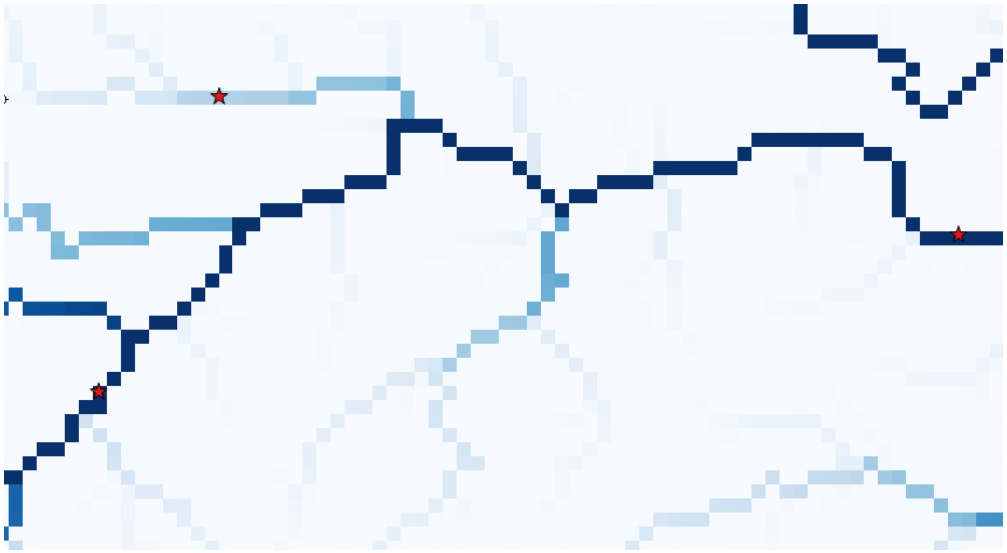

Figure 37: Adding points to the locations Shapefile layer using the accuflux.map.

3. If you are finished with adding the points, then you again can click the “Toggle Editing” button and Save your edits.

4. The next step involves converting the “locations” Shapefile layer to a raster layer. This can be done using the “v.to.rast.attribute” tool in QGIS under Processing Toolbox (see Figure 38).
5. Within this toolbox (Figure 39) set the “locations” layer as “Input vector layer”, make sure that the “id” column is selected, set the “GRASS region extent” by specifying the **clone.map** layer, and set the “GRASS region cellsize” as determined before. Finally, choose a “Rasterized” layer name (e.g. “locations.tif”) and click Run.
6. The final step again involves converting the resulting GeoTiff raster from step 5) to a PCRaster *.map format. This can be done using the Raster → Conversion → Translate tool (see Figure 30 and Figure 31). The only additional step required here is to click the “Edit” button (see Figure 40) and add the following syntax: **-ot Float32** (see Figure 41).
7. Finally click OK, and again OK, and again OK, and Close to finish the conversion.

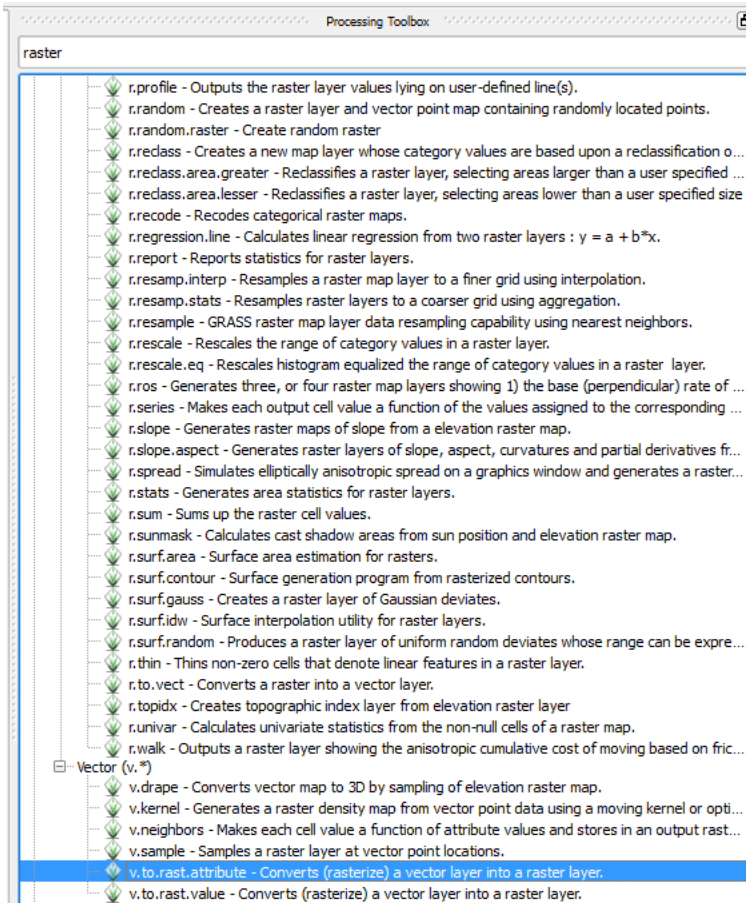

Figure 38: Selecting the v.to.rast.attribute tool from the Processing Toolbox.

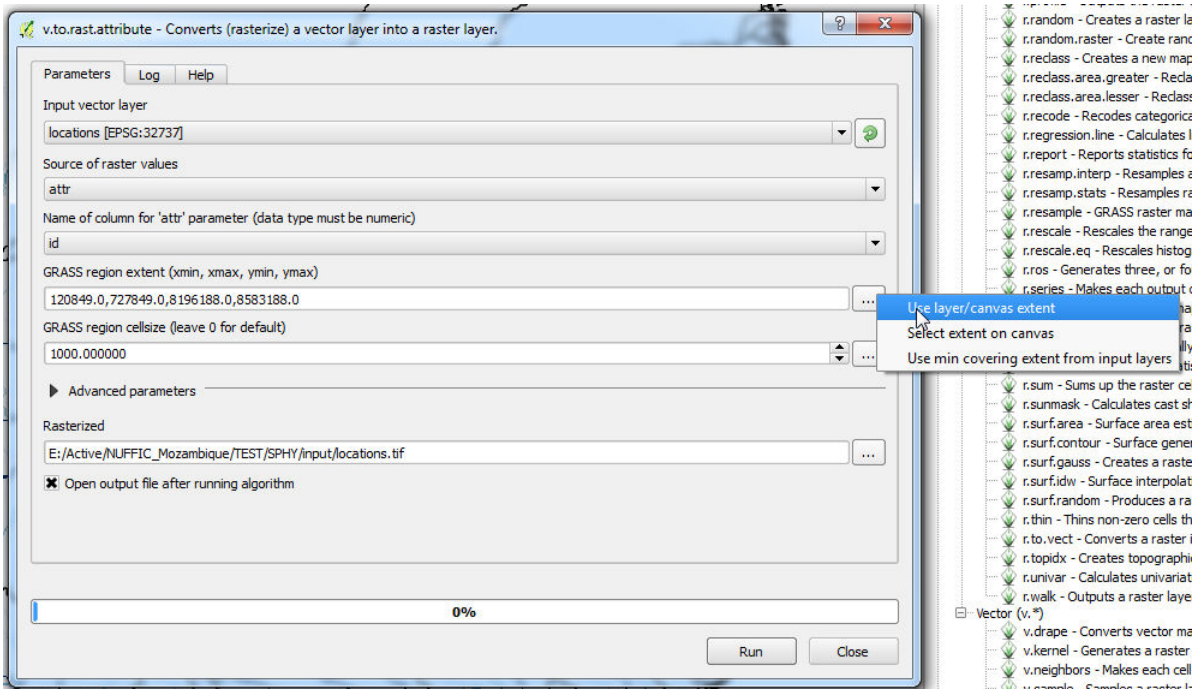

Figure 39: Setting the options in the v.to.rast.attribute tool.

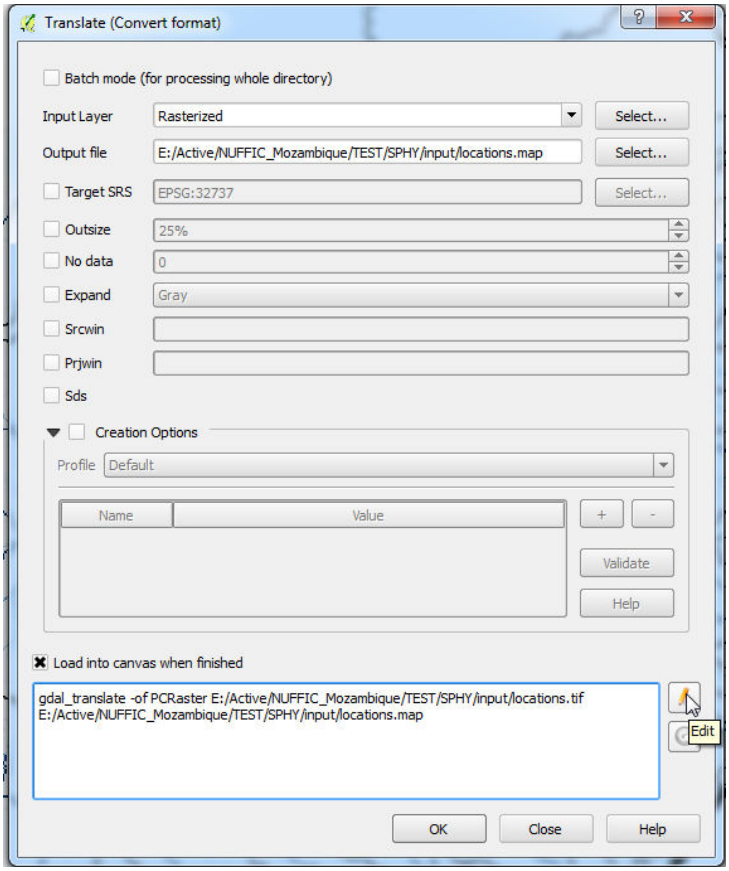

Figure 40: Editing the command for Translation.

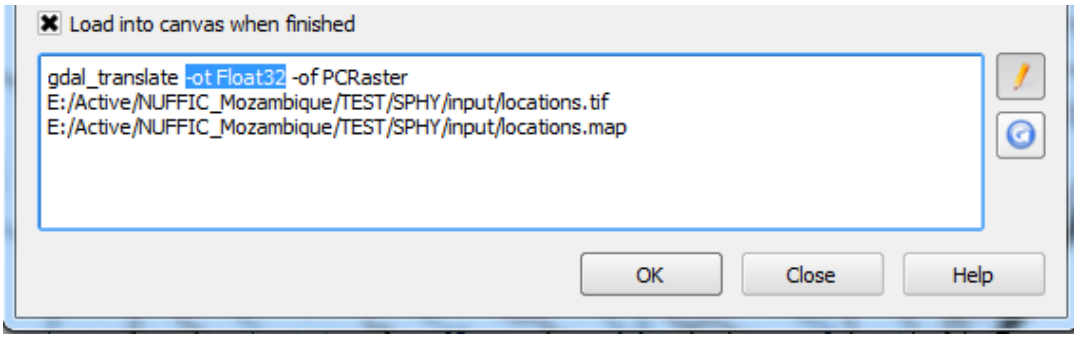

Figure 41: Adding the "-ot Float32" syntax to the command for Translation.

The resulting "locations.map" is of the Float32 data format (scalar). As can be seen Table 12 from it is required to have a nominal format for station files. This can be achieved by typing the following command in the Windows Command line:

pcrcalc locs.map = nominal(locations.map)

You can use **locs.map** and **ldd.map** to delineate the catchments of the points in **locs.map**. Use the subcatchment command for that:

pcrcalc catchment.map = subcatchment(ldd.map, locs.map)

5.6 Glacier table

The glacier table allows for a sub-grid representation of the glacier processes, by creating a grid at a finer resolution than the model grid. The glacier table is only required for the SPHY version higher 3.0 and higher. The glacier table contains eight elements (Table 10, Table 11).

Table 10: Elements of the glacier table

Name	Description
U_ID	Unique ID that is set at smaller spatial scale to account for sub grid heterogeneity in the glacier cover
MOD_ID	Individual ID of each cell of the SPHY model
GLAC_ID	ID of the individual glaciers in the model area, from the RGI inventory, from glacier ID 1 to X (with X being the maximum number of glacier)
MOD_H	Elevation of model ID cell
MOD_GLAC	Elevation of subgrid cell
DEBRIS	A flag (0 or 1) to identify if the cell is debris-covered
FRAC_GLAC	The fraction of the cell that is covered by glacier
ICE_DEPTH	Ice thickness of the cell

Table 11: Example of Glacier table

U_ID	MOD_ID	GLAC_ID	MOD_H	GLAC_H	DEBRIS	FRAC_GLAC	ICE_DEPTH
1	61122	89	3946	3946	1	0.002	0
2	61123	89	3928	3928	1	0.368	5.28
3	61124	89	3897	3897	1	0.189	7.04
4	61937	89	3950	3950	1	0.446	17.31
…	…	…	…	…	…	…	…

The suggested method to process these inputs can be summarized in 4 steps:

1- Create model vector grid (fishnet) (MOD_ID)
2- Intersect with the glacier outlines (GLAC_ID)

3- Create subgrid variability grid (U_ID)
4- Calculate elevation, glacier thickness, debris cover and glacier fraction (MOD_H, GLAC_H, DEBRIS, FRAC_GLAC, ICE_DEPTH)

Step 1: Create model vector grid (MOD_ID)

Open a model input raster file with the spatial extent and grid size in QGIS. This could be the clone.map, dem.map, latitude.map, or any raster model grid input. In the Vector Creation toolbox, select the “Create grid” tool. For the “Grid extent”, select the option “Calculate from layer”, and select the model raster. For “Horizontal spacing” and “Vertical spacing”, set the grid size of your model. Set name to “MOD_ID”.

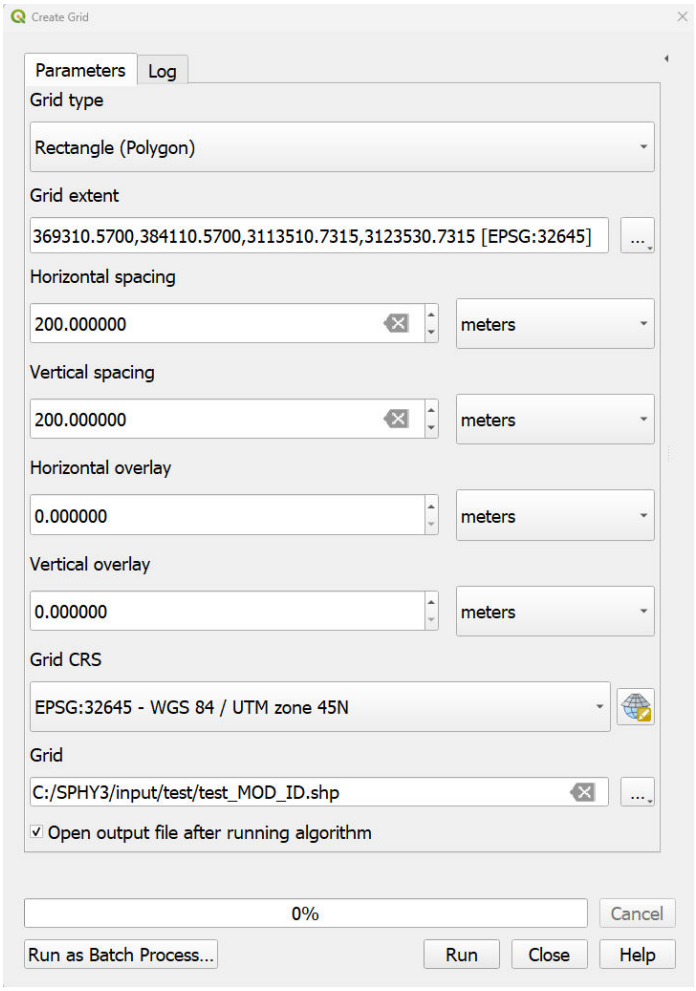

Figure 42: Creating Model_ID grid. Set the Horizontal and Vertical spacing to the model grid resolution.

This new vector layer contains polygons for each grid of your model domain, with value starting at 1 in the upper left corner. In the attribute table of your “MOD_ID” layer (right click on layer, select “Open attribute table” and deleted the attributes “left”, ‘”top”, ‘”right”, “bottom” to keep only the column “id” using the “Delete field” in the attribute table. Rename this attribute to “MOD_ID” using the tool “Rename field” in the Vector table toolbox. This is now your MOD_ID vector layer.

Step 2: Create GLAC_ID, MOD_H and glac_id.map,

Import the vector layer of glacier outline in the model area. This could come from manually digitized glacier areas or from an inventory like RGI7 (RGI 7.0 Consortium, 2023). Clip the glacier outline vector to the model area using the Vector Overlay toolbox “Clip” tool and reproject to the desired projection to

match your model projection (toolbox Vector general, “reproject layer” tool). Open the attribute table of the glacier outline layer and create a new attribute using the field calculator (Figure 43).

Using the GDAL toolbox, use the “Rasterize (vector to raster) to transform the GLAC_ID vector layer to a raster layer GLAC_ID” (Figure 44), followed by transforming to a .map file by using the PCRaster toolbox with ther tool “Convert to PCRaster format”, with format " NOMINAL” and named glac_id.map. This is an input for the glacier module in SPHY.

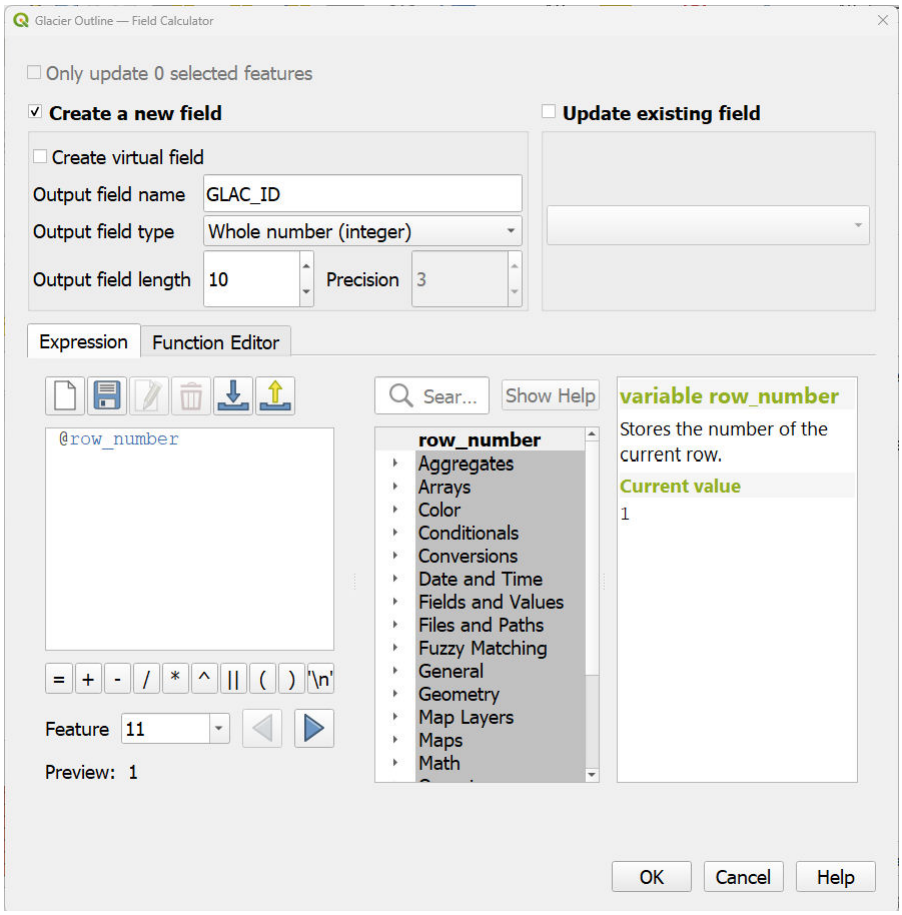

Figure 43: Create GLAC_ID attribute

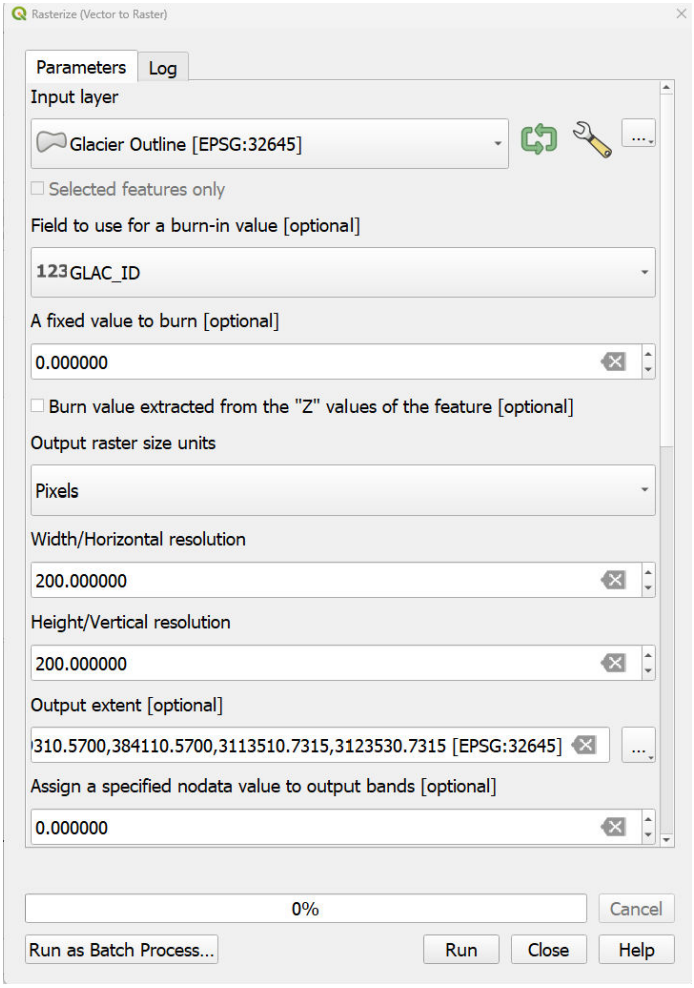

Figure 44: Rasterize glacier outline to obtain GLAC_ID map layer

You now need to intersect the MOD_ID grid with the glacier outline to obtain a grid that covers only the glacier area. To do so, intersect the glacier outline vector layer with the MODEL_ID grid (Vector overlay toolbox, “intersection” tool) with input layer “MOD_ID” and overlay layer “Glacier Outline”. The resulting layer (GLAC_ID) has two attributes: MOD_ID, from the original grid of the model domain, and “GLAC_ID”, the value of the individual glaciers (Figure 45).

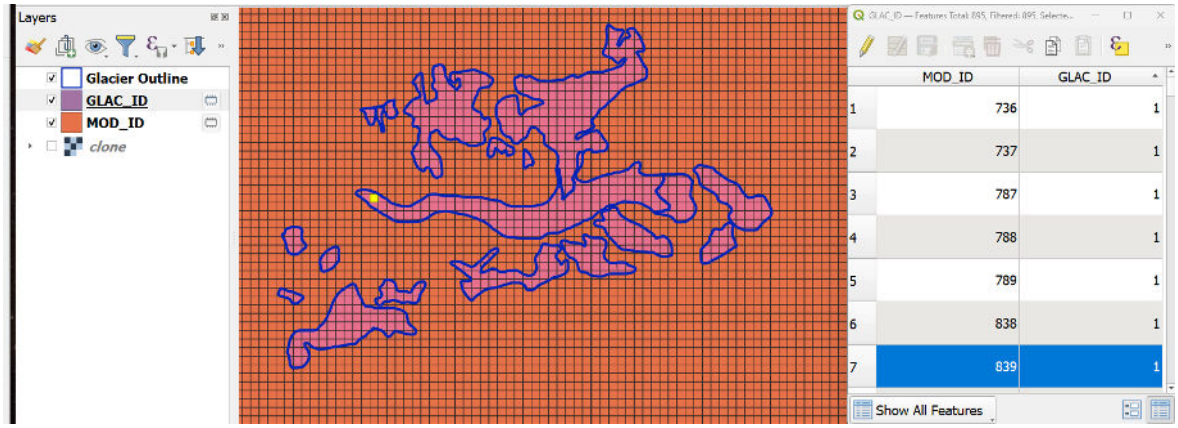

Figure 45: The GLAC_ID layer (in pink) with two attributes, GLAC_ID and MOD_ID as shown in the attribute table for a cell on the glacier toe highlighted in yellow, with MOD ID 839 and GLAC_ID 1. The orange grid in the background correspond to the model ID grid. At this stage, the cell size of the GLAC_ID and MOD_ID are the same size.

The elevation of the MOD_ID cells over the glacier area, which corresponds to the column “MOD_H” in the glacier table, can now be calculated. Import the DEM for your model area. Then, open the tool “Zonal Statistics” in the toolbox Raster analysis (Figure 46). For “Statistics to calculate”, select “mean”. Using the tool “rename field”, rename the resulting field to “MOD_H”. The resulting raster has three attributes: MOD_ID, GLAC_ID, MOD_H.

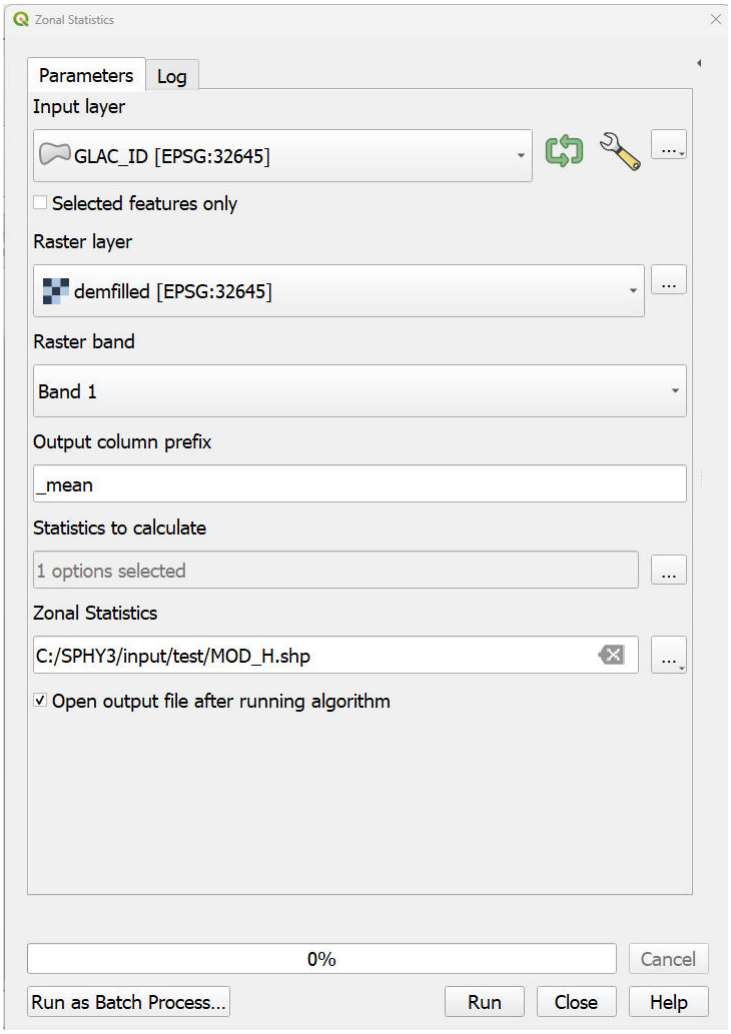

Figure 46: Using the "Zonal statistics" tool to calculate the elevation of the glacier grid

STEP 3: Create sub-grid variability (U_ID)

In this step, the smaller grid to account to calculate glacier processes at a higher resolution is created. Also, in some cases, some grid cells have 2 different glaciers within them, so we have to create a smaller gid system to account for this sub-grid variability (Figure 47). To create the U_ID (the smaller scale grid), follow the same steps as to create the MOD_ID (step 1), but select a smaller spatial resolution as needed. Create a new attribute, named U_ID, to start the values at 1 (same as Figure 43 to obtain GLAC_ID, using the rows as index). Keep only the attribute U_ID in the vector layer. Intersect the U_ID with the MOD_ID vector layer to keep only the smaller grid in the glacier area (using the “Intersect” tool). The resulting vector layer U_ID has four attributes: MOD_ID, GLAC_ID, MOD_H, and U_ID (Figure 48).

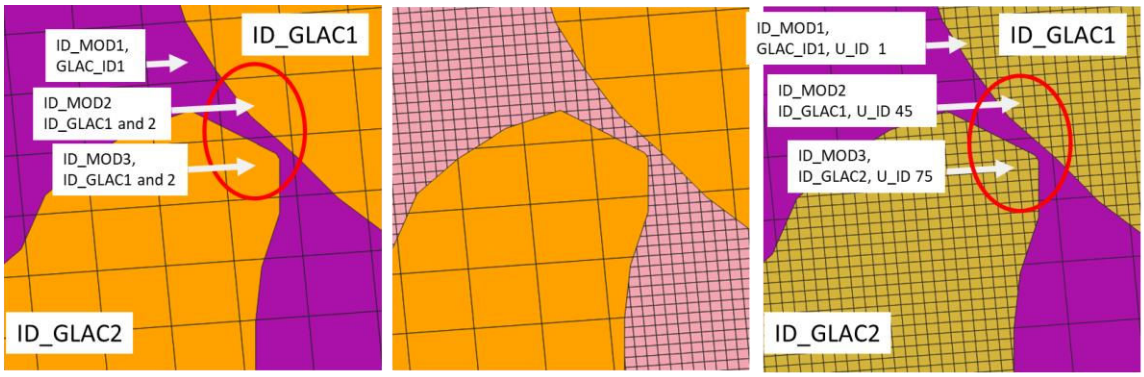

In purple is the background model ID grid, and in orange is the grid clipped to the glacier area.
For some cell, there is only 1 glacier ID per mod_ID cell, which works well (ex, ID_MOD1). In other cells, like ID_MOD2 and ID_MOD3, there are 2 different glacier per cell (ID_GLAC 1 and ID_GLAC2).

To address this, we create a smaller grid cell to account for sub-grid glacier heterogeneity – shown in pink.

This small grid is then clipped to the glacier outline (shown in yellow) and each small grid becomes a U_ID grid. Each cell of the smaller scale U_ID grid has a unique ID as well as the GLAC_ID and the MOD_ID.

Figure 47: The need for a smaller grid to account for the multiple glacier in one cell model cell

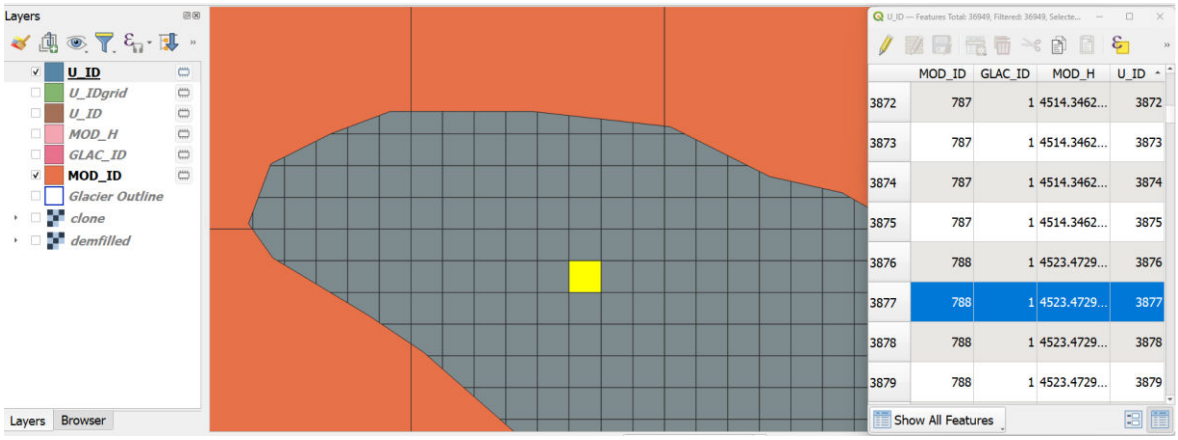

Figure 48: The U_ID layer showing the smaller scale grid cell, with the four attributes (MOD_ID, GLAC_ID, MOD_H, and U_ID). The orange background correspond to the larger MOD_ID grid.

Step 4: Calculate the elevation (U_MOD), glacier thickness (ICE_DEPTH), debris cover (DEBRIS) and glacier fraction (GLAC_FRAC):

In this step, we use the finer grid U_ID to calculate the values for each grid cell for the various dataset: elevation, the presence of debris, the ice thickness and the fraction glacier cover.

For the H_GLAC (elevation of the glacier), follow the same step as for the MOD_H calculation with the Zonal Statistics tool (Figure 46) using the original DEM, or an updated, finer resolution DEM is needed. Once again, you can rename the field to ICE_DEPTH and remove any attribute that are superfluous.

For glacier thickness (ICE_DEPTH), first load your ice thickness data into QGIS, then use the Zonal Statistic tool. If the ice thickness dataset is not continuous, or comes with multiple files, first merge into a single raster using toolbox SAGA Next Gen (needs to be downloaded as a plugin) raster tools with tool Mosaicking. Set “Overlapping areas” to “maximum”, and create a text file list with all the files to be used in the mosaic. Then using the “Zonal Statistics” tools to calculate the ice thickness for each U_ID

cell. Once again, you can rename the field to ICE_DEPTH and remove any attribute that are superfluous.

Some ice thickness might show as zero due to some misalignment of the product of a missing glacier in the ice thickness database. For these cases, you can set a fixed value as the glacier thickness. To do so, in the attribute table, open the field calculator, and for the ICE_DEPTH field, set the expression: if("ICE_DEPTH" is NULL, 25, " ICE_DEPTH") (Figure 49). Repeat the procedure for ice_depth values that are 0.

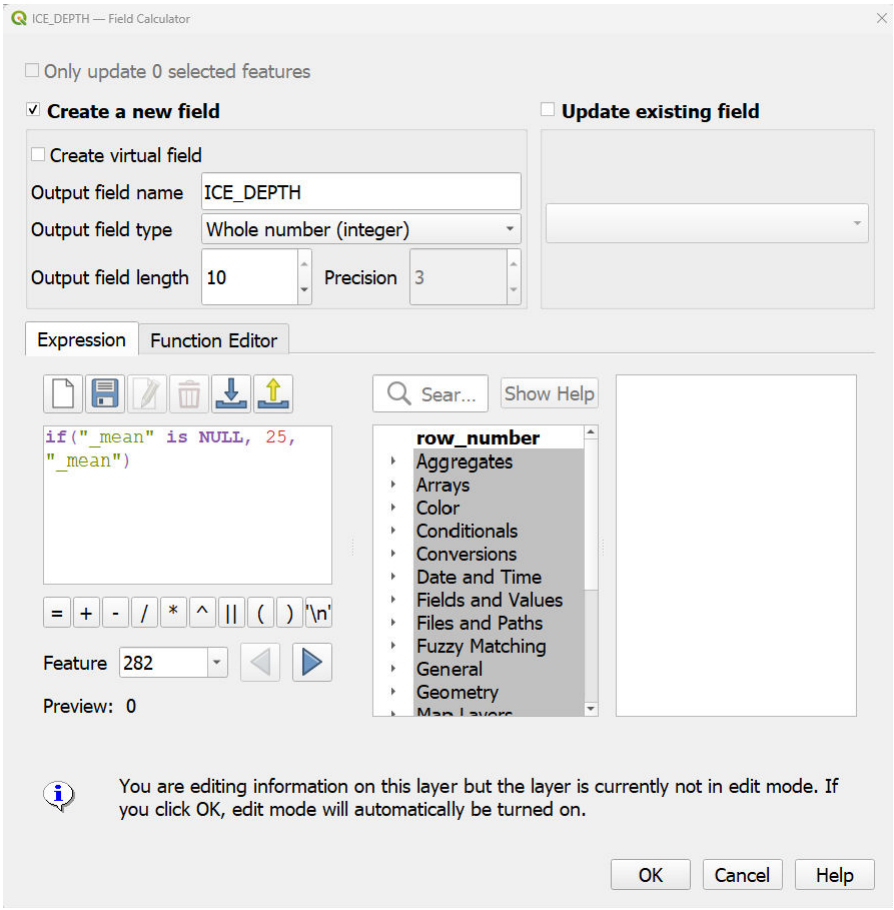

Figure 49: Replacing "NULL" values with ice thickness of 25 m, using the layer "_MEAN", THE OUTPUT OF THE Zonal Statistics tool.

For the debris-cover, import the debris-cover file, and if in vector format, rasterized using the GDAL toolbox, with tool "Rasterize (vector to raster), with the same resolution as the U_ID. Set the burn in value to 1. Using the "Zonal statistics" tool, calculate the presence of debris for each pixel of the U_ID vector. Using the field calculator, change the "NULL" values to "0" (if("_mean" is NULL, 0, "_mean"), as in Figure 49 DEBRIS should be either 0 or 1.

For the fraction of glacier cover in a given cell (GLAC_FRAC), first calculate the area of each polygon with the Vector Geometry toolbox, with tool "add geometry attribute". This adds area and perimeter to the attribute table. Based on the cell size, you can now calculate the ratio of the cell covered by the glacier. For example, in this case, if the cell is 25 x 25m, the maximum area is 625. Using the field calculator, you can divide the "area" attribute by the maximum area of each cell, giving you the glacier fraction. GLAC_FRAC should be higher than 0 and maximum of 1.

You should now have a vector layer with eight attributes corresponding to the the 8 columns needed in the glacier table, with the spatial resolution of the smaller grid capturing the glacier processes at higher resolution. Once all the calculation are done and checked, export file as .csv, organize column titles and order, and this gives you the glacier table needed as a SPHY input (Figure 50).

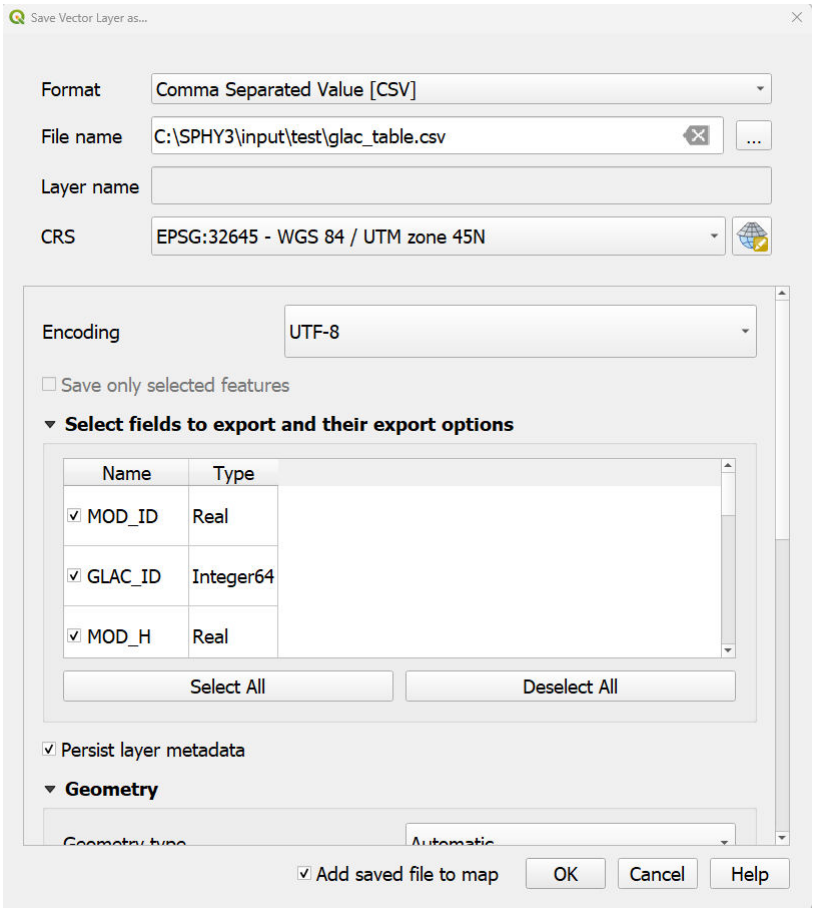

Figure 50: Exporting the vector layer as glac_table.csv.

5.7 Soil hydraulic properties

All processes related to the soil, such as infiltration, percolation, and capillary rise, are determined based on soil hydraulic properties. These include field capacity, saturated water content, wilting point, permanent wilting point and saturated hydraulic conductivity. These soil properties need to be provided for the root zone and the subzone. PCRaster maps can be provided for each of these properties, which can be obtained from field measurements or through the application of pedotransfer functions. The output from pedotransfer functions is also available at global scale, for instance from the Harmonized World Soil Database. The user may also provide soil texture (sand and clay fractions), organic matter and bulk density maps. Then, the soil hydraulic properties are determined through the application of pedotransfer functions (Saxton and Rawls, 2006). FutureWater developed a global map of soil hydraulic properties (HiHydroSoil, Simons et al., 2020)

5.8 Other static input maps

Similar as the DEM, you can reproject and resample other static model input data and convert them to PCRaster format maps using the reprojection and resampling functions in QGIS (step 1-9 from Section 5.3). Note that different data types are used for PCRaster maps. You can convert maps from one data

type to another using the command line functions boolean(), nominal(), ordinal(), scalar(), directional() or ldd(). For example to convert the scalar type landuse.map to a nominal landuse.map, type:

pcrcalc landuse_nominal.map = nominal(landuse.map)

For details regarding the input readers are referred to Appendix 2: Input and Output description.

Table 12: Data types used in SPHY.

data type	description attributes	domain	Example
boolean	boolean	0 (false), 1 (true)	suitable/unsuitable, visible/non visible
nominal	classified, no order	-2^{31} ... 2^{31}, whole values	soil classes, land use classes, discharge stations, administrative regions
Ordinal	classified, order	-2^{31} ... 2^{31}, whole values	succession stages, income groups
Scalar	continuous, lineair	-10^{37}...10^{37}, real values	elevation, temperature
directional	continuous, directional	0 to 2 pi (radians), or to 360 (degrees), and -1 (no direction), real values	aspect
Ldd	local drain direction to neighbour cell	1...9 (codes of drain directions)	drainage networks, wind directions

5.9 Meteorological forcing map series

Meteorological forcing map-series are series of input maps with the time step indicated in each filename. The filenames have a strict format with 8 characters before a dot (.), and three characters behind the dot. For example the average temperature maps can have the format **tavg0000.001**, **tavg0000.002**, etc. To generate forcing data you have two options:

1) interpolate point station data to grids at the model extent and resolution, and convert to PCRaster grid format.
2) resample existing gridded meteorological data products to model extent and resolution and convert to PCRaster grid format.
3) Depending on the number of time steps in your model you will probably need to write a script to batch this process and repeat it automatically for multiple time steps. A script like this can be created in any scripting language like for example Python or R. This procedure is automated in the SPHY preprocessor plugin but it only works with old version of QGIS (Terink et al., 2015b).

5.10 Open water evaporation

Open water evaporation is determined in reservoirs and lakes, only when the reservoir and/or lake module is used. To use the open water evaporation algorithm, the ETOpenWaterFLAG should be set to 1. Then the kc-value of open water evaporation should be provided, for which a value of 1.2 is commonly used. Finally, a map should be provided with the fraction per cell occupied by open water, in which each water body covers at least the lake or reservoir ID map. The latter is important for the calculation of the changes in lake and reservoir volume based on the open water evaporation estimates. The map is also used to partly switch-off the soil-water processes in the corresponding cells, depending on the fraction of the cell occupied by open water.

5.11 Dynamic vegetation module

Usage of the dynamic vegetation module in SPHY requires the availability of a time series of NDVI maps of the study area. These are prepared in the same format and naming conventions as the meteorological forcing map series (**ndvi0000.001**, etc.). NDVI maps for SPHY applications are typically derived from satellite-based sensors such as Sentinel-2, Landsat 8, or MODIS. As these satellites do not have daily overpass frequencies and clouds sometimes hinder the acquisition of high-quality images, daily NDVI maps are unlikely to be available. When SPHY is run with daily time steps, the model takes the most recent NDVI image until a new one is available from the forcing map series.

The NDVI is used within SPHY as an important indicator of vegetation vigor and amount of vegetation. It allows for dynamic simulation of processes such as evapotranspiration, interception and canopy storage. To couple NDVI with Kc (see Eq. 3), it is required to set maximum and minimum NDVI values that are linked to max and min Kc. Although these can be introduced as constant values, when modeling heterogeneous areas, it is recommended to provide the model with spatial maps of these constants varied by land use/land cover class. Similarly, $\mathrm{LAI}_{\max}$ (see Eq. 6) typically depends on vegetation type and should be listed in a lookup table. Table 14 shows the $\mathrm{LAI}_{\max}$ values for a certain number of vegetation types.

Table 13: Overview of mandatory inputs to the SPHY dynamic vegetation module

Parameter	Spatial map [SM], single value [SV]	For maps: Boolean [BO], Nominal [NO], Scalar [SC], Directional [DI]. For single value: Integer [IN] or Float [FL]	Unit	Parameter determination	Name
Kc_{max}	**SM**, SV	SC	[-]	Free	kcmax_utm.map
Kc_{min}	**SM**. SV	SC	[-]	Free	kcmin_utm.map
$NDVI_{max}$	**SM**, SV	SC	[-]	Observable	ndvimax.map
$NDVI_{min}$	**SM**, SV	SC	[-]	Observable	ndvimin.map
NDVI	SM	FL	[-]	Observable	forcing mapseries (ndvi0000.*)

Table 14: LAI_{max} values for different vegetation types (Sellers et al., 1996).

Vegetation type	LAI_{max} [-]
Broadleaf evergreen trees	7
Broadleaf deciduous trees	7
Mixed trees	7.5
Needleleaf evergreen trees	8
High latitude deciduous trees	8
Grass with 10 - 40% woody cover	5
Grass with <10% woody cover	5
Shrubs and bare soil	5
Moss and lichens	5
Bare	5
Cultivated	6

5.12 Soil erosion model input

The soil erosion model input can be found in the SEDIMENT module part of the config file and the subsequent 6 modules related to the different soil erosion models included in SPHY. The first step is to

select a soil erosion model, which include: MUSLE (1), MMF (2), INCA (3), SHETRAN (4), DHSVM (5) and HSPF (6).

The rock fraction map is used by MUSLE, MMF and SHETRAN, and can be ignored for the other 3 soil erosion models. The rock fraction map should be provided in the range between 0-1. Rock fraction values can be obtained by the empirical formulations by (Poesen et al., 1998), which determine rock fraction based on slope gradient.

The soil erosion models use the accumulated runoff to determine the detachment by runoff. This can lead to unrealistic soil erosion estimates in large study areas (>10 km^2), where water accumulates into channels and rivers. To prevent this from happening, the model can ignore the detachment by runoff in the channels and rivers with a predefined upstream area (km^2). To use this feature, the exclChannelsFLAG should be set to 1.

For all soil erosion models, the user needs to provide a table with land use specific model parameters, such as ground cover and plant height. These tables are linked with the land use map provided under LANDUSE.

In the following subsections the model specific parameters for the MMF soil erosion model are discussed. In the following subsections the model specific parameters are discussed.

5.12.1 MMF

The MMF soil erosion model requires the following land use specific model parameters (Table 15):

Table 15: MMF_table

Land use class	Plant height (PH)	Stem density (NV)	Stem diameter (D)	Canopy cover (CC)	Ground cover (GC)	No erosion	Tillage	Manning	No vege-tation
-99	1	2	3	4	5	6	7	8	9
1	10	0.5	0.4	0.8	0.65	0	0	0.2	0
2	0.5	4	0.2	0.5	0.5	0	0	0.1	0
3	0.2	20	0.15	0.3	0.35	0	1	0	1
…	…								…

Values for the plant height, stem density, stem diameter, canopy cover and ground cover can be found in Table 3 of (Morgan and Duzant, 2008) however, this table is mostly focused on British crop types and natural vegetation. Still, this table gives some suggestions for different vegetation types, which may help to define the model parameters for other geographical regions. The “no erosion” column is used to indicate with 0 (erosion) or 1 (no erosion) which land use types do not experience erosion, such as water and pavement. In case of no erosion, the sediment taken into transport will be set to 0. The “tillage” column indicates which land use classes apply tillage, i.e. 0 for no tillage and 1 for tillage. In case of tillage, the Manning’s roughness coefficient for soil will be obtained with the surface roughness parameter RFR (see below). The “Manning” column can be used to provide a Manning’s coefficient for irregular-spaced vegetation, commonly used for natural cover types (e.g. forest and shrubland). This column will be ignored in case it is set to 0, then the Manning’s roughness coefficient for vegetation will be determined with the stem density and stem diameter. When another value is provided, then the stem density and stem diameter will be ignored, and the provided Manning’s coefficient will be considered. Manning’s coefficient values for different vegetation conditions can be obtained from (Chow, 1959). The “no vegetation” column is used to ignore the Manning’s roughness coefficient for vegetation. This can be useful in the case of orchards, where the stem density is very low, which may result in unrealistic Manning’s roughness values.

Stem density, stem diameter and ground cover are commonly used for model calibration. Although literature values are available, these values are difficult to obtain for large study areas and may differ from agricultural field to agricultural field or from forest to forest.

The MMF soil erosion model may consider the changes of vegetation conditions in case of a sow-harvest cycle. In that case, the harvestFLAG should be set to 1. Another land use specific table (Table 16) should be provided, which gives the values for the period between harvest and sowing (commonly a fallow period):

Table 16: MMF_harvest

Land use class	Sowing	Harvest	Plant height (PH)	Stem density (NV)	Stem diameter (D)	Canopy cover (CC)	Ground cover (GC)	Tillage
-99	1	2	3	4	5	6	7	8
1	102	241	0.05	500	0.01	0.3	0.35	1
2	278	51	0	0	0	0	0	0
3	0	0	0	0	0	0	0	0
…			…					

In the "sowing" and "harvest" column the days of the year (julian dates) should be provided of sowing and harvest, respectively. The other columns are similar to the MMF_table, with the difference that the values provided here (MMF_harvest) will be considered in the period between harvest and sowing and the MMF_table between sowing and harvest. When a land use class does not consider the sowing-harvest cycle (e.g. natural vegetation or orchards/vineyards), the dates should be set to 0.

Intensity of the erosive rain can be provided with the PrecInt model parameter Morgan and Duzant (2008) propose 10 mm h^{-1} for temperate climates, 25 mm h^{-1} for tropical climates and 30 mm h^{-1} for strongly seasonal climates (e.g. Mediterranean, tropical monsoon). The intensity of the erosive precipitation will be based on the rainfall intensity obtained from the rainfall input when the infiltration excess surface runoff is used (i.e. Infil_excess = 1 in the INFILTRATION section of the config file).

The canopy cover values provided in the two tables, i.e. MMF_table and MMF_harvest, will be ignored when CanopyCoverLAIFlag is set to 1. In that case, the canopy cover will be obtained from the LAI determined by the vegetation module

The detachability of the soil by raindrop impact should be provided for each texture class. Based on laboratory experiments, (Quansah, 1982) proposed $K_c = 0.1$, $K_z = 0.5$ and $K_s = 0.3$ g J^{-1}. Similarly, the detachability of the soil by runoff should be provided for each texture class, for which (Quansah, 1982) proposed $DR_c = 1.0$, $DR_z = 1.6$ and $DR_s = 1.5$ g mm^{-1}.

The particle diameter of the three textural classes should be provided, for which Morgan and Duzant (2008) proposes $2 \cdot 10^{-6}$ m for clay, $60 \cdot 10^{-6}$ m for silt and $200 \cdot 10^{-6}$ m for sand.

The Manning's roughness coefficient for bare soil should be provided, for which a default value of 0.015 s $m^{1/3}$ should be a reasonable first estimate.

The flow depth of bare soil, in-field flow depth and flow depth for transport capacity are used in the immediate deposition calculation. Values of, respectively, 0.005, 0.1 and 0.25 m are taken as default values.

The surface roughness parameter RFR is used for land use classes that apply tillage (see MMF_table and MMF_harvest). Morgan and Duzant (2008) provide a table (Table IV) with common values for RFR for different ploughing equipment.

The sediment and flow density are commonly set to 2650 and 1000 kg m^{-3}, where the flow density may be slightly higher (e.g. 1100 kg m^{-3}) for runoff on hillslopes (Abrahams et al., 2001).

The fluid viscosity is nominally set to 0.001 kg m^{-1} s^{-1}, but often taken as 0.0015 to allow for the effects of the sediment in the flow (Morgan and Duzant, 2008).

Table 17: Model parameters

Model parameter	Model variable	Unit	Range/default
Plant height	PH	m	0-50
Stem density	NV	stems m^{-2}	0-10,000
Stem diameter	D	m	0-5
Canopy cover	CC	-	0-1
Ground cover	GC	-	0-1
No erosion		-	0 or 1
Tillage		-	0 or 1
Manning	n	s $m^{-1/3}$	0.01-0.5
No vegetation		-	0 or 1
Sowing		day of the year	1-365
Harvest		day of the year	1-365
Intensity of the erosive rain	I	mm h^{-1}	10-50
Detachability of the soil by raindrop impact	K_c, K_z, K_s	g J^{-1}	0.1, 0.5, 0.3
Detachability of the soil by runoff	DR_c, DR_z, DR_s	g mm^{-1}	1.0, 1.6, 1.5
Particle diameter	δ_c, δ_z, δ_s,	m	$2 \cdot 10^{-6}$, $60 \cdot 10^{-6}$, $200 \cdot 10^{-6}$
Bare soil Manning's roughness coefficient	n_{soil}	s $m^{-1/3}$	0.015
Flow depth bare soil	d_{bare}	m	0.005
Flow depth in field	d_{field}	m	0.1
Flow depth transport capacity	d_{TC}	m	0.25
Surface roughness parameter for tillage	RFR	cm m^{-1}	6-48
Sediment density	ρ_s	kg m^{-3}	2650
Flow density	ρ	kg m^{-3}	1100
Fluid viscosity	η	kg m^{-1} s^{-1}	0.0015

5.12.2 Soil erosion model calibration

Each soil erosion model can be calibrated in more or less the same way, except for the MUSLE model, which is typically applied without model calibration. All other models include several parameters that can be used for model calibration. Soil erodibility is often used for calibration, to adjust the soil erosion values for land use classes that do not have ground cover, such as frequently ploughed orchards. Model parameters related to ground cover and more specific vegetation characteristics (e.g. stem density, stem diameter and root cohesion) are subsequently used to calibrate the soil erosion for specific land use types. We refer to Eekhout and De Vente (2020) and Eekhout et al. (2021), in which all 6 soil erosion models were applied and give some specific recommendations for model calibration.

5.12.3 Soil erosion model output

The soil erosion models generate the sediment taken into transport as output, which is given in tons per cell. Soil erosion is frequently reported in ton ha^{-1} yr^{-1} or kg km^{-2} yr^{-1}, hence, post-processing of the output data is needed to determine the more commonly used soil erosion output formats.

The process-based soil erosion models (i.e. MMF, INCA, SHETRAN, DHSVM and HSPF) also allow to give the detachment by raindrop impact and detachment by runoff as output. Similar to the sediment taken into transport output, the detachment by raindrop impact and runoff are given in ton per cell. The MMF model also generates the immediate deposition as model output in ton per cell.

5.13 Sediment transport

The current sediment transport module only works with the MMF soil erosion model. The sediment transport module incorporates a transport capacity equation, which is forced by two model parameters, i.e. TC_β and TC_γ.(Prosser and Rustomji, 2000b) suggest adopting a value of 1.4 for both model parameters. However, these two parameters are frequently used for model calibration, for instance, when measured sediment concentration or reservoir sediment yield data are available.

The sediment transport equation includes a roughness factor, that accounts for the effect of vegetation on sediment transport. The roughness factor is based on the vegetation characteristics, as provided in the land use specific mmf_table. This approach works well for headwater areas, where overland flow can be assumed on the hillslopes. However, for larger study areas, where the water accumulates into river channels, the roughness factor has an important influence on how much sediment is transported downstream. When a river flows through a densely vegetated land use class (e.g. a forest), much of the sediment will be deposited. This might be unrealistic, because the sediment transport will be unaffected by the forest. Instead, the flow is mostly affected by the composition of the riverbed, which mostly consists of sand and/or gravel, with a lower Manning's roughness coefficient than the surrounding land use. To overcome this, the model may account for a much channel bed specific Manning's roughness value. To use this feature, the user needs to set manningChannelFLAG to 1. Next, the upstream area needs to be provided (upstream_km2), from which river channels are assumed. And finally, the channel Manning's roughness coefficient should be provided, which will override the Manning's values determined by the vegetation characteristics. Typical channel Manning's value can be obtained from (Chow, 1959).

When the reservoir module is used, the sediment transport module accounts for the trapping efficiency of the reservoirs. The trapping efficiency should be provided by the user in the TrapEffTab look-up table:

Table 18: TrapEffTab

Reservoir ID	Trapping efficiency (TE)
-99	1
1	0.95
2	0.89
3	0.64
…	…

In this table, the reservoir IDs should correspond to the ones used in the reservoir module. The trapping efficiency can be based on the equation by Brown (1943), which uses the reservoir capacity and drainage basin as input. This advanced sediment transport algorithm uses a 2-phase approach. In the first phase the transport capacity is applied to the sediment taken into transport, as determined by the soil erosion model. In the second phase the trapping efficiency determines the fraction of the sediment that is trapped by the reservoir and the fraction that is routed in downstream direction of the reservoir. When several

reservoirs are located in the same river (i.e. in sequence), this 2-phase approach is repeated as many times as reservoirs are present in the same river. The user needs to provide a table that indicates the order of the reservoirs, starting with the most upstream located reservoir (with a value of 0) down to the downstream located reservoirs. Figure 51 shows an example of the Segura River catchment, where the most upstream located reservoirs all have an order of 1 (but get a value of 0 I the ResOrder table). The order increases in downstream direction, where the last reservoir (which is actually the catchment outlet), has the highest order of 6 (5 in the ResOrder table).

Table 19: ResOrder

Reservoir ID	Trapping efficiency (TE)
1	0
2	0
3	0
4	1
5	1
6	2
…	…

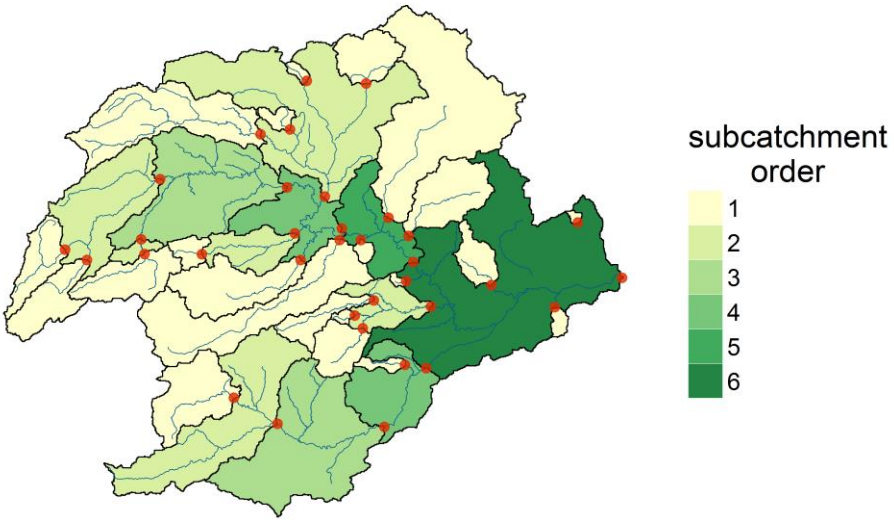

Figure 51: Example of the subcatchment order in the sediment transport routine.

The sediment transport model generates several model output variables. This includes sediment deposition (SedDep), which shows where and how much sediment is deposited in the study area, this output variable is usually stored as a yearly map. The sediment flux (SedFlux) shows how much sediment is transported through each grid cell. The sediment flux can be stored as a yearly map or can be obtained as a time series at the station cells. The latter can be used for model calibration when time series of sediment concentrations are available. In that case, the sediment transport should be divided by the discharge to get sediment concentration. When the reservoir module is used, the model can obtain sediment yield data at each of the reservoirs using the SedYld variable. Depending on the application, a time series or map output can be used.

Table 20: Model parameters

Model parameter	Model variable	Unit	Range/default
Model parameter TC_{β}	β	-	1-1.8
Model parameter TC_{γ}	γ	-	0.9-1.8

Manning channel flag		-	0 or 1
Upstream area for channel Manning		km^2	> cell area
Channel Manning's roughness value	n	$m\ s^{-1/3}$	0.025-0.15
Trapping efficiency	TE	-	0-1

6 Reporting and other utilities

6.1 Reporting

SPHY includes a large number of processes from which output can be generated through maps and timeseries. In a separate csv-file, the user can decide how map output should be generated for 50+ model variables. The csv-file has 6 columns: name, map, avg, timeseries, filename and comment. By default the csv-file is named reporting.csv and is located in the SPHY directory. To output variables other than the defaults, users must place the 'reporting.csv' file in the input directory, where SPHY map inputs are located.

The first column refers to the variable name in the model, which should not be changed.

In the second column the user can decide with which frequency the map (sum) output should be generated. This is usually used for water balance fluxes, such as precipitation, evapotranspiration and runoff and for sediment transport output:

Table 21: Variables from which the sum should be reported

Code	Meaning	Number of maps generated	Common application
Y	Yearly sum	Number years in simulation	Water balance fluxes, e.g. precipitation, evapotranspiration, runoff
M	Monthly sum	Number of months in simulation (12 * number of years)	Water balance fluxes, e.g. precipitation, evapotranspiration, runoff
D	Daily output	Each time step	Not commonly used
MS	Long-term average monthly sum	12 maps	Water balance fluxes, e.g. precipitation, evapotranspiration, runoff

The third column is used to indicate the output variables that should be generated as an average. This is most commonly used for water balance storage components, such as canopy, snow, rootzone and groundwater storage, but also for plant water stress:

Table 22: Variables from which the average should be reported

Code	Meaning	Number of maps generated	Common application
Y	Yearly average	Number years in simulation	Water balance storage components, e.g. snow, rootzone and groundwater storage
M	Monthly average	Number of months in simulation (12 * number of years)	Water balance storage components, e.g. snow, rootzone and groundwater storage
MA	Long-term monthly average	12 maps	Water balance storage components, e.g. snow, rootzone and groundwater storage

In the second and third column more than one output frequency can be selected, separated with a “+” symbol. For example, when the user wants to get yearly and long-term average monthly output, the following combination should be provided: “Y+MA”.

The fourth column is used to indicate which variables should generate timeseries. In this case only one frequency can be used, which is daily. The time series will be generated at the stations, hence, the output file will contain 1 column with the time steps of the simulation, which is followed by one column per station. Time series output is generally used for routed runoff and sediment flux:

Table 23: Variable from from which a time series should be reported

Code	Meaning	Number of time steps	Common application
D	Daily time series	All time steps	Routed runoff and sediment flux

In the fifth column the user can define the filename (prefix). The maximum number of characters used here depends on the number of simulated time steps. The file names of map output (sum or average maps) is constructed as follows, in case of daily (D) output: SedFlxD0.001, SedFlxD0.002, SedFlxD0.003, etc. In this case, a prefix of 6 characters is used (i.e. SedFlx). The model will crash in case the simulation has more than 9999 time steps. In case of more than 9999 time steps, a prefix of maximum 5 characters should be used (e.g. SedFlx): SdFlxD10.000, SdFlxD10.001, SdFlxD10.002, etc.

The sixth column provides comments for each of the model variables, such as the full name and the unit.

In column 2-4, NONE indicates that no output will be generated. Only model output will be generated for model variables that are considered during the simulation. So, if the reporting csv-table indicates that sediment flux should be reported, but the sediment transport module is not used (i.e. SedTransFLAG = 0 in the config file), then no sediment flux will be generated. For further details regarding the output files readers are referred to in Appendix 2: Input and Output description.

Table 24: Example of the reporting file

Model name	Map	Avg	Timeseries	Filename	Comment
TotPrec	Y	NONE	NONE	Prec	PRECIPITATION in mm
PlantStress	NONE	MA	NONE	Pws	PLANT WATER STRESS dimensionless
StorRootW	NONE	Y	NONE	Rootw	ROOTZONE STORAGE in mm
QallRAtot	NONE	NONE	D	QAll	ROUTED TOTAL RUNOFF in m3/s
…	…	…	…	…	…

Users can also add new variables to the reporting file. This can be done by adding a new line to the reporting file with a reference to the variable name in question. Keep in mind to use a filename that has less than 5 characters (column 5). In addition, the following code should be added to the SPHY model code below where the variable is defined:

self.reporting.reporting(self, pcr, 'VariableNameReporting', VariableNameModel)

The VariableNameReporting should coincide with the variable name of the first column of the reporting file. The VariableNameModel should coincide with the variable name in the model code. These two variable names could be identical, but this is up to the user.

6.2 NetCDF

The SPHY model allows the climate forcing to be read directly from NetCDF format instead of the usual daily pcraster map input. The model runs will slow down when using the NetCDF input, because each time step the data need to be interpolated onto the model grid. It is advisable to use the common pcraster map input instead of the NetCDF input in case model calibration, when many model runs are needed

using the same climate period and extent. However, the NetCDF input can be useful for scenario model runs, for instance in climate change impact assessments.

The NetCDF input can be used for precipitation and temperature (daily average, minimum and maximum). Here we explain how to use the NetCDF input for precipitation. All steps are identical for each of the three temperature inputs. To use the NetCDF input, first the precNetcdfFLAG should be set to 1. The location of the NetCDF file should be indicated under precNetcdf, which is the file with a *.nc extension. The input variable precNetcdfInput is used to give some specific information about how the data are stored in the NetCDF file, each element is separated by a comma (","). The information can be obtained by reading the NetCDF file in R, python or other programming or GIS software. The information includes:

- Variable name: This is the variable name given in the NetCDF file. For precipitation this can include precipitation, pcp, prec, etc. For temperature this can include temp, tavg, tmin, tmax, avgtemp, mintemp, maxtemp, etc.
- X-coordinate: The x-coordinate is a variable stored in the NetCDF file. In case of a rectangular grid, this is often indicated with an X, lon or longitude. In case of a rotated grid, this is often indicated with rlon.
- Y-coordinate: The y-coordinate is a variable stored in the NetCDF file. In case of a rectangular grid, this is often indicated with an Y, lat or latitude. In case of a rotated grid, this is often indicated with rlat.
- Interpolation method: There are three interpolation methods implemented: linear, cubic or nearest neighbor. It is suggested to use linear or nearest neighbor interpolation for precipitation input. The cubic interpolation technique may result in negative values in case the NetCDF input includes many 0 values and occasional positive values. For temperature input, all three interpolation techniques can be used. For more information on the difference between the three interpolation techniques see: https://docs.scipy.org/doc/scipy/reference/generated/scipy.interpolate.griddata.html
- Multiplication factor: Often precipitation NetCDF data are stored in mm * 10 format. This to decrease the size of the NetCDF files. In that case a multiplication factor of 0.1 is needed to let the model know that the data first need to be multiplied by 0.1 before further processing.
- EPSG code NetCDF file: The coordinate system of the NetCDF file is most likely different than the coordinate system of the SPHY project. The coordinate system of the NetCDF file is needed to make the necessary transformations of the coordinates and data interpolation. The coordinate system of the NetCDF file can be found by reading the NetCDF in R, python or any GIS program. Each coordinate system is linked to a so-called EPSG code. For instance, the WGS84 coordinate system has EPSG code 4326. In that case, the input will be "epsg:4326". The code can be found in the following website: https://spatialreference.org/. NetCDF file often use rotated pole coordinates. In that case the word "rotated" should be provided. To make the necessary transformations to the coordinates, the NetCDF script will search for the grid_north_pole_latitude and grid_north_pole_longitude variables inside the NetCDF file. Beware, the script will crash in case these variables do not exist.
- EPSG code model domain: Similar to the EPSG code of the NetCDF file, the same needs to be provided of the model domain. See above for information on how to find the EPSG code of the model domain.

The NetCDF input can be for example:

precNetcdfInput = pcp,X,Y,linear,0.1,epsg:25830,epsg:25830

- Variable name: pcp
- X-coordinate: X
- Y-coordinate: Y
- Interpolation method: linear

- Multiplication factor: 0.1
- EPSG code NetCDF file: epsg:25830
- EPSG code model domain: epsg:25830

precNetcdfInput = precipitation,rlon,rlat,linear,1,rotated,epsg:25830

- Variable name: precipitation
- X-coordinate: rlon
- Y-coordinate: rlat
- Interpolation method: linear
- Multiplication factor: 1
- EPSG code NetCDF file: rotated
- EPSG code model domain: epsg:25830

7 Bibliography

Abbott, M. B., Bathurst, J. C., Cunge, J. A., O'Connell, P. E., and Rasmussen, J.: An introduction to the European Hydrological System — Systeme Hydrologique Europeen, "SHE", 1: History and philosophy of a physically-based, distributed modelling system, J Hydrol (Amst), 87, 45–59, https://doi.org/10.1016/0022-1694(86)90114-9, 1986.

Abrahams, A. D., Li, G., Krishnan, C., and Atkinson, J. F.: A sediment transport equation for interrill overland flow on rough surfaces, Earth Surf Process Landf, 26, 1443–1459, https://doi.org/10.1002/esp.286, 2001.

ADB: Consultant's Report Regional Technical Assistance: Water and Adaptation Interventions in Central and West Asia, 2012.

Allen, R. G., Pereira, L. S., Raes, D., and Smith, M.: Crop evapotranspiration – Guidelines for computing crop water requirements, FAO Irrigation and drainage paper, 56, 1998a.

Allen, R. G., Pereira, L. S., Raes, D., and Smith, M.: Crop evapotranspiration: Guidelines for computing crop requirements, Irrigation and Drainage Paper No. 56, FAO, 300 pp., https://doi.org/10.1016/j.eja.2010.12.001, 1998b.

Allen, R. G., Pereira, L. S., Raes, D., and Smith, M.: Crop evapotranspiration: Guidelines for computing crop requirements, Irrigation and Drainage Paper No. 56, FAO, 300 pp., https://doi.org/10.1016/j.eja.2010.12.001, 1998c.

Andersson, E.: User guide to ECMWF forecast products. Version 1.1, 2013.

Ariathurai, R. and Arulanandan, K.: Erosion Rates of Cohesive Soils, Journal of the Hydraulics Division, 104, 279–283, 1978.

Bartholomeus, R. P., Witte, J.-P. M., van Bodegom, P. M., van Dam, J. C., and Aerts, R.: Critical soil conditions for oxygen stress to plant roots: Substituting the Feddes-function by a process-based model, J Hydrol (Amst), 360, 147–165, https://doi.org/10.1016/j.jhydrol.2008.07.029, 2008.

Bastiaanssen, W. G. M., Allen, R. G., Droogers, P., D'Urso, G., and Steduto, P.: Twenty-five years modeling irrigated and drained soils: State of the art, Agric Water Manag, 92, 111–125, https://doi.org/10.1016/j.agwat.2007.05.013, 2007.

Batjes, N. H., Dijkshoorn, J. A., van Engelen, V. W. P., Fischer, G., Jones, A., Montanarella, L., Petri, M., Prieler, S., Teixeira, E., Wilberg, D., and Shi, X.: Harmonized World Soil Database (version 1.1), Rome, Italy and Laxenburg, Austria, 2009.

Batjes, N. H., Dijkshoorn, J. A., van Engelen, V. W. P., Fischer, G., Jones, A., Montanarella, L., Petri, M., Prieler, S., Teixeira, E., and Shi, X.: Harmonized World Soil Database (version 1.2), 2012.

van Beek, L. P. H. and Bierkens, M. F. P.: The Global Hydrological Model PCR-GLOBWB: Conceptualization, Parameterization and Verification, Utrecht, 2008.

Beven, K.: Kinematic subsurface stormflow, Water Resour Res, 17, 1419–1424, https://doi.org/10.1029/WR017i005p01419, 1981.

Beven, K. and Germann, P.: Macropores and water flow in soils, Water Resour Res, 18, 1311–1325, https://doi.org/10.1029/WR018i005p01311, 1982.

Beven, K. J.: Rainfall-runoff modelling: the primer, John Wiley & Sons, Ltd, Chichester, UK, 1–457 pp., https://doi.org/10.1002/9781119951001, 2012.

Bicknell, B. R., Imhoff, J. C., Kittle, J. L., Donigian, A. S., and Johanson, R. C.: Hydrological Simulation Program – FORTRAN, 1993.

Bierkens, M. F. P. and van Beek, L. P. H.: Seasonal Predictability of European Discharge: NAO and Hydrological Response Time, J Hydrometeorol, 10, 953–968, https://doi.org/10.1175/2009JHM1034.1, 2009.

Biswas, A. K. and Tortajada, C.: Future Water Governance: Problems and Perspectives, Int J Water Resour Dev, 26, 129–139, https://doi.org/10.1080/07900627.2010.488853, 2010.
Bontemps, S., Defourny, P., Bogaert, E., Arino, O., Kalogirou, V., and Ramos Perez, J.: GLOBCOVER 2009. Products Description and Validation Report, 2011.
Bouwer, H.: Infiltration of Water into Nonuniform Soil, Journal of the Irrigation and Drainage Division, 95, 451–462, 1969.
Bracken, C., Rajagopalan, B., and Prairie, J.: A multisite seasonal ensemble streamflow forecasting technique, Water Resour Res, 46, https://doi.org/10.1029/2009WR007965, 2010.
Bramer, L. M., Hornbuckle, B. K., and Caragea, P. C.: How Many Measurements of Soil Moisture within the Footprint of a Ground-Based Microwave Radiometer Are Required to Account for Meter-Scale Spatial Variability?, Vadose Zone Journal, 12, 1–13, https://doi.org/10.2136/vzj2012.0100, 2013.
Brandt, C. J.: Simulation of the size distribution and erosivity of raindrops and throughfall drops, Earth Surf Process Landf, 15, 687–698, https://doi.org/10.1002/esp.3290150803, 1990.
Brown, C. B.: Discussion of Sedimentation in reservoirs, Proceedings of the American Society of Civil Engineers, 69, 1493–1500, 1943.
Brown, L. C. and Foster, G. R.: storm Erosivity Using Idealized Intensity Distributions, Transactions of the ASAE, 30, 0379–0386, https://doi.org/10.13031/2013.31957, 1987.
Brutsaert, W.: De Saint-Venant Equations Experimentally Verified, J. Hydr. Eng. Div.-ASCE, 97, 1387–1401, 1971.
Carlson, T. N. and Ripley, D. A.: On the relation between NDVI, fractional vegetation cover, and leaf area index, Remote Sens Environ, 62, 241–252, https://doi.org/10.1016/S0034-4257(97)00104-1, 1997.
Choi, K., Arnhold, S., Huwe, B., and Reineking, B.: Daily Based Morgan-Morgan-Finney (DMMF) Model: A Spatially Distributed Conceptual Soil Erosion Model to Simulate Complex Soil Surface Configurations, Water (Basel), 9, 278, https://doi.org/10.3390/w9040278, 2017.
Chow, V. Te: Open-Channel Hydraulics, McGraw-Hill Book Company, New York, US, 728 pp., https://doi.org/ISBN 07-010776-9, 1959.
Chow. V. Te: Open-Channel Hydraulics, McGraw-Hill Book Company, New York, US., 1959.
Clark, M. P., Slater, A. G., Rupp, D. E., Woods, R. A., Vrugt, J. A., Gupta, H. V., Wagener, T., and Hay, L. E.: Framework for Understanding Structural Errors (FUSE): A modular framework to diagnose differences between hydrological models, Water Resour Res, 44, https://doi.org/10.1029/2007WR006735, 2008.
Clark, M. P., Nijssen, B., Lundquist, J. D., Kavetski, D., Rupp, D. E., Woods, R. A., Freer, J. E., Gutmann, E. D., Wood, A. W., Brekke, L. D., Arnold, J. R., Gochis, D. J., and Rasmussen, R. M.: A unified approach for process-based hydrologic modeling: 1. Modeling concept, Water Resour Res, 51, 2498–2514, https://doi.org/10.1002/2015WR017198, 2015a.
Clark, M. P., Nijssen, B., Lundquist, J. D., Kavetski, D., Rupp, D. E., Woods, R. A., Freer, J. E., Gutmann, E. D., Wood, A. W., Gochis, D. J., Rasmussen, R. M., Tarboton, D. G., Mahat, V., Flerchinger, G. N., and Marks, D. G.: A unified approach for process-based hydrologic modeling: 2. Model implementation and case studies, Water Resour Res, 51, 2515–2542, https://doi.org/10.1002/2015WR017200, 2015b.
Contreras, S., Hunink, J., and Baille, A.: Building a Watershed Information System for the Campo de Cartagena basin (Spain) integrating hydrological modeling and remote sensing, Wageningen, 2014.
Dai, A.: Drought under global warming: a review, WIREs Climate Change, 2, 45–65, https://doi.org/10.1002/wcc.81, 2011.

van Dam, J. C., Huygen, J., Wesseling, J. G., Feddes, R. A., Kabat, P., van Walsum, P. E. V., Groenendijk, P., and van Diepen, C. A.: Theory of SWAP version 2.0; simulation of water flow, solute transport and plant growth in the soil-water-atmosphere-plant environment, Tech. rep., 1997.

Deb S.K. and Shukla M.K.: Soil hydrology, land use and agriculture: measurement and modelling, edited by: Shukla, M. K., CAB International, UK, https://doi.org/10.1079/9781845937973.0000, 2011.

Doten, C. O., Bowling, L. C., Lanini, J. S., Maurer, E. P., and Lettenmaier, D. P.: A spatially distributed model for the dynamic prediction of sediment erosion and transport in mountainous forested watersheds, Water Resour Res, 42, https://doi.org/10.1029/2004WR003829, 2006.

Droogers, P. and Aerts, J.: Adaptation strategies to climate change and climate variability: A comparative study between seven contrasting river basins, Physics and Chemistry of the Earth, Parts A/B/C, 30, 339–346, https://doi.org/10.1016/j.pce.2005.06.015, 2005.

Droogers, P. and Bouma, J.: Simulation modelling for water governance in basins, Int J Water Resour Dev, 30, 475–494, https://doi.org/10.1080/07900627.2014.903771, 2014.

Droogers, P. and Immerzeel, W. W.: Wat is het beste model?, H2O Tijdschrift voor watervoorziening en waterbeheer, 38–41, 2010.

Droogers, P., Immerzeel, W. W., Terink, W., Hoogeveen, J., Bierkens, M. F. P., van Beek, L. P. H., and Debele, B.: Water resources trends in Middle East and North Africa towards 2050, Hydrol Earth Syst Sci, 16, 3101–3114, https://doi.org/10.5194/hess-16-3101-2012, 2012.

EEA: EU-DEM layers, Copernicus data and information funded by the European Union, 2014.

Eekhout, J. P. and De Vente, J.: How soil erosion model conceptualization affects soil loss projections under climate change, Progress in Physical Geography: Earth and Environment, 44, 212–232, https://doi.org/10.1177/0309133319871937, 2020.

Eekhout, J. P. C., Terink, W., and de Vente, J.: Assessing the large-scale impacts of environmental change using a coupled hydrology and soil erosion model, Earth Surface Dynamics, 6, 687–703, https://doi.org/10.5194/esurf-6-687-2018, 2018.

Eekhout, J. P. C., Millares-Valenzuela, A., Martínez-Salvador, A., García-Lorenzo, R., Pérez-Cutillas, P., Conesa-García, C., and de Vente, J.: A process-based soil erosion model ensemble to assess model uncertainty in climate-change impact assessments, Land Degrad Dev, 32, 2409–2422, https://doi.org/10.1002/ldr.3920, 2021.

Endrizzi, S., Dall' Amico, M., Gruber, S., and Rigon, R.: GEOtop Users Manual. User Manual Version 1.0, Zurich, 2011.

Endrizzi, S., Gruber, S., Dall'Amico, M., and Rigon, R.: GEOtop 2.0: simulating the combined energy and water balance at and below the land surface accounting for soil freezing, snow cover and terrain effects, Geosci Model Dev, 7, 2831–2857, https://doi.org/10.5194/gmd-7-2831-2014, 2014.

EPA: Modeling at EPA, http://www.epa.gov/epahome/models.html, 2014.

Epema, G. F. and Riezebos, H. T.: Fall velocity of waterdrops at different heights as a factor influencing erosivity of simulated rain, in: Rainfall simulation runoff and soil erosion, edited by: de Ploey, J., 1–17, 1983.

Essery, R., Morin, S., Lejeune, Y., and B Ménard, C.: A comparison of 1701 snow models using observations from an alpine site, Adv Water Resour, 55, 131–148, https://doi.org/10.1016/j.advwatres.2012.07.013, 2013.

FAO: CropWater Information, http://www.fao.org/nr/water/cropinfo.html, 2013.

Farr, T. G., Rosen, P. A., Caro, E., Crippen, R., Duren, R., Hensley, S., Kobrick, M., Paller, M., Rodriguez, E., Roth, L., Seal, D., Shaffer, S., Shimada, J., Umland, J., Werner, M., Oskin,

M., Burbank, D., and Alsdorf, D.: The Shuttle Radar Topography Mission, Reviews of Geophysics, 45, RG2004, https://doi.org/10.1029/2005RG000183, 2007.
Feddes, R. A., Kowalik, P. J., and Zaradny, H.: Simulation of field water use and crop yield., Pudoc, Wageningen, 1978.
Finger, D., Pellicciotti, F., Konz, M., Rimkus, S., and Burlando, P.: The value of glacier mass balance, satellite snow cover images, and hourly discharge for improving the performance of a physically based distributed hydrological model, Water Resour Res, 47, https://doi.org/10.1029/2010WR009824, 2011.
Foglia, L., Hill, M. C., Mehl, S. W., and Burlando, P.: Sensitivity analysis, calibration, and testing of a distributed hydrological model using error-based weighting and one objective function, Water Resour Res, 45, https://doi.org/10.1029/2008WR007255, 2009.
van Genuchten, M. Th.: A Closed-form Equation for Predicting the Hydraulic Conductivity of Unsaturated Soils, Soil Science Society of America Journal, 44, 892–898, https://doi.org/10.2136/sssaj1980.03615995004400050002x, 1980.
Gill, M. A.: Flood routing by the Muskingum method, J Hydrol (Amst), 36, 353–363, https://doi.org/10.1016/0022-1694(78)90153-1, 1978.
Gopalan, K., Wang, N.-Y., Ferraro, R., and Liu, C.: Status of the TRMM 2A12 Land Precipitation Algorithm, J Atmos Ocean Technol, 27, 1343–1354, https://doi.org/10.1175/2010JTECHA1454.1, 2010.
Govers, G.: Misapplications and Misconceptions of Erosion Models, in: Handbook of Erosion Modelling, edited by: Morgan, R. P. C. and Nearing, M. A., John Wiley & Sons, Ltd, Chichester, UK, 117–134, https://doi.org/10.1002/9781444328455.ch7, 2011.
Goward, S. N. and Huemmrich, K. F.: Vegetation canopy PAR absorptance and the normalized difference vegetation index: An assessment using the SAIL model, Remote Sens Environ, 39, 119–140, https://doi.org/10.1016/0034-4257(92)90131-3, 1992.
Grantz, K., Rajagopalan, B., Clark, M., and Zagona, E.: A technique for incorporating large-scale climate information in basin-scale ensemble streamflow forecasts, Water Resour Res, 41, https://doi.org/10.1029/2004WR003467, 2005.
Hall, D. K., Riggs, G. A., Salomonson, V. V, DiGirolamo, N. E., and Bayr, K. J.: MODIS snow-cover products, Remote Sens Environ, 83, 181–194, https://doi.org/10.1016/S0034-4257(02)00095-0, 2002.
Hansen, E. and Engelund, F.: A Monograph on Sediment Transport in Alluvial Streams, Copenhagen, Denmark, 1967.
Hargreaves, G. H. and Samani, Z. A.: Reference Crop Evapotranspiration from Temperature, Appl Eng Agric, 1, 96–99, https://doi.org/10.13031/2013.26773, 1985.
Heber Green, W. and Ampt, G. A.: Studies on Soil Phyics., J Agric Sci, 4, 1–24, https://doi.org/10.1017/S0021859600001441, 1911.
HEC: Hydrologic Engineering Center (HEC) computer software for hydrologic engineering and planning analysis, http://www.hec.usace.army.mil/software/, 2014.
Hengl, T., Mendes de Jesus, J., Heuvelink, G. B. M., Ruiperez Gonzalez, M., Kilibarda, M., Blagotić, A., Shangguan, W., Wright, M. N., Geng, X., Bauer-Marschallinger, B., Guevara, M. A., Vargas, R., MacMillan, R. A., Batjes, N. H., Leenaars, J. G. B., Ribeiro, E., Wheeler, I., Mantel, S., and Kempen, B.: SoilGrids250m: Global gridded soil information based on machine learning, PLoS One, 12, e0169748, https://doi.org/10.1371/journal.pone.0169748, 2017.
Herrera, S., Fernández, J., and Gutiérrez, J. M.: Update of the Spain02 gridded observational dataset for EURO-CORDEX evaluation: assessing the effect of the interpolation

methodology, International Journal of Climatology, 36, 900–908, https://doi.org/10.1002/joc.4391, 2016.
Hersbach, H., Bell, B., Berrisford, P., Hirahara, S., Horányi, A., Muñoz-Sabater, J., Nicolas, J., Peubey, C., Radu, R., Schepers, D., Simmons, A., Soci, C., Abdalla, S., Abellan, X., Balsamo, G., Bechtold, P., Biavati, G., Bidlot, J., Bonavita, M., De Chiara, G., Dahlgren, P., Dee, D., Diamantakis, M., Dragani, R., Flemming, J., Forbes, R., Fuentes, M., Geer, A., Haimberger, L., Healy, S., Hogan, R. J., Hólm, E., Janisková, M., Keeley, S., Laloyaux, P., Lopez, P., Lupu, C., Radnoti, G., de Rosnay, P., Rozum, I., Vamborg, F., Villaume, S., and Thépaut, J.: The ERA5 global reanalysis, Quarterly Journal of the Royal Meteorological Society, 146, 1999–2049, https://doi.org/10.1002/qj.3803, 2020.
Hewlett, J. D.: Water Management, USDA Forest Service, Southeastern Forest Experiment Station, Ashville, 1961.
Hijmans, R. J., Cameron, S. E., Parra, J. L., Jones, P. G., and Jarvis, A.: Very high resolution interpolated climate surfaces for global land areas, International Journal of Climatology, 25, 1965–1978, https://doi.org/10.1002/joc.1276, 2005.
Hock, R.: Temperature index melt modelling in mountain areas, J Hydrol (Amst), 282, 104–115, https://doi.org/10.1016/S0022-1694(03)00257-9, 2003.
Hock, R.: Glacier melt: a review of processes and their modelling, Progress in Physical Geography: Earth and Environment, 29, 362–391, https://doi.org/10.1191/0309133305pp453ra, 2005.
Hooghoudt, S.: Bijdragen tot de kennis van eenige natuurkundige grootheden van den grond. No. 7. Algemeene beschouwing van het probleem van de detailontwatering en de infiltratie door middel van parallel loopende drains, greppels, slooten en kanalen., Versl. Landbouwkd. Onderz, 46, 515–707, 1940.
Horton, R. E.: The Rôle of infiltration in the hydrologic cycle, Eos, Transactions American Geophysical Union, 14, 446–460, https://doi.org/10.1029/TR014i001p00446, 1933.
von Hoyningen-Huene, J.: Die Interzeption des Niederschlags in landwirtschaftlichen Pflanzenbeständen, Arbeitsbericht Deutscher Verband fur Wasserwirtschaft und Kulturbau, DWK, 1981.
Immerzeel, W., Lutz, A. F., and Droogers, P.: Climate Change Impacts on the Upstream Water Resources of the Amu and Syr Darya River Basins, Wageningen, 2012a.
Immerzeel, W. W. and Bierkens, M. F. P.: Asia's water balance, Nat Geosci, 5, 841–842, https://doi.org/10.1038/ngeo1643, 2012.
Immerzeel, W. W. and Droogers, P.: Calibration of a distributed hydrological model based on satellite evapotranspiration, J Hydrol (Amst), 349, 411–424, https://doi.org/10.1016/j.jhydrol.2007.11.017, 2008.
Immerzeel, W. W., Droogers, P., de Jong, S. M., and Bierkens, M. F. P.: Large-scale monitoring of snow cover and runoff simulation in Himalayan river basins using remote sensing, Remote Sens Environ, 113, 40–49, https://doi.org/10.1016/j.rse.2008.08.010, 2009.
Immerzeel, W. W., van Beek, L. P. H., and Bierkens, M. F. P.: Climate Change Will Affect the Asian Water Towers, Science (1979), 328, 1382–1385, https://doi.org/10.1126/science.1183188, 2010.
Immerzeel, W. W., van Beek, L. P. H., Konz, M., Shrestha, A. B., and Bierkens, M. F. P.: Hydrological response to climate change in a glacierized catchment in the Himalayas, Clim Change, 110, 721–736, https://doi.org/10.1007/s10584-011-0143-4, 2012b.
Irrisoft: Irrisoft: Database and on-line Applications in Irrigation, Drainage & Hydrology, 2014.
Jacob, D., Petersen, J., Eggert, B., Alias, A., Christensen, O. B., Bouwer, L. M., Braun, A., Colette, A., Déqué, M., Georgievski, G., Georgopoulou, E., Gobiet, A., Menut, L., Nikulin, G., Haensler, A., Hempelmann, N., Jones, C., Keuler, K., Kovats, S., Kröner, N., Kotlarski, S.,

Kriegsmann, A., Martin, E., van Meijgaard, E., Moseley, C., Pfeifer, S., Preuschmann, S., Radermacher, C., Radtke, K., Rechid, D., Rounsevell, M., Samuelsson, P., Somot, S., Soussana, J.-F., Teichmann, C., Valentini, R., Vautard, R., Weber, B., and Yiou, P.: EURO-CORDEX: new high-resolution climate change projections for European impact research, Reg Environ Change, 14, 563–578, https://doi.org/10.1007/s10113-013-0499-2, 2014.

Jin, C. X., Römkens, J. M., and Griffioen, F.: Estimating manning's roughness coefficient for shallow overland flow in non-submerged vegetative filter strips, Transactions of the ASAE, 43, 1459–1466, 2000.

de Jong, S. and Jetten, V.: Distributed, quantitative assessment of canopy storage capacity by Hyperspectral Remote Sensing, 2010.

Karssenberg, D.: The value of environmental modelling languages for building distributed hydrological models, Hydrol Process, 16, 2751–2766, https://doi.org/10.1002/hyp.1068, 2002.

Karssenberg, D., Burrough, P. A., Sluiter, R., and de Jong, K.: The PCRaster Software and Course Materials for Teaching Numerical Modelling in the Environmental Sciences, Transactions in GIS, 5, 99–110, https://doi.org/10.1111/1467-9671.00070, 2001.

Karssenberg, D., Schmitz, O., Salamon, P., de Jong, K., and Bierkens, M. F. P.: A software framework for construction of process-based stochastic spatio-temporal models and data assimilation, Environmental Modelling & Software, 25, 489–502, https://doi.org/10.1016/j.envsoft.2009.10.004, 2010.

Kerby, W. S.: Time of concentration for overland flow., Civil Engineering, 29, 1959.

Khanal, S., Lutz, A. F., Kraaijenbrink, P. D. A., van den Hurk, B., Yao, T., and Immerzeel, W. W.: Variable 21st Century Climate Change Response for Rivers in High Mountain Asia at Seasonal to Decadal Time Scales, Water Resour Res, 57, https://doi.org/10.1029/2020WR029266, 2021.

Kirpich, Z. P.: Time of concentration of small agricultural watersheds. , Civil Engineering, 10, 1940.

Van Der Knijff, J. M., Younis, J., and De Roo, A. P. J.: LISFLOOD: a GIS-based distributed model for river basin scale water balance and flood simulation, International Journal of Geographical Information Science, 24, 189–212, https://doi.org/10.1080/13658810802549154, 2010.

Kokkonen, T., Koivusalo, H., Jakeman, A., and Norton, J.: Construction of a degree-day snow model in the light of the ten iterative steps in model development, in: iEMSs Third Biennial Meeting: "Summit on Environmental Modelling and Software"., 2006.

Kozak, J. A., Ahuja, L. R., Green, T. R., and Ma, L.: Modelling crop canopy and residue rainfall interception effects on soil hydrological components for semi-arid agriculture, Hydrol Process, 21, 229–241, https://doi.org/10.1002/hyp.6235, 2007.

Krysanova, V., Müller-Wohlfeil, D.-I., and Becker, A.: Development and test of a spatially distributed hydrological/water quality model for mesoscale watersheds, Ecol Modell, 106, 261–289, https://doi.org/10.1016/S0304-3800(97)00204-4, 1998.

Krysanova, V., Wechsung, J., Arnold, R., Srinivasan, R., and Williams, J.: PIK Report Nr. 69 "SWIM (Soil and Water Integrated Model), User Manual," Potsdam, 2000.

Krysanova, V., Hattermann, F., Huang, S., Hesse, C., Vetter, T., Liersch, S., Koch, H., and Kundzewicz, Z. W.: Modelling climate and land-use change impacts with SWIM: lessons learnt from multiple applications, Hydrological Sciences Journal, 60, 606–635, https://doi.org/10.1080/02626667.2014.925560, 2015.

Lall, U.: Debates—The future of hydrological sciences: A (common) path forward? One water. One world. Many climes. Many souls, Water Resour Res, 50, 5335–5341, https://doi.org/10.1002/2014WR015402, 2014.

Lambert, J. J., Daroussin, J., Eimberck, M., Le Bas, C., Jamagne, M., King, D., and Montanarella, L.: Soil Geographical Database for Eurasia & The Mediterranean: Instructions Guide for Elaboration at scale 1:1,000,000 version 4.0. EUR 20422 EN., Ispra, Italy, 2003.

Lazar, A. N., Butterfield, D., Futter, M. N., Rankinen, K., Thouvenot-Korppoo, M., Jarritt, N., Lawrence, D. S. L., Wade, A. J., and Whitehead, P. G.: An assessment of the fine sediment dynamics in an upland river system: INCA-Sed modifications and implications for fisheries, Science of The Total Environment, 408, 2555–2566, https://doi.org/10.1016/j.scitotenv.2010.02.030, 2010.

Liang, X., Lettenmaier, D. P., Wood, E. F., and Burges, S. J.: A simple hydrologically based model of land surface water and energy fluxes for general circulation models, Journal of Geophysical Research: Atmospheres, 99, 14415–14428, https://doi.org/10.1029/94JD00483, 1994.

Liang, X., Wood, E. F., and Lettenmaier, D. P.: Surface soil moisture parameterization of the VIC-2L model: Evaluation and modification, Glob Planet Change, 13, 195–206, https://doi.org/10.1016/0921-8181(95)00046-1, 1996.

Lindström, G., Pers, C., Rosberg, J., Strömqvist, J., and Arheimer, B.: Development and testing of the HYPE (Hydrological Predictions for the Environment) water quality model for different spatial scales, Hydrology Research, 41, 295–319, https://doi.org/10.2166/nh.2010.007, 2010.

Liu, Y., Gupta, H., Springer, E., and Wagener, T.: Linking science with environmental decision making: Experiences from an integrated modeling approach to supporting sustainable water resources management, Environmental Modelling & Software, 23, 846–858, https://doi.org/10.1016/j.envsoft.2007.10.007, 2008.

Lukey, B. T., Bathurst, J. C., Hiley, R. A., and Ewen, J.: SHETRAN sediment transport component: equations and algorithms., Newcastle, United Kingdom, 1995.

Lutz, A. F., Droogers, P., and Immerzeel, W.: Climate Change Impact and Adaptation on the Water Resources in the Amu Darya and Syr Darya River Basins., Wageningen, 2012.

Lutz, A. F., Immerzeel, W. W., Gobiet, A., Pellicciotti, F., and Bierkens, M. F. P.: Comparison of climate change signals in CMIP3 and CMIP5 multi-model ensembles and implications for Central Asian glaciers, Hydrol Earth Syst Sci, 17, 3661–3677, https://doi.org/10.5194/hess-17-3661-2013, 2013.

Lutz, A. F., Immerzeel, W. W., Shrestha, A. B., and Bierkens, M. F. P.: Consistent increase in High Asia's runoff due to increasing glacier melt and precipitation, Nat Clim Chang, 4, 587–592, https://doi.org/10.1038/nclimate2237, 2014.

Lutz, A. F., Immerzeel, W. W., Kraaijenbrink, P. D. A., Shrestha, A. B., and Bierkens, M. F. P.: Climate Change Impacts on the Upper Indus Hydrology: Sources, Shifts and Extremes, PLoS One, 11, e0165630, https://doi.org/10.1371/journal.pone.0165630, 2016.

Manning R.: On the flow of water in open channels and pipes., Transactions of the Institution of Civil Engineers of Ireland, 20, 161–207, 1891.

Marshall, J. S. and Palmer, W. M. K.: THE DISTRIBUTION OF RAINDROPS WITH SIZE, Journal of Meteorology, 5, 165–166, https://doi.org/10.1175/1520-0469(1948)005<0165:TDORWS>2.0.CO;2, 1948.

McPhee, J., Rubio-Alvarez, E., Meza, R., Ayala, A., Vargas, X., and Vicuna, S.: An Approach to Estimating Hydropower Impacts of Climate Change from a Regional Perspective, in: Watershed Management 2010, 13–24, https://doi.org/10.1061/41143(394)2, 2010.

Meehl, G. A., Covey, C., Delworth, T., Latif, M., McAvaney, B., Mitchell, J. F. B., Stouffer, R. J., and Taylor, K. E.: THE WCRP CMIP3 Multimodel Dataset: A New Era in Climate Change

Research, Bull Am Meteorol Soc, 88, 1383–1394, https://doi.org/10.1175/BAMS-88-9-1383, 2007.
Mendoza, P. A., McPhee, J., and Vargas, X.: Uncertainty in flood forecasting: A distributed modeling approach in a sparse data catchment, Water Resour Res, 48, https://doi.org/10.1029/2011WR011089, 2012.
Monteith, J. L.: Principles of environmental physics. , Edward Arnold, London, 241 pp., https://doi.org/10.1002/qj.49710042414, 1973.
Morgan, R. P. C.: Soil Erosion and Conservation, 3rd ed., Blackwell Science Ltd, Malden, USA, 2005.
Morgan, R. P. C. and Duzant, J. H.: Modified MMF (Morgan–Morgan–Finney) model for evaluating effects of crops and vegetation cover on soil erosion, Earth Surf Process Landf, 33, 90–106, https://doi.org/10.1002/esp.1530, 2008.
Morgan, R. P. C., Quinton, J. N., Smith, R. E., Govers, G., Poesen, J. W. A., Auerswald, K., Chisci, G., Torri, D., Styczen, M. E., and Folly, A. J. V.: The European soil erosion model (EUROSEM): documentation and user guide (No. Version 3.6), Silsoe, United Kingdom, 1998.
Morris, E. M. and Woolhiser, D. A.: Unsteady one-dimensional flow over a plane: Partial equilibrium and recession hydrographs, Water Resour Res, 16, 355–360, https://doi.org/10.1029/WR016i002p00355, 1980.
Myneni, R. B. and Williams, D. L.: On the relationship between FAPAR and NDVI, Remote Sens Environ, 49, 200–211, https://doi.org/10.1016/0034-4257(94)90016-7, 1994.
Nash, J. E. and Sutcliffe, J. V.: River flow forecasting through conceptual models part I — A discussion of principles, J Hydrol (Amst), 10, 282–290, https://doi.org/10.1016/0022-1694(70)90255-6, 1970.
Neitsch, S. L., Arnold, J. G., Kiniry, J. R., and Williams, J. R.: Soil and Water Assessment Tool (SWAT). Theoretical Documentation, College Station, Texas, 2009.
Niu, G.-Y., Yang, Z.-L., Mitchell, K. E., Chen, F., Ek, M. B., Barlage, M., Kumar, A., Manning, K., Niyogi, D., Rosero, E., Tewari, M., and Xia, Y.: The community Noah land surface model with multiparameterization options (Noah-MP): 1. Model description and evaluation with local-scale measurements, J Geophys Res, 116, D12109, https://doi.org/10.1029/2010JD015139, 2011.
Oogathoo, S., Prasher, S., Rudra, R., and Patel, R.: Calibration and validation of the MIKE SHE model in Canagagigue Creek watershed, in: Agricultural and biosystems engineering for a sustainable world. , in: International Conference on Agricultural Engineering, 2008.
Parajka, J. and Blöschl, G.: Spatio-temporal combination of MODIS images – potential for snow cover mapping, Water Resour Res, 44, https://doi.org/10.1029/2007WR006204, 2008.
Park, S. W., Mitchell, J. K., and Scarborough, J. N.: Soil Erosion Simulation on Small Watersheds: A Modified ANSWERS Model, Transactions of the ASAE, 25, 1581–1588, https://doi.org/10.13031/2013.33771, 1982.
Pechlivanidis, I., Jackson, B., McIntyre, N., and Weather, H.: Catchment scale hydrological modelling: A review of model types, calibration approaches and uncertainty analysis methods in the context of recent developments in technology and applications, Global NEST journal , 13, 193–214, 2011.
Peng, D., Zhang, B., and Liu, L.: Comparing spatiotemporal patterns in Eurasian FPAR derived from two NDVI-based methods, Int J Digit Earth, 5, 283–298, https://doi.org/10.1080/17538947.2011.598193, 2012.
Petryk, S. and Bosmajian, G.: Analysis of flow through vegetation, Journal of the Hydraulics Division, 101, 871–884, 1975.

Piechota, T. C., Chiew, F. H. C., and Dracup, J. A.: Seasonal streamflow forecasting in eastern Australia and the El Niño – Southern Oscillation , Water Resour Res, 34, 3035–3044, 1998.
Poesen, J.: Soil erosion in the Anthropocene: Research needs, Earth Surf Process Landf, 43, 64–84, https://doi.org/10.1002/esp.4250, 2018.
Poesen, J. W., van Wesemael, B., Bunte, K., and Benet, A. S.: Variation of rock fragment cover and size along semiarid hillslopes: a case-study from southeast Spain, Geomorphology, 23, 323–335, 1998.
Pomeroy, J. W., Gray, D. M., Brown, T., Hedstrom, N. R., Quinton, W. L., Granger, R. J., and Carey, S. K.: The cold regions hydrological model: a platform for basing process representation and model structure on physical evidence, Hydrol Process, 21, 2650–2667, https://doi.org/10.1002/hyp.6787, 2007.
Prosser, I. P. and Rustomji, P.: Sediment transport capacity relations for overland flow, Progress in Physical Geography: Earth and Environment, 24, 179–193, https://doi.org/10.1177/030913330002400202, 2000.
Quansah, C.: Laboratory experimentation for the statistical derivation of equations for soil erosion modelling and soil conservation design, Cranfield Institute of Technology, 365 pp., 1982.
Rafn, E. B., Contor, B., and Ames, D. P.: Evaluation of a Method for Estimating Irrigated Crop-Evapotranspiration Coefficients from Remotely Sensed Data in Idaho, Journal of Irrigation and Drainage Engineering, 134, 722–729, https://doi.org/10.1061/(ASCE)0733-9437(2008)134:6(722), 2008.
Ragettli, S. and Pellicciotti, F.: Calibration of a physically based, spatially distributed hydrological model in a glacierized basin: On the use of knowledge from glaciometeorological processes to constrain model parameters, Water Resour Res, 48, https://doi.org/10.1029/2011WR010559, 2012.
Ragettli, S., Cortés, G., McPhee, J., and Pellicciotti, F.: An evaluation of approaches for modelling hydrological processes in high-elevation, glacierized Andean watersheds, Hydrol Process, 28, 5674–5695, https://doi.org/10.1002/hyp.10055, 2014.
Ragettli, S., Pellicciotti, F., Immerzeel, W. W., Miles, E. S., Petersen, L., Heynen, M., Shea, J. M., Stumm, D., Joshi, S., and Shrestha, A.: Unraveling the hydrology of a Himalayan catchment through integration of high resolution in situ data and remote sensing with an advanced simulation model, Adv Water Resour, 78, 94–111, https://doi.org/10.1016/j.advwatres.2015.01.013, 2015.
Refshaard, J. and Storm, B.: MIKE SHE, 1995.
Regonda, S. K., Rajagopalan, B., Clark, M., and Zagona, E.: A multimodel ensemble forecast framework: Application to spring seasonal flows in the Gunnison River Basin, Water Resour Res, 42, https://doi.org/10.1029/2005WR004653, 2006.
Reid, T. D., Carenzo, M., Pellicciotti, F., and Brock, B. W.: Including debris cover effects in a distributed model of glacier ablation, Journal of Geophysical Research: Atmospheres, 117, https://doi.org/10.1029/2012JD017795, 2012.
Renard, K. G., Foster, G. R., Weesies, G. A., McCool, D. K., and Yoder, D. C.: Predicting soil erosion by water: a guide to conservation planning with the Revised Universal Soil Loss Equation (RUSLE), https://doi.org/DC0-16-048938-5 65–100, 1997.
RGI 7.0 Consortium: Randolph Glacier Inventory - A Dataset of Global Glacier Outlines, Version 7.0., 2023.
Rigon, R., Bertoldi, G., and Over, T. M.: GEOtop: A Distributed Hydrological Model with Coupled Water and Energy Budgets, J Hydrometeorol, 7, 371–388, https://doi.org/10.1175/JHM497.1, 2006.

Rockström, J., Falkenmark, M., Lannerstad, M., and Karlberg, L.: The planetary water drama: Dual task of feeding humanity and curbing climate change, Geophys Res Lett, 39, https://doi.org/10.1029/2012GL051688, 2012.

Rollenbeck, R. and Bendix, J.: Rainfall distribution in the Andes of southern Ecuador derived from blending weather radar data and meteorological field observations, Atmos Res, 99, 277–289, https://doi.org/10.1016/j.atmosres.2010.10.018, 2011.

Van Rompaey, A. J. J., Verstraeten, G., Van Oost, K., Govers, G., and Poesen, J.: Modelling mean annual sediment yield using a distributed approach, Earth Surf Process Landf, 26, 1221–1236, https://doi.org/10.1002/esp.275, 2001.

Roussel, M. C., Thompson, D. B., Fang, X., Cleveland, T. G., and Garcia, C. A.: Timing-parameter estimation for applicable Texas watersheds, 2005.

Samain, B., Simons, G. W. H., Voogt, M. P., Defloor, W., Bink, N.-J., and Pauwels, V. R. N.: Consistency between hydrological model, large aperture scintillometer and remote sensing based evapotranspiration estimates for a heterogeneous catchment, Hydrol Earth Syst Sci, 16, 2095–2107, https://doi.org/10.5194/hess-16-2095-2012, 2012.

Samaniego, L., Kumar, R., and Attinger, S.: Multiscale parameter regionalization of a grid-based hydrologic model at the mesoscale, Water Resour Res, 46, https://doi.org/10.1029/2008WR007327, 2010.

Sangrey, D. A., Harrop-Williams, K. O., and Klaiber, J. A.: Predicting Ground-Water Response to Precipitation, Journal of Geotechnical Engineering, 110, 957–975, https://doi.org/10.1061/(ASCE)0733-9410(1984)110:7(957), 1984.

Saxton, K. E. and Rawls, W. J.: Soil Water Characteristic Estimates by Texture and Organic Matter for Hydrologic Solutions, Soil Science Society of America Journal, 70, 1569–1578, https://doi.org/10.2136/sssaj2005.0117, 2006.

Schaner, N., Voisin, N., Nijssen, B., and Lettenmaier, D. P.: The contribution of glacier melt to streamflow, Environmental Research Letters, 7, 034029, https://doi.org/10.1088/1748-9326/7/3/034029, 2012.

Schmitz, O., Karssenberg, D., van Deursen, W. P. A., and Wesseling, C. G.: Linking external components to a spatio-temporal modelling framework: Coupling MODFLOW and PCRaster, Environmental Modelling & Software, 24, 1088–1099, https://doi.org/10.1016/j.envsoft.2009.02.018, 2009.

Schmitz, O., Karssenberg, D., de Jong, K., de Kok, J.-L., and de Jong, S. M.: Map algebra and model algebra for integrated model building, Environmental Modelling & Software, 48, 113–128, https://doi.org/10.1016/j.envsoft.2013.06.009, 2013.

Sellers, P. J., Tucker, C. J., Collatz, G. J., Los, S. O., Justice, C. O., Dazlich, D. A., and Randall, D. A.: A Revised Land Surface Parameterization (SiB2) for Atmospheric GCMS. Part II: The Generation of Global Fields of Terrestrial Biophysical Parameters from Satellite Data, J Clim, 9, 706–737, https://doi.org/10.1175/1520-0442(1996)009<0706:ARLSPF>2.0.CO;2, 1996.

Serrano-Notivoli, R., Beguería, S., Saz, M. Á., Longares, L. A., and de Luis, M.: SPREAD: a high-resolution daily gridded precipitation dataset for Spain – an extreme events frequency and intensity overview, Earth Syst Sci Data, 9, 721–738, https://doi.org/10.5194/essd-9-721-2017, 2017.

Sheffield, J., Goteti, G., and Wood, E. F.: Development of a 50-Year High-Resolution Global Dataset of Meteorological Forcings for Land Surface Modeling, J Clim, 19, 3088–3111, https://doi.org/10.1175/JCLI3790.1, 2006.

Simons, G. W. H., Koster, R., and Droogers, P.: HiHydroSoil v2.0 - A high resolution soil map of global hydraulic properties, Wageningen, 2020.

Singh, P. and Kumar, N.: Impact assessment of climate change on the hydrological response of a snow and glacier melt runoff dominated Himalayan river, J Hydrol (Amst), 193, 316–350, https://doi.org/10.1016/S0022-1694(96)03142-3, 1997.
Sloan, P. G. and Moore, I. D.: Modeling subsurface stormflow on steeply sloping forested watersheds, Water Resour Res, 20, 1815–1822, https://doi.org/10.1029/WR020i012p01815, 1984.
Smedema, L. K. and Rycroft, D. W.: Land Drainage-Planning and Design of Agricultural Drainage Systems., Cornell University Press, Ithaca, New York, 1983.
Sorg, A., Bolch, T., Stoffel, M., Solomina, O., and Beniston, M.: Climate change impacts on glaciers and runoff in Tien Shan (Central Asia), Nat Clim Chang, 2, 725–731, https://doi.org/10.1038/nclimate1592, 2012.
Sperna Weiland, F. C., van Beek, L. P. H., Kwadijk, J. C. J., and Bierkens, M. F. P.: The ability of a GCM-forced hydrological model to reproduce global discharge variability, Hydrol Earth Syst Sci, 14, 1595–1621, https://doi.org/10.5194/hess-14-1595-2010, 2010.
Taylor, K. E., Stouffer, R. J., and Meehl, G. A.: An Overview of CMIP5 and the Experiment Design, Bull Am Meteorol Soc, 93, 485–498, https://doi.org/10.1175/BAMS-D-11-00094.1, 2012.
Terink, W., Lutz, A. F., and Simons, G. W. H.: SPHY: Spatial Processes in HYdrology. Case-studies for training., 2015a.
Terink, W., Lutz, A. F., and Immerzeel, W. W.: SPHY: Spatial Processes in HYdrology. Graphical User-Interfaces (GUIs)., 2015b.
Terink, W., Lutz, A. F., Simons, G. W. H., Immerzeel, W. W., and Droogers, P.: SPHY v2.0: Spatial Processes in HYdrology, Geosci Model Dev, 8, 2009–2034, https://doi.org/10.5194/gmd-8-2009-2015, 2015c.
Themeßl, M. J., Gobiet, A., and Heinrich, G.: Empirical-statistical downscaling and error correction of regional climate models and its impact on the climate change signal, Clim Change, 112, 449–468, https://doi.org/10.1007/s10584-011-0224-4, 2012.
Tollner, E. W., Barfield, B. J., Haan, C. T., and Kao, T. Y.: Suspended Sediment Filtration Capacity of Simulated Vegetation, Transactions of the ASAE, 19, 0678–0682, https://doi.org/10.13031/2013.36095, 1976.
Tucker, C. J.: Red and photographic infrared linear combinations for monitoring vegetation, Remote Sens Environ, 8, 127–150, https://doi.org/10.1016/0034-4257(79)90013-0, 1979.
USGS: Landsat 8: U.S. Geological Survey Fact Sheet, 2013–3060 pp., 2013.
USGS: Water Resources Applications Software, 2014.
VanderKwaak, J. E. and Loague, K.: Hydrologic-Response simulations for the R-5 catchment with a comprehensive physics-based model, Water Resour Res, 37, 999–1013, https://doi.org/10.1029/2000WR900272, 2001.
Venetis, C.: A STUDY ON THE RECESSION OF UNCONFINED ACQUIFERS, International Association of Scientific Hydrology. Bulletin, 14, 119–125, https://doi.org/10.1080/02626666909493759, 1969.
de Vente, J., Poesen, J., Verstraeten, G., Van Rompaey, A., and Govers, G.: Spatially distributed modelling of soil erosion and sediment yield at regional scales in Spain, Glob Planet Change, 60, 393–415, https://doi.org/10.1016/j.gloplacha.2007.05.002, 2008.
de Vente, J., Poesen, J., Verstraeten, G., Govers, G., Vanmaercke, M., Van Rompaey, A., Arabkhedri, M., and Boix-Fayos, C.: Predicting soil erosion and sediment yield at regional scales: Where do we stand?, Earth Sci Rev, 127, 16–29, https://doi.org/10.1016/j.earscirev.2013.08.014, 2013a.
de Vente, J., Poesen, J., Verstraeten, G., Govers, G., Vanmaercke, M., Van Rompaey, A., Arabkhedri, M., and Boix-Fayos, C.: Predicting soil erosion and sediment yield at regional

scales: Where do we stand?, Earth Sci Rev, 127, 16–29, https://doi.org/10.1016/j.earscirev.2013.08.014, 2013b.
Verbunt, M., Gurtz, J., Jasper, K., Lang, H., Warmerdam, P., and Zappa, M.: The hydrological role of snow and glaciers in alpine river basins and their distributed modeling, J Hydrol (Amst), 282, 36–55, https://doi.org/10.1016/S0022-1694(03)00251-8, 2003.
Vicuña, S., Garreaud, R. D., and McPhee, J.: Climate change impacts on the hydrology of a snowmelt driven basin in semiarid Chile, Clim Change, 105, 469–488, https://doi.org/10.1007/s10584-010-9888-4, 2011.
van Vuuren, D. P., Edmonds, J., Kainuma, M., Riahi, K., Thomson, A., Hibbard, K., Hurtt, G. C., Kram, T., Krey, V., Lamarque, J. F., Masui, T., Meinshausen, M., Nakicenovic, N., Smith, S. J., and Rose, S. K.: The representative concentration pathways: An overview, Clim Change, 109, 5–31, https://doi.org/10.1007/s10584-011-0148-z, 2011.
Wada, Y., van Beek, L. P. H., van Kempen, C. M., Reckman, J. W. T. M., Vasak, S., and Bierkens, M. F. P.: Global depletion of groundwater resources, Geophys Res Lett, 37, https://doi.org/10.1029/2010GL044571, 2010.
Wagener, T., Sivapalan, M., Troch, P. A., McGlynn, B. L., Harman, C. J., Gupta, H. V., Kumar, P., Rao, P. S. C., Basu, N. B., and Wilson, J. S.: The future of hydrology: An evolving science for a changing world, Water Resour Res, 46, https://doi.org/10.1029/2009WR008906, 2010.
Wagner, P. D., Fiener, P., Wilken, F., Kumar, S., and Schneider, K.: Comparison and evaluation of spatial interpolation schemes for daily rainfall in data scarce regions, J Hydrol (Amst), 464–465, 388–400, https://doi.org/10.1016/j.jhydrol.2012.07.026, 2012.
Wheeler, T. and von Braun, J.: Climate Change Impacts on Global Food Security, Science (1979), 341, 508–513, https://doi.org/10.1126/science.1239402, 2013.
Wicks, J. M.: Physically-based mathematical modelling of catchment sediment yield, University of Newcastle upon Tyne, 1988.
Wicks, J. M. and Bathurst, J. C.: SHESED: a physically based, distributed erosion and sediment yield component for the SHE hydrological modelling system, J Hydrol (Amst), 175, 213–238, https://doi.org/10.1016/S0022-1694(96)80012-6, 1996.
Wigmosta, M. S., Vail, L. W., and Lettenmaier, D. P.: A distributed hydrology-vegetation model for complex terrain, Water Resour Res, 30, 1665–1679, https://doi.org/10.1029/94WR00436, 1994.
Williams, J. R.: HYMO flood routing, J Hydrol (Amst), 26, 17–27, https://doi.org/10.1016/0022-1694(75)90122-5, 1975.
Williams, J. R.: The EPIC Model., in: Computer Models of Watershed Hydrology, edited by: Singh, V. P., Water Resources Publications, Highlands Ranch, 909–1000, 1995.
Wischmeier, W. H. and Smith, D. D.: Predicting rainfall erosion losses, Agriculture handbook no. 537, 285–291, https://doi.org/10.1029/TR039i002p00285, 1978.
Wischmeier, W. H., Johnson, C. B., and Cross, B. V.: A Soil Erodibility Nomograph for Farmland and Construction Sites, J Soil Water Conserv, 189–193, 1971.
Woolhiser, D. A., Smith, R. E., and Goodrich, D. C.: KINEROS, A Kinematic Runoff and Erosion Model: Documentation and user manial., Washington, D.C., 1990.
Yalin, M. S.: An Expression for Bed-Load Transportation, Journal of the Hydraulics Division, 89, 221–250, https://doi.org/10.1061/JYCEAJ.0000874, 1963.
Yatagai, A., Kamiguchi, K., Arakawa, O., Hamada, A., Yasutomi, N., and Kitoh, A.: APHRODITE: Constructing a Long-Term Daily Gridded Precipitation Dataset for Asia Based on a Dense Network of Rain Gauges, Bull Am Meteorol Soc, 93, 1401–1415, https://doi.org/10.1175/BAMS-D-11-00122.1, 2012.

Copyright

Appendix 1: Input and Output

Table 25: Overview of SPHY model parameters. The last column indicates whether the parameter is observable, or can be determined by calibration (free).

Acronym	Description	Units	Parameter determination
Kc	Crop coefficient	–	Free
Kc_{max}	Maximum crop coefficient	–	Free
Kc_{min}	Minimum crop coefficient	–	Free
$NDVI_{max}$	Maximum NDVI	–	Observable
$NDVI_{min}$	Minimum NDVI	–	Observable
$FPAR_{max}$	Maximum fraction of absorbed photosynthetically active radiation	–	Free
$FPAR_{min}$	Minimum fraction of absorbed photosynthetically active radiation	–	Free
T_{crit}	Temperature threshold for precipitation to fall as snow	°C	Free
DDF_s	Degree-day factor for snow	$mm\,°C^{-1}\,day^{-1}$	Free
SSC	Water storage capacity of snowpack	$mm\,mm^{-1}$	Free
GlacF	Glacier fraction of grid cell	–	Observable
DDF_{CI}	Degree-day factor for debris-free glaciers	$mm\,°C^{-1}\,day^{-1}$	Free
DDF_{DC}	Degree-day factor for debris-covered glaciers	$mm\,°C^{-1}\,day^{-1}$	Free
F_{CI}	Fraction of GlacF that is debris free	–	Observable
F_{DC}	Fraction of GlacF that is covered with debris	–	Observable
GlacROF	Fraction of glacier melt that becomes glacier runoff	–	Free
$SW_{1,sat}$	Saturated soil water content of first soil layer	mm	Observable
$SW_{1,fc}$	Field capacity of first soil layer	mm	Observable
$SW_{1,pF3}$	Wilting point of first soil layer	mm	Observable
$SW_{1,pF4.2}$	Permanent wilting point of first soil layer	mm	Observable
$K_{sat,1}$	Saturated hydraulic conductivity of first soil layer	$mm\,day^{-1}$	Observable
$SW_{2,sat}$	Saturated soil water content of second soil layer	mm	Observable
$SW_{2,fc}$	Field capacity of second soil layer	mm	Observable
$K_{sat,2}$	Saturated hydraulic conductivity of second soil layer	$mm\,day^{-1}$	Observable
$SW_{3,sat}$	Saturated soil water content of groundwater layer	mm	Observable
slp	Slope of grid cell	$m\,m^{-1}$	Observable
δ_{gw}	Groundwater recharge delay time	day	Free
α_{gw}	Baseflow recession coefficient	day^{-1}	Free
BF_{tresh}	Threshold for baseflow to occur	mm	Free
kx	Flow recession coefficient	–	Free

Appendix 2: Input and Output description

This appendix provides an overview of the input that is required by the SPHY model, and the output that can be reported by the SPHY model. It should be noted that the current version of the SPHY model GUI (version 1.0) does not support the interaction with all the input that can be specified in the SPHY model configuration file (*.cfg). This will be implemented in future versions of the GUI. Table 26 specifies the model input that can be specified in the current version of the SPHY model GUI. An overview of the output that can be reported by the model is shown in Table 27.

Table 26: Overview of SPHY model input.

Map or parameter name	Interface tab	Spatial map [SM], single value [SV], or table [TB]	For maps: Boolean [BO], Nominal [NO], Scalar [SC], Directional [DI]. For single value: Integer [IN] or Float [FL]	Units
Clone map	General settings	SM	BO	[-]
DEM map	General settings	SM	SC	[MASL]
Slope map	General settings	SM	SC	[-]
Sub-basins map	General settings	SM	NO	[-]

Stations map	General settings	SM	NO	[-]
Precipitation	Climate	SM	SC	[mm/d]
Avg. daily temperature	Climate	SM	SC	[°C]
Max. daily temperature	Climate	SM	SC	[°C]
Min. daily temperature	Climate	SM	SC	[°C]
Latitude zones	Climate	SM	SC	[latitude]
Solar constant	Climate	SV	FL	[MJ/m^2/min]
Field capacity	Soils	SV	SC	[mm/mm]
Saturated content	Soils	SV	SC	[mm/mm]
Permanent wilting point	Soils	SV	SC	[mm/mm]
Wilting point	Soils	SV	SC	[mm/mm]
Saturated hydraulic conductivity	Soils	SV	SC	[mm/d]
Rootlayer thickness	Soils	SM, SV	SC, IN	[mm]
Sublayer thickness	Soils	SM, SV	SC, IN	[mm]
Maximum capillary rise	Soils	SV	IN	[mm]
Groundwater layer thickness	Groundwater	SM, SV	SC, IN	[mm]
Saturated groundwater content	Groundwater	SM, SV	SC, IN	[mm]
Initial groundwater storage	Groundwater	SM, SV	SC, IN	[mm]
Baseflow threshold	Groundwater	SM, SV	SC, IN	[mm]
deltaGw	Groundwater	SM, SV	SC, IN	[d]
alphaGw	Groundwater	SM, SV	SC, FL	[-]
Land use map	Land use	SM	NO	[-]
Crop coefficients lookup table	Land use	TB	FL	[-]
Initial glacier fraction	Glaciers	SM	SC	[-]
Clean ice glacier fraction	Glaciers	SM	SC	[-]
Debris covered glacier fraction	Glaciers	SM	SC	[-]
GlacF	Glaciers	SM, SV	SC, FL	[-]
DDFDG	Glaciers	SM, SV	SC, FL	[mm/°C/d]
DDFG	Glaciers	SM, SV	SC, FL	[mm/°C/d]
SnowIni	Snow	SM, SV	SC, IN	[mm]
SnowWatStore	Snow	SM, SV	SC, IN	[mm]
SnowSC	Snow	SM, SV	SC, FL	[-]
DDFS	Snow	SM, SV	SC, FL	[mm/°C/d]
Tcrit	Snow	SV	FL	[°C]
Recession coefficient	Routing	SM, SV	SC, FL	[-]
Flow direction	Routing	SM	DI	[-]

Routed total runoff	Routing	SM, SV	SC, FL	[m^3/s]
Routed rainfall runoff	Routing	SM, SV	SC, FL	[m^3/s]
Routed baseflow runoff	Routing	SM, SV	SC, FL	[m^3/s]
Routed snow runoff	Routing	SM, SV	SC, FL	[m^3/s]
Routed glacier runoff	Routing	SM, SV	SC, FL	[m^3/s]

Table 27: Overview of SPHY model output (Report options tab).

Output variable	Spatial map [SM] or time-series [TS]	Output frequency: daily [D], monthly [M], or annual [A]	Units	Option to report sub-basin average flux in mm: yes [Y] or no [N].
Baseflow runoff	SM, TS	D, M, A	mm	N
Capillary rise	SM, TS	D, M, A	mm	N
ETa	SM, TS	D, M, A	mm	Y
ETp	SM, TS	D, M, A	mm	N
Glacier melt	SM, TS	D, M, A	mm	Y
Glacier percolation	SM, TS	D, M, A	mm	N
Glacier runoff	SM, TS	D, M, A	mm	N
Groundwater recharge	SM, TS	D, M, A	mm	N
Precipitation	SM, TS	D, M, A	mm	Y
Rain runoff	SM, TS	D, M, A	mm	N
Rainfall	SM, TS	D, M, A	mm	N
Rootzone drainage	SM, TS	D, M, A	mm	N
Rootzone percolation	SM, TS	D, M, A	mm	N
Routed baseflow runoff	SM, TS	D, M, A	m^3/s	Y
Routed glacier runoff	SM, TS	D, M, A	m^3/s	Y
Routed rain runoff	SM, TS	D, M, A	m^3/s	Y
Routed snow runoff	SM, TS	D, M, A	m^3/s	Y
Routed total runoff	SM, TS	D, M, A	m^3/s	Y
Snow	SM, TS	D, M, A	mm	N
Snow melt	SM, TS	D, M, A	mm	N
Snow runoff	SM, TS	D, M, A	mm	N
Subzone percolation	SM, TS	D, M, A	mm	N
Surface runoff	SM, TS	D, M, A	mm	N
Total runoff	SM, TS	D, M, A	mm	N

The output variables in SPHY can be of two types (a) Time-series (TS) (b) Spatial maps (SM). The TS will always have the extension ".tss". The first column represents the time-step. It always starts at 1 and ends at final step of simulation. So, if the simulation is between 01-01-2003 and 31-12-2003, then 1 represents 01-01-2003 and 365 represents 31-12-2003. The number of columns, except the first column,

in a 'tss' file represents the number of outlet points created initially in the model. The DTS, MTS, ATS represents daily, monthly and annual timeseries depending on the user choice on aggregation (see Table 28). **R**Tot, **S**Tot, **G**Tot, **B**Tot, QAll represents rainfall-runoff, snowmelt runoff, glaciermelt runoff, baseflow, and Total runoff. The 'Tot' term represents that the components are routed, and the units are in cubic meter per second. The SM with prefixes Rain, Snow, Glac, Base, QAll are self-explanatory. The additional r after each prefix represents that flow are not routed and units are in mm. For instance, Snowr represents the non-routed snowmelt-runoff in mm. The suffix 'r' represents its runoff but not routed. The prefix D, M, Y represents the aggregation level daily, monthly and yearly. So, if the file name is SnowrM then its monthly spatial non-routed runoff and so on. Note that the extension of the SM files follows similar concept as of TS. For instance, BTotM000.365 represents the average of routed baseflow for the month of January (the year will be start of simulation), BTotM000.365 represents the average of routed baseflow for the month of December and BTotM000.396 represents the average of routed baseflow for the month of January next year and so on. There are also some glacier related csv output files GLAC_T.csv (glacier temperature), Prec_GLAC (precipitation over glaciers), Rain_GLAC.csv (rain over glaciers), Snow_GLAC.csv (snow over glaciers), ActSnowMelt_GLAC.csv (actual snowmelt from glaciers), TotalSnowStore_GLAC.csv (total snow storage over glaciers), GlacR.csv (glacier runoff) and so on. Note the first column represents the timestep and other columns represent individual glaciers in the study region. There are many outputs that can be generated from SPHY, so users are suggested to read the configuration file and the relevant script as the description of the variable is included as comments.

Table 28: Description of the most common output files.

Output file	Spatial map [SM] or time-series [TS]	Units	Description
RTotDTS.tss	TS	m^3/s	This is daily rainfall-runoff time series data at each station
STotDTS.tss	TS	m^3/s	This is daily snowmelt runoff time series data at each station
GTotDTS.tss	TS	m^3/s	This is daily glaciermelt runoff time series data at each station
BTotDTS.tss	TS	m^3/s	This is daily baseflow time series data at each station
QAllDTS.tss	TS	m^3/s	This is daily total runoff time series data at each station
RainrM00.031	SM	mm	This is non-routed spatial rainfall-runoff for the month of January. M represents the monthly timestep. The 031 represents the last timestep of a particular month.
SnowrM00.031	SM	mm	This is non-routed spatial snowmelt runoff for the month of January. M represents the monthly timestep. The 031 represents the last timestep of a particular month.
GlacrM00.031	SM	mm	This is non-routed spatial glacier melt runoff for the month of January. M represents the monthly timestep. The 031 represents the last timestep of a particular month.
BaserM00.031	SM	mm	This is non-routed spatial baseflow for the month of January. M represents the monthly timestep. The 031 represents the last timestep of a particular month.
TotrM000.031	SM	mm	This is non-routed spatial total runoff for the month of January. M represents the monthly timestep. The 031 represents the last timestep of a particular month.
RTotM000.031	SM	m^3/s	This is routed spatial rainfall-runoff for the month of January. M represents the monthly timestep. The 031 represents the last timestep of a particular month.
STotM000.031	SM	m^3/s	This is routed spatial snowmelt runoff for the month of January. M represents the monthly timestep. The 031 represents the last timestep of a particular month.

GTotM000.031	SM	m^3/s	This is routed spatial glaciermelt runoff for the month of January. M represents the monthly timestep. The 031 represents the last timestep of a particular month.
BTotM000.031	SM	m^3/s	This is routed spatial baseflow for the month of January. M represents the monthly timestep. The 031 represents the last timestep of a particular month.
QAllM000.031	SM	m^3/s	This is routed spatial total runoff for the month of January. M represents the monthly timestep. The 031 represents the last timestep of a particular month.

Appendix 3: Soil erosion model input

The most used soil erosion model is the MMF model. However, in SPHY other erosion models are also implemented. This appendix describes those erosion models and how to use them in SPHY.

MUSLE

The optional K-factor map (soil erodibility) can be provided here. The Wischmeier et al. (1971) formulations are used (see section 2.8) when this is left empty. In that case, a sand, clay and organic matter map should be provided in the PEDOTRANSFER section of the config file (even when the pedotransferfunctions are not used, i.e. if PedotransferFLAG = 0).

The P-factor map indicates the support practice factor, which indicates how conservation measures reduce soil erosion. While other model parameters may also be used to indicate soil conservation, such as the C-factor, this factor is often considered to be 1.

A look-up table needs to be defined for the land use specific model parameters. The user needs to provide a PCRaster table file (*.tbl), where each row represents a land use class. The following data need to be provided:

Table 29: musle_table

Land use class	C-factor	Retardance coefficient
-99	1	2
1	0.05	0.1
2	0.4	0.4
3	0.2	0.8
…	…	…

The values for C-factor and retardance coefficient can be obtained from several sources. Successful applications with the MUSLE soil erosion model were obtained with the C-factor and retardance coefficient values obtained from Table 30 and Table 31, respectively.

Table 30: C-factor values for different land use classes (de Vente et al., 2009).

Land use classes	C-factor
Urban areas	0
Non-irrigated arable land	0.44
Irrigated land	0.25
Rice fields	0.05
Orchards	0.35
Fruit tree plantations	0.30

Heterogeneous agricultural areas	0.30
Deciduous/evergreen forest	0.002
Coniferous forest	0.004
Mixed forest	0.003
Natural grassland	0.08
Shrubs and transitional woodland / Matorral	0.03
Bare surfaces above 1000 m elevation	0.12
Water surfaces	0

Table 31: Retardance coefficient values for different terrains (Roussel et al., 2005).

Generalized terrain description	Dimensionless retardance coefficient (N)
Pavement	0.02
Smooth, bare, packed soil	0.1
Poor grass, cultivated row crops, or moderately rough packed surfaces	0.2
Pasture, average grass	0.4
Deciduous forest	0.6
Dense grass, coniferous forest, or deciduous forest with deep litter	0.8

Table 32: Range for different model parameters

Model parameter	Model variable	Unit	Range/default
Soil erodibility factor	K	kg h MJ-1 mm-1	0.02-0.69
Erosion control practice factor	P	-	0-1
Crop and management factor	C	-	0-1
Retardance coefficient	N	-	0-1

INCA

The INCA soil erosion model requires the following land use specific model parameters (inca_table):

Table 33: inca_table

Land use class	Vegetation cover (V)	Ground cover (C_g)	Calibration parameter (a_4)	No erosion
-99	1	2	3	4
1	8.5	0.65	0.7	0
2	5	0.35	1.5	0
3	3.5	0.3	5	0
…	…			

The vegetation cover (V) is similar to the canopy cover of the other soil erosion models but multiplied with a factor 10. The vegetation cover is determined by LAI · 10 in case the vegetation module is used. The ground cover (C_g) and "no erosion" columns are similar to the ones used by MMF. The calibration parameter a_4 is described below.

The soil erodibility for splash (E_{SP}) and flow erosion (E_{FL}) can be used for model calibration and have default values of 0.005 kg m^{-2} s^{-1} and 0.003 kg km^{-2} s^{-1}.

The splash detachment scaling parameter C_{X1} is a constant with a value of 3 s m^{-1}.

The model parameters a_1-a_6 include constants and parameters that can be used for model calibration. The constants include a_2 (=0 m^2 s^{-1}), a_3 (=0.15) and a_5 (=0 m^2 s^{-1}). The other parameters can be used for model calibration. The calibration parameter a_4 can be given as a fixed value for all model domain or be land use specific using inca_table (Table 33).

Table 34: Model parameters

Model parameter	Model variable	Unit	Range/default
Vegetation cover	V	-	0-10
Ground cover	C_g	-	0-1
No erosion		-	0 or 1
Soil erodibility for splash erosion	E_{SP}	kg m^{-2} s^{-1}	0.005
Soil erodibility for flow erosion	E_{FL}	kg km^{-2} s^{-1}	0.003
Splash detachment scaling parameter	C_{X1}	s m^{-1}	3
Flow erosion scaling factor	a_1	s m^{-2}	7-15
Flow erosion direct runoff threshold	a_2	m^2 s^{-1}	0
Flow erosion non-linear coefficient	a_3	-	0.15
Transport capacity scaling factor	a_4	kg m^{-2} km^{-2}	0.7-10
Transport capacity direct runoff threshold	a_5	m^2 s^{-1}	0
Transport capacity non-linear coefficient	a_6	-	0.73-0.9

SHETRAN

The SHETRAN soil erosion model requires the following land use specific model parameters (shetran_table):

Table 35: Shetran_table

Land use class	Leaf drip diameter (d_l)	Leaf drip distance (X)	Ground cover (C_g)	Canopy cover (Cc)	Manning (n)	No erosion
-99	1	2	3	4	5	6
1	0.005	10	0.65	0.85	0.2	0
2	0.004	0.5	0.35	0.6	0.1	0
3	0.006	0.3	0.3	0.35	0.05	0
…	…	…	…	…	…	…

The leaf drip diameter should be specified per land use class, with a typical value of around 0.005 m. See Table 4.2 of Wicks (1988) for values per land use class. The leaf drip distance is similar to the plant height used in the other models. The same holds for ground and canopy cover, for which the latter is ignored in case the vegetation module is used. Table 4.2 of Wicks (1988) gives also suggestions for these model parameters. The Manning's roughness should be specified for all land use classes. The "no erosion" (0 or 1) column prevents erosion from happening, for instance for water and paved land use classes.

The raindrop impact soil erodibility coefficient k_r is typically between 0.1-70 J^{-1}, while the overland flow soil erodibility coefficient k_f is typically between 0.5-20 · 10^{-6} kg m^{-2} s^{-1}.

The flow and sediment density can be assumed to be 1100 and 2650 kg m^{-3}, respectively.

The particle diameter of the three textural classes should be provided, which can be assumed similar to the values provided by (Morgan and Duzant, 2008) for the MMF model.

The median grain size D_{50} can be provided, but when left empty, the median grain size will be estimated from the particle diameter and texture maps.

The width-to-depth ratio is used to determine the size of the rills, for the calculation of the flow velocity. Typical values range from 1-3.

The immediate deposition is determined using a transport capacity equation, for which two options are available, i.e. (1) Yalin (1963) and (2) Hansen and Engelund (1967).

Table 36: Model parameters

Model parameter	Model variable	Unit	Range/default
Leaf drip diameter	d_l	m	0.003-0.007
Leaf drip distance	X	m	0-50
Ground cover	C_g	-	0-1
Canopy cover	C_c	-	0-1
Manning	n	s $m^{-1/3}$	0.01-0.5
No erosion		-	0 or 1
Raindrop impact soil erodibility coefficient	k_r	J^{-1}	0.1-70
Overland flow soil erodibility coefficient	k_f	kg m^{-2} s^{-1}	0.5-20 · 10^{-6}
Flow density	ρ	kg m^{-3}	1100
Sediment density	ρ_s	kg m^{-3}	2650
Particle diameter	δ_c, δ_z, δ_s,	m	2 · 10^{-6}, 60 · 10^{-6}, 200 · 10^{-6}
Median grain size	D_{50}	µm	1-2000
Width-to-depth ratio	WD	-	1-3
Capacity equation			1 or 2

DHSVM

The DHSVM soil erosion model requires the following land use specific model parameters (dhsvm_table):

Table 37: Dhsvm_table

Land use class	Leaf drip diameter (D)	Leaf drip distance (X)	Ground cover (C_g)	Canopy cover (Cc)	Manning (n)	Root cohesion (COH_r)	No erosion
-99	1	2	3	4	5	6	7
1	0.005	10	0.65	0.85	0.2	15	0
2	0.004	0.5	0.35	0.6	0.1	1.5	0
3	0.006	0.3	0.3	0.35	0.05	10	0
…	…	…	…	…	…	…	…

The leaf drip diameter should be specified per land use class, with a typical value of around 0.005 m. See Table 4.2 of Wicks (1988) for values per land use class. The leaf drip distance is similar to the

plant height used in the other models. The same holds for ground and canopy cover, for which the latter is ignored in case the vegetation module is used. Table 4.2 of Wicks (1988) gives also suggestions for these model parameters. The Manning's roughness should be specified. The root cohesion can be obtained from the EUROSEM manual (Morgan et al., 1998), see also Table 38. The "no erosion" column (0 or 1) prevents erosion from happening, for instance for water and paved land use classes.

Table 38: Guide values for root cohesion (COHr; kPa), based on Morgan et al. (1998)

Vegetation type	Soil cohesion (COHr) (kPa)
Barley	0.2-0.6
Grass	1-8
Marram grass	1.5-15
Chaparral, matorral	0.3-3
Alfalfa	10
Alder	2-12
Sitka spruce	4-12
Hemlock	1-8
Willow	6
Poplar	2
Maple	4-6
Pines	4-10
Coniferous forest	1-17.5
Candlenut	15-35
Acacia	1-5

A soil class map (SoilClass) should be provided, which is subsequently used to assign soil cohesion values to the soil classes. The soil cohesion values should be provided in a table, i.e. dhsvm_cohesion_table:

Table 39: Dhsvm_cohesion_table

Soil class	Soil cohesion (COH)
-99	1
1	10
2	3
3	15
…	…

The values for soil cohesion can be obtained from the EUROSEM manual (Morgan et al., 1998), which gives soil cohesion estimates per soil type based on the USDA soil texture classification.

The raindrop impact soil erodibility coefficient k_r is typically between 0.1-70 J^{-1}.

The critical stream power SP_{cr} is typically 0.004 kg m s^{-3}.

The median grain size D_{50} can be provided, but when left empty, the median grain size will be estimated from the particle diameter and texture maps.

The width-to-depth ratio is used to determine the size of the rills, for the calculation of the flow velocity. Typical values range from 1-3.

The minimum water depth should be provided for stability reasons. A value of 0.001 m should give satisfying results.

The flow and sediment density can be assumed to be 1100 and 2650 kg m^{-3}, respectively.

The particle diameter of the three textural classes should be provided, which can be assumed similar to the values provided by (Morgan and Duzant, 2008c) for the MMF model.

Table 40: Model parameters

Model parameter	Model variable	Unit	Range/default
Leaf drip diameter	D	m	0.003-0.007
Leaf drip distance	X	m	0-50
Ground cover	C_g	-	0-1
Canopy cover	C_c	-	0-1
Manning	n	s $m^{-1/3}$	0.01-0.5
Root cohesion	COH_r	kPa	0.2-35
No erosion		-	0 or 1
Soil cohesion	COH	kPa	2-44
Raindrop impact soil erodibility coefficient	k_r	J^{-1}	0.1-70
Critical stream power	SP_{cr}	kg m s^{-3}	0.004
Flow density	ρ	kg m^{-3}	1100
Sediment density	ρ_s	kg m^{-3}	2650
Particle diameter	δ_c, δ_z, δ_s,	m	$2 \cdot 10^{-6}$, $60 \cdot 10^{-6}$, $200 \cdot 10^{-6}$
Median grain size	D_{50}	µm	1-2000
Width-to-depth ratio	WD	-	1-3
Minimum water depth	h_{min}	m	0.001

HSPF

The HSPF soil erosion model requires the following land use specific model parameters (hspf_table):

Table 41: Hspf_table

Land use class	Ground cover (CR)	Soil scour detachment (KGER)	No erosion
-99	1	2	3
1	0.65	0.03	0
2	0.5	0.2	0
3	0.35	0.5	0
…	…	…	…

Ground cover is similar to all other soil erosion models, specified per land use class. The soil scour detachment coefficient (KGER) is a model parameter that is a soil erodibility parameter for detachment by runoff. The “no erosion” column (0 or 1) prevents erosion from happening, for instance for water and paved land use classes.

The P-factor map indicates the support practice factor, which indicates how conservation measures reduce soil erosion, which factor is often considered to be 1.

The rainfall detachment coefficient KRER is similar to the USLE K-factor. The Wischmeier et al. (1971) formulations are used (see section 2.8) when this is left empty. In that case, a sand, clay and

organic matter map should be provided in the PEDOTRANSFER section of the config file (even when the pedotransferfunctions are not used (i.e. if PedotransferFLAG = 0). The rainfall detachment exponent JRER is an exponent in the detachment by raindrop impact formulation.

Similar model parameters exist for the washoff detachment, i.e. KSER and JSER, and for scour detachment, i.e. KGER and JRER. The soil scour detachment KGER should be left empty when the land use specific values are provided in hspf_table.

The fraction by which detached sediment storage decreases per time step is defined by AFFIX.

Table 42: Model parameters

Model parameter	Model variable	Unit	Range/default
Ground cover	CR	-	0-1
Soil scour detachment	KGER	-	0.01-0.5
No erosion			0 or 1
Support practice factor	SMPF	-	0-1
Rainfall detachment coefficient	KRER	-	0.14-0.45
Rainfall detachment exponent	JRER	-	1.5-3
Washoff detachment coefficient	KSER	-	0.1-5
Washoff detachment exponent	JSER	-	1.5-2.5
Soil scour detachment coefficient	KGER	-	0.01-0.5
Soil scour detachment exponent	JGER	-	1-2
Fraction of sediment storage decrease	AFFIX	-	0.05